Alma Mater Studiorum · Università di Bologna

Scuola di Scienze
Corso di Laurea Magistrale in Fisica

Mechanical and electrical characterization of wearable textile pressure and strain sensors based on PEDOT:PSS

Relatore:
Prof. Enrico G. Campari

Correlatore:
Prof.ssa Beatrice Fraboni
Dott. Marta Tessarolo

Presentata da:
Luca Possanzini

Sessione II
Anno Accademico 2016/2017

Alle mie nipoti Caterina, Giorgia e Gemma

"Una vita tranquilla e modesta porta più gioia del perseguimento del successo legato ad una agitazione perenne."

Albert Einstein

Abstract

Wearable technology refers to various types of electronic devices that can be incorporated into clothes or accessories and that can be comfortably worn on the body. They are widely used in the fields of health, medicine, fitness, sport, disabilities and education.

In this thesis, wearable textile pressure and strain sensors has been developed and theoretical models that described the sensing behaviors are reported. The active parts of the wearable textile sensors are based on the intrinsic conductive polymer (PEDOT:PSS). To treat the fabrics with the conductive solution, drop-casting method and screen printing technique, has been evaluated.

On one hand, the theory developed for cotton fabric demonstrated that it is possible to change the pressure response range of the textile pressure sensors, changing the ethylene glycol concentration in PEDOT:PSS solution, and fixing the sensors configuration. In order to evaluate a real life application, textile pressure sensor has been fabricated on a sport technical elastic fabric. Similar behaviors has been obtained proving the validity of the proposed model.

Then, the fabrication process and the electro-mechanical characterization of wearable textile strain sensors are described. Range tests and stability tests performed on these strain sensors give information about the performance in terms of gauge factors and reliability. The sensing mechanism is thoroughly analyzed by a theoretical model based on fabric properties and on the wale-course structure deformations typical of knitted textiles.

The results obtained during this work allows the developments of a new generations of textile pressure and strain sensors that can be easily worn in daily life.

Sommario

Il termine *tecnologia indossabile* si riferisce a quei dispositivi elettronici incorporati negli indumenti od accessori che possono essere comodamente indossati. Essi sono ampiamente utilizzati in campo medico, sportivo, educativo o per monitorare disabilità.

In questa tesi sono stati sviluppati sensori di pressione e di deformazione tessili, proponendo il modello teorico che ne descrive il comportamento. L'elemento attivo di tali sensori tessili è basato sul polimero intrinsecamente conduttivo (PEDOT:PSS). La soluzione conduttiva è stata depositata sui tessuti tramite il metodo *drop-casting* e la tecnica *screen printing*.

La teoria sviluppata per il tessuto di cotone ha dimostrato che è possibile cambiare il range di pressione in cui i sensori rispondono cambiando la concentrazione di glicole etilenico presente nella soluzione di PEDOT:PSS pur mantenendo la geometria dei sensori inalterata.

Per realizzare un'applicazione reale, il sensore di pressione tessile è stato fabbricato su un tessuto tecnico sportivo elastico. Comportamenti simili sono stati ottenuti dimostrando la validità del modello proposto.

Successivamente, sono presentati i processi di fabbricazione e la caratterizzazione elettro-meccanica di sensori di deformazione tessili. *Range tests* e *stability tests* eseguiti su questi sensori di deformazione forniscono notizie circa le loro prestazioni:affidabilità e gauge factor. Il meccanismo di rilevamento è stato analizzato con un modello teorico basato sulle proprietà del tessuto e sulla deformazione della struttura *wale-course* tipica dei tessuti a maglia.

I risultati ottenuti durante questo lavoro permettono lo sviluppo di una nuova generazione di sensori di pressione e di deformazione tessili che potranno essere comodamente indossati nella vita di tutti i giorni.

Contents

Introduction

Wearable technology refers to various types of electronic devices that can be incorporated into cloths and accessories which can be comfortably worn on the body. During the last few years, this field of research has attracted a great deal of attention and it has experienced a strong expansion. The implications and uses of wearable technology are far reaching and it can influence the fields of health, medicine, fitness, aging, disabilities, education, transportation, enterprise, finance, gaming and music. Inside this new and promising field of interest, tremendous effort has been put into the development of smart textiles, which are generally fabricated by integrating electrical circuits into traditional textiles to modify their functionalities. Generally speaking, these textiles are defined as "smart" because they have the functions that enable them to directly respond to mechanical, thermal, chemical and electrical stimuli coming from the surrounding environment. Potential applications of smart textiles and fabrics may include wearable computing fabrics, antistatic garments, tactile textile sensors and thermal, pressure or strain sensing for medical and athletic applications.

In this thesis, wearable textile pressure and strain sensors has been developed and the theoretical models that describe the sensing behavior are reported. The active parts of the wearable textile sensors are based on the intrinsic conductive polymer (PEDOT:PSS), changing the electrical properties with different concentration of EG as second dopant. To treat the fabrics with the conductive solution, drop-casting method and screen printing technique, which are efficient and low-cost deposition methods, have been evaluated. A complete mechanical characterization of compressive and tensile properties of the textiles used to fabricate the sensors has been performed.

The working principle of textile pressure sensors has been studied and developed using woven cotton fabric as substrate. The results found in this context are applied in a sport technical elastic fabric for a real life application. In order to understand the piezoresistive behavior of PEDOT:PSS, fixing the geometry configuration of the pressure sensors, various solution formulations of the conductive polymers has been

investigated. This leads to an understand of how different solvents and additive concentrations influence the electrical and piezoresistive properties, and also the textile pressure sensors performances.

Similarly, the relevant electrical and mechanical properties of wearable textile strain sensors based on elastic fabric have been studied. Range tests and stability tests performed on these strain sensors give information about the performance in terms of gauge factors and reliability. Then, the sensing mechanisms is thoroughly analyzed, based on the experimental observation of deformation characteristics of knitted fabric. Finally, the sensing behavior of the textile strain sensor is qualitatively described as a function of additive concentration at different tensile strain.

Chapter 1 introduces generalities about wearable sensors and it gives a description of working principle of wearable pressure and strain sensors. At the end of the chapter, a brief presentation of sensing elements realized directly on fabric materials is proposed.

Chapter 2 gives an introduction about polymers physics presenting their properties and classification. After an overview on conducting polymers, doping mechanisms and the main features of PEDOT:PSS, with its potential applications, are described.

Chapter 3 explains the general characteristics of the fabrics used as substrate for the textile pressure and strain sensors. It reports the chemical compounds used to realize different conductive solution formulations. The basis of the two deposition methods to treat the fabric substrate are also described. Finally, the morphological, electrical and mechanical characterization methods used in this thesis are presented.

Chapter 4 provides a comparison of the electrical responses between different PEDOT:PSS solution deposited as thin films on glass substrate and coated on cotton fabric. Morphological characterization has been carried out by means atomic force microscope and scanning electron microscope, whereas Van der Pauw method has been used to analyze the electrical properties.

Chapter 5 is focused on the techniques used to characterize the mechanical behaviors of cotton, elastic and high performance sport technical fabrics. After a brief overview in rheology theory, the results of creep-relaxation experiment, recovery test and stress-strain trend are reported both in compression and tension modes.

Chapter 6 presents the results related to wearable textile pressure sensors. First of all, the geometry configuration and layout of the fabricated sensors are described. Then, a pressure sensing model and the description of electrical-mechanical characterization procedure are proposed. The second part of the chapter shows the cotton pressure sensors responses and the interpretation of piezoresistive behaviors of PEDOT:PSS. A first comparison between the performance of pressure sensors based on

different PEDOT:PSS formulation is pointed out. The final section of this chapter is devoted to the results of the pressure sensors realized on the sport technical elastic fabric to achieve real life applications.

Chapter 7 reports the results for the wearable textile strain sensors. The chapter begins with an explanation of the fabrication method and electrical-mechanical characterization procedures. The results provided by range and stability tests, as well as the interpretation of textile strain sensor mechanism, are reported in the last section.

Chapter 1

Wearable electronic

1.1 Wearable sensors: features and classification

The technological advancement in the past three decades has impacted our lives and wellbeing significantly. One of its important areas are flexible and wearable electronic devices: they have attracted considerable attention because of their great potential applications, in areas such as wearable displays, smart clothing, human motion and health monitor [1, 2, 3]. The proliferation of mobile devices, internet and cloud computing has sparked a new era of Internet of Things (IoT), thus allowing researchers to create application-specific solutions based on the interconnection between physical objects and the internet. The U.S. National Intelligence Council gives this definition of IoT: "The Internet of Things is the general idea of things, especially everyday objects, that are readable, recognizable, locatable, addressable, and controllable via the Internet - whether via RFID (Radio-Frequency IDentification), wireless LAN (Local Area Network), wide-area network, or other means [4]." In particular, everyday objects that have not previously seemed electronic at all are starting to be online with embedded sensors and microprocessors, communicating with each other and the Internet.

The terms "wearable technology" or "wearable devices" refer to electronic technologies or tiny computers with sensing, processing, storage and communications capabilities that are incorporated into items of clothing and accessories which can comfortably be worn on the body. Overall, wearable technology is a perfect example of interaction of humans and technology and covers a very broad area that requires a mixture of expertise derived from disjointed accademic fields of science and technology that normally may not interact with each other.

A sensor is defined as "a device used to detect, locate, or quantify energy or matter, giving a signal for the detection of a physical or chemical property to which

the device responds" [5]. The physical sensors (different for a chemical sensor) can detects a change in a physical stimulus and turns that stimulus into a signal that can be measured or recorded. The regular activities of human body generate various physical stimuli, such as body and skin heat, blood pressure, pulse, skin strain and infrared radiation. A wearable sensor is a particular kind of sensor that can be integrated (insert) - or directly fabricated - on cloths.

Recently, the rapid development in new sensing materials, fabrication processes and electrical sensing techniques has contributed to significant progress in the achievement of flexible and stretchable physical sensing devices. Many of these sensing devices with high sensitivity are fabricated on microstructured and nanostructured materials and show unique useful properties such as transparency, extreme thinness, ultralight weight, ultra-conformality and technological compatibility with large areas. During this time, many efforts are being made to realize novel wearable sensors in different research field: track the user's physical activities in the area of rehabilitation or monitor chemical parameters to obtain complete information about a wearer's health.

The world of wearables is transforming our lives and figure 1.1 shows some of the main application of wearable technologies. The latest discoveries on sensing capabilities enable the realization of different chemical sensors devices that can potentially monitor electrolytes [6], metabolites [7], heavy metals [8], toxic gases [9] directly on the body in various biofluids (such as sweat [10], tears[11] and saliva [12]) or physical sensors devices monitoring the heart beat rate [13], the jugular venous pulse[14], the voice [15], muscle movement, [16], bodily motion [17], and the temperature of the human body [18].

The wearable sensors are classified as single function or multi-functional and can be invasive or non-invasive. The latter wearable sensors which are in contact with the body could either monitor the individual or the surrounding environment. Active or passive is a different way to classify its according to whether or not they need power to operate. Yet another view of wearable sensors is the mode in which the signals are transmitted for processing - wired or wireless. Examples of single function, non-invasive, in contact with the body, passive and wired wearable sensors shall be presented in this work such as a special kind of pressure and strain sensors developed coating a fabrics with a conductive ink. The fabrication of these particular sensors will be described better in the next chapters. They can be used to realize special technical sports equipment for bikers that could monitor the pressure exerted by the wearer. The pressure sensors shall be realized directly on the fabric used to realize the sport suit. They allow to monitor the pressure distribution on the saddle and they must operate until at least 100 kPa.

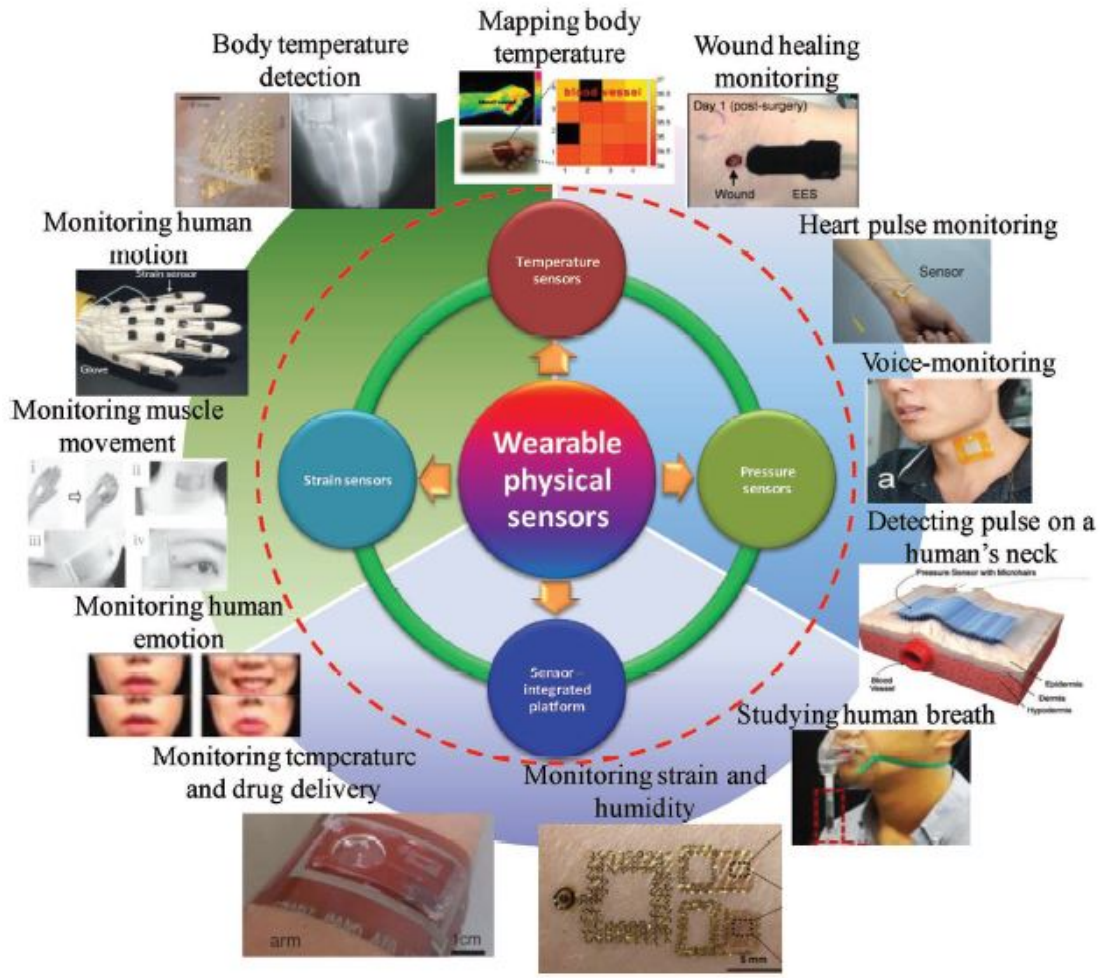

Figure 1.1: Overview of characteristic properties of recently developed wearable physical sensors for monitoring human activity and personal healthcare using temperature, pressure and strain sensors [19].

The wearable sensors system consisting of various components and devices, ranging from various types of small physical sensors (temperature, pressure and strain sensors) and actuators to multimedia devices including transmission modules and self-sustainable power supplies. These systems, which are conformally in contact with the surface of organs or the skin thanks to their main features, support complex healthcare applications and enable low-cost wearable, non-invasive alternatives for continuous monitoring of health, mobility and activities generated from the human body. Fundamentally, wearable system can carry out the following basic functions or unit operations in each of the scenarios shown in the last figure:

- sense;
- process (analyze);
- store;
- transmit;

The specifics of each function will depend on the application domain and on the wearer. The main features required of an ideal wearable system, which is the key to their successful use, are shown in figure 1.2. From a physical standpoint, their must be lightweight, invisible and with a variable form factor. The responsiveness of a wearable system is critical, especially when used for real-time data acquisition and control. They must be easily configurable for the desired end-use application and must be continuos monitoring

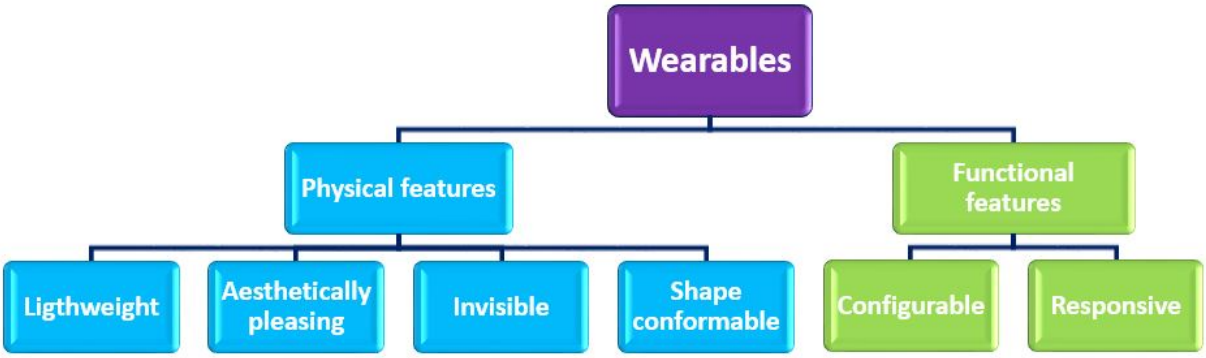

Figure 1.2: Main features of wearable systems.

This thesis will focus on the wearable sensors that respond to physical motion such as pressure or strain: these sensors will be realized directly on fabric to improve the wearer comfort and make they invisible.

1.2 Pressure wearable sensors

Many efforts has been done in the development of stratchable wearable sensors and in this section are presented only some of the latest and more substantial successful examples of these sensors for the detection of pressure, as well as novel sensor structures with their technological innovations and challenges [20].

The examples of wearable sensors reported in this section are realized on flexible and stretchable substrate of plastic materials and can be added to cloths or attached

on the surface of skin. They don't use directly the textile like substrate but can be use like external accessories.

The detection of *pressure* is of great importance to diagnose, prevent and treat various diseases or sports injuries in athletes. The pressure produced by human-body activity varies from a low-pressure regime (< 10 kPa) to a medium-pressure regime (< 100 kPa) and a high-pressure regime (> 100 kPa) [21]. Various regime of pressure will be generate by different position of the human body. The pressures produced by intra-body pressure or by tactile touch are collocated in the low-pressure regime, < 10 kPa, instead the pressure produced in the foot by the body weight is in the high-pressure regime, > 100 kPa. Between this two range is collocated the medium-pressure regime, < 100 kPa, generated by the heart rate, blood pressure wave, respiration rate or radial artery wave.

A powerful pressure sensor must reach an high sensitivity in the range of interest and this depends on the application. The sensing mechanism of the most relevant wearable pressure sensors includes piezoelectricity, piezoresistivity and capacitance. Depending on the active materials and device structure, each of these sensing mechanisms has its own characteristics.

1.2.1 Piezoelectric pressure sensors

Piezoelectric-based pressure sensors rely on the piezoelectric effect, which occurs when dipoles reorient under pressure to form an internal polarization. This polarization results in the generation of charge on the crystal face that is proportional to the applied pressure. An electric charge proportional to the applied pressure is generated when a piezoelectric material is stressed and taking advantage of this effect.

Only particular materials show a piezoelectric behavior and one of these in the *lead zirconate titanate* (PZT). A practical example of a piezoelectric pressure sensor relies on PZT is realized by Dagdeviren et al. [22] that introduced this material in a MOSFET (*metal metal oxide semiconductor field effect transistor*) configuration as gate electrode. The resulting devices is small, lightweight, stretchable and presented high responsivity, high detection resolution (detection limit $0,005$ Pa), fast response times (ca. 0,1 ms), low hysteresis and high stability. It works in the low pressure regime and can be applied on wrist, neck and throat for monitoring blood pressure (figure 1.3).

1.2.2 Piezoresistive pressure sensors

Piezoresistive-based pressure sensors rely on the piezoresistive effect, which occurs when the electrical resistivity of a material changes in response to applied mechan-

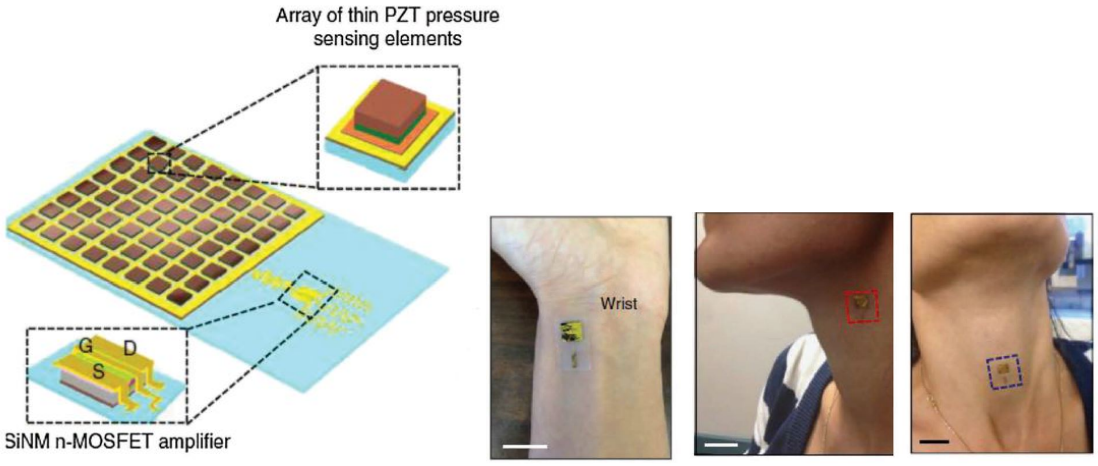

(a) (b)

Figure 1.3: a) Schematic of pressure sensors includes a square array of PZT thin-film transducer and MOSFET. b) Photograph of the sensors placed on a wrist, neck and throat. [22]

ical strain. In contrast to the piezoelectric effect, the piezoresistive effect causes a change only in electrical resistance, not in electric potential. In semi-conducting materials, the strain from the applied force impacts the material's band structure, which makes it easier or more difficult for electrons to be excited into the conduction band. Consequently, the density of current carriers is altered and the material's resistance changes. Usually the resistance change in metals is mostly due to the change of geometry resulting from applied mechanical stress. However, even though the piezoresistive effect is small in those cases it is often not negligible. Some metals display piezoresistivity that is much larger than the resistance change due to geometry (e.g. platinum alloys). In the piezoresistive pressure sensors, a combination of geometry deformation and piezorevistive intrinsic behavior of material, give informations about the applied load.

Traditionally, active materials for piezoresistive pressure sensors have mainly been based on elastomer composites that contain *carbon nano tubes* CNTs [23, 24, 25] , metal particles [26] and conductive polymers (CPs) [27], which are incorporated into elastomers (e.g., polydimethylsiloxane (PDMS) or polyurethane (PU)) to generate piezoresistive behavior.

An example of resistive pressure sensor is proposed by Choong [27] and is formed by a micropyramidal array of PDMS coated with a conductive elastomeric composite of PEDOT:PSS (poly(3,4-ethylenedioxythiophene) polystyrene sulfonate) and polyurethane dispersion (PUD). This structure serves as a piezoresistive electrode.

Applying an external pressure on the counter electrode lay on the top of micropyramidal, there are changes of the contact interface resistance (R_{CI}) and of the piezoresistive electrode resistance (R_{PE}). When an electrical current flow through the contact area bridging the two terminals, the resistance change induce a potential difference with respect to the counter and piezoresistive electrodes (figure 1.4). The pressure sensor with its microstructure enables measurement of the blood pressure of a human, demonstrating its promising application in personal healthcare.

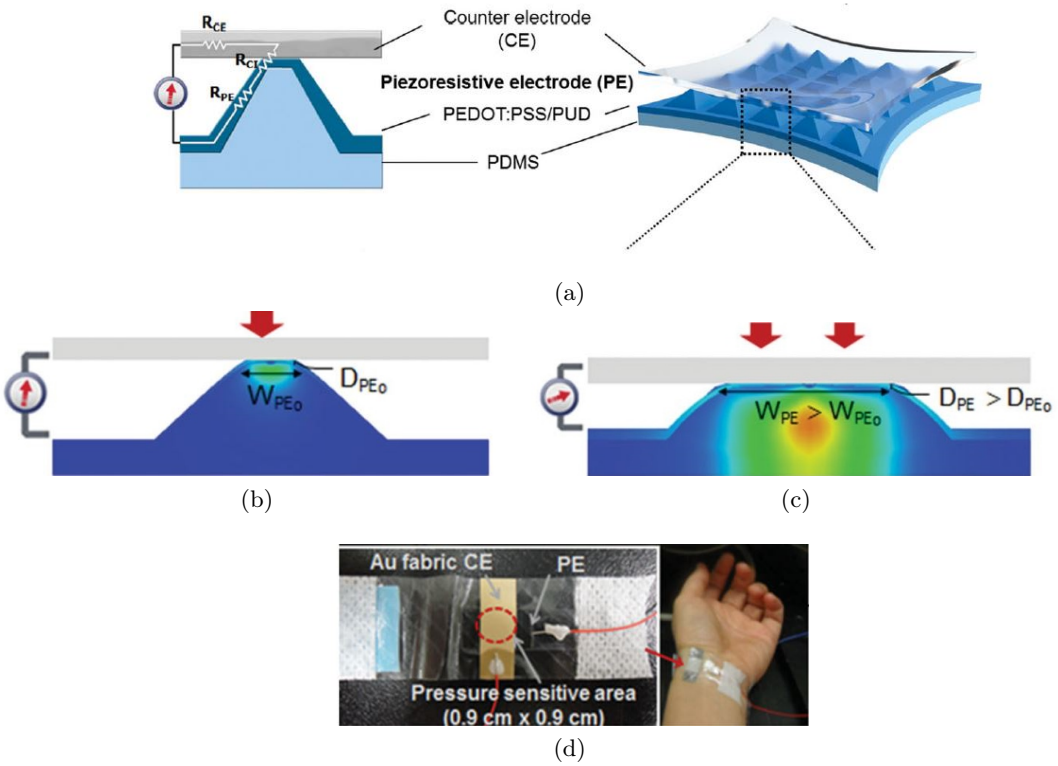

Figure 1.4: a) Circuit model used to derive the sensing principle of the sensor, which relies on the change of the pyramid's geometry (resulting in a resistance variation) in response to pressure. b - c) Effects of the different applied pressure. d) The pressure sensors with pyramid geometry attached on the wrist for real-time monitoring of blood pressure [27].

1.2.3 Capacitive pressure sensors

The *capacitive*-based pressure sensor can monitor the external applied pressure detecting the capacitance change of a capacitor. A capacitor is a passive electronic component that stores energy in the form of an electrostatic field. It consists of two conducting plates separated by an insulating material (dielectric). The practical formula to compute the capacitance C knowing only the geometrical parameters is

$C = \epsilon_0 \epsilon_r A/d$, where ϵ_0 is the electric constant, ϵ_r is the relative static permittivity of the dielectric, A is the area of the two plates, and d is the thickness of the dielectric. Therefore the capacitance between two conductive pads depends on their size, relative position and the properties of the nonconductive material in-between. Changes in d are commonly used for the detection of pressure in capacitive pressure sensors.

Many research groups worked to develop transparent and stretchable capacitive pressure sensors by using carbon nanotube CNTs [28, 29], silver nano wires AgNWs[30] and conductive ionic materials[31] as electrodes. For example, Mannsfeld et al. [21] and Schwart et al. [32], fabricated a flexible OFET (*organic field effect transistor*) with a microstructured PDMS as a gate dielectric layer to realize a pressure sensor (figure 1.5). It show high sensitivity (8,4 kPa^{-}1), fast responsivity (<10 ms), high stability and low power consumption. When attached on the human wrist, this sensor can monitoring in real-time the radial artery pulse wave.

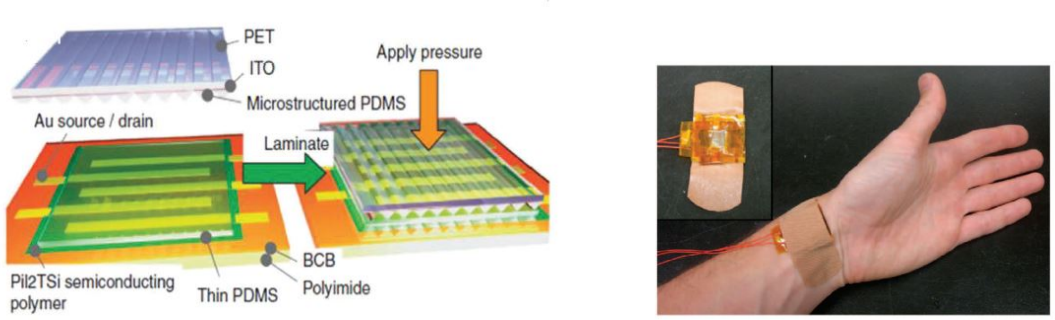

(a) (b)

Figure 1.5: a) Schematic illustration of the fabrication process of a pressure-sensitive OFET [32], b) pressure sensor attached on to the wrist of a test person.

Foot plantar pressure system

The main focus of this thesis is related on the medium and high pressure regimes. A very practical application of pressure sensors working in this range are the foot plantar pressure measurement system. The plantar pressure systems available on the market or in research laboratories vary in sensor configuration to meet different application requirements. Typically the configuration is one of three types: pressure distribution platforms, imaging technologies with complex image processing software and in-shoe systems. In designing plantar pressure measurement devices the key requirements are spatial resolution, sampling frequency, accuracy, sensitivity and calibration. In the recent years was developed many example of foot plantar pressure

sensors reported in Razak's work [33]. The main characteristic of this system to be mobile and wearable for monitoring activities of daily life are the wireless connection and low power consumption.

In-shoe sensors are flexible and embedded in the shoe such that measurements reflect the interface between the foot and the shoe making it very portable (figure 1.6). Another practical application of pressure measurement system is to measure the saddle pressure distribution of a biker while he is riding. Such system allows the recording of the loads exerted on saddle surface evaluating pedaling style and pressure patterns distribution that can give important informations to improve comfort and prevent some injuries (the seat pressure during cycling can compress specific neurovascular tissues over the perineum leading to genital pathologies).

(a) (b) (c)

Figure 1.6: a) An in-shoe based foot plantar pressure sensor by Pedar Novel [34], b) and an in-shoe based foot plantar pressure sensor F-Scan System developed by Tekscan [35], c) Saddle pressure sensors system by GebioMized.

1.3 Strain wearable sensors

A strain sensor or strain gauge is a sensor used for the purpose of measuring the deformation of objects. Normally, a strain gauge consists of an insulating flexible backing which supports a metallic foil pattern. It can be easily attached on an object for monitoring its deformation. For applications in e-skin and human motion monitoring in medicine, flexible and stretchable strain sensors has developed using sensing materials such as CNTs [36, 37], graphene [38, 39], reduced graphene oxide (R-GO) [40], R-GO composites [41], organic semiconductors [42], GaInSn [43] and conductive polymers [44].

These sensors can be attached on clothing or in the human body and are present different sensing mechanism of these sensors including piezoelectricity, piezoresistivity and capacitive. The strain sensors study in this thesis are piezoresistive based and only an overview of these kind of wearable sensors is shown.

1.3.1 Piezoresistive strain sensors

The following examples of piezoresistive strain sensors use a plastic material as substrate and the sensing part can be realized with various materials each of which with their advantages.

A good option to realize the sensing layers is with CNTs and Slobodian et al. [45] introduced a stretchable strain sensor based on a CNT/PU composite. It can be easily embedded in flexible and stretchable material exhibiting a multi-directional detection, multifunctionality and high strain resolution.

Also graphene (Gr) is another candidate for developing piezoresistive strain sensors because it has good mechanical and electrical properties. Under applied tensile strain, the hexagonal structure near the edge of the Gr film would partially be destroyed leading a change in the electronic band structure and resistance (work of Li et al. [46]).

Further, PEDOT:PSS with its optical transparency, light weight, high flexibility, simple fabrication and piezoresistivity behaviors has been widely used for realize strain sensors applications. An example of low-cost, flexible PEDOT:PSS strain sensor was fabbricated by Latessa et al.[47]. This sensor has a gauge factor (ratio of relative change in electrical resistance R, to the mechanical strain ϵ, $GF = \frac{\Delta R}{R}/\epsilon$) of $17,8$ and a response to bending angle in the range of 0 - 60° in both directions. As will be seen in the subsequent chapters, the addition of common additives, such as dimethylsulfoxide (DMSO), has effects on the mechanical properties of PEDOT:PSS. Savagatrup et al. [90] reasoned that PEDOT:PSS films containing 5% DMSO might behave as a piezoresistive strain sensor for applications requiring extreme mechanical deformation. These devices exhibited detectable responses at 20% strain and high mechanical robustness through elastic deformation. The sensing devices proposed are suitable for application of monitoring human motion.

1.4 Textile sensors

In the last years, wearable devices are rapidly emerging and forming a new segment - “Wearable Intern of Things ” [49] - due to their capability of sensing, computing, communication and can continuously tracked individuals without they noticing. To realize this purpose the concept of wearable sensors made a step forward: passing from indicating the insertion of small electronic equipment into textile to the broader meaning that includes any electronic device directly realized in a textile form. These sensors are now so intimately interwoven into the fabrics that they are not pervasive and are operationally “invisible” to end-users. The user interface is simple and this,

coupled with the invisibility of the "embedded" technology in the various devices, has contributed to the proliferation of these sensors in various applications [50].

Wearable textile sensors are actually very popular and this is proven by the novel Levi's Commuter Trucker Jacket that recently was put on sale. Surely, this is representing the first application available to the wider public and it is just a starting point for future devices development. This new product is a jacket, washable, durable and comfortable but, with Jacquard technology, the wearer can perform common digital tasks - like starting or stopping music, getting directions or reading incoming text messages - by simply swiping or tapping the jacket sleeve (figure 1.7).

Figure 1.7: Levi's Commuter Trucker Jacket with Jacquard technology developed by Google.

There are many efforts to develop new wearable textile sensors and this new results show that the works in this expansion field is reasonable.

The textiles have many characteristic that make them suitable for wearable applications since they are:

- flexible, strong, lightweight and generally withstand different types of operational (stress/strain) and harsh environmental conditions;
- unique in combining strength and flexibility in the same structure, and so they conform to the desired shape when bent but retain their strength;
- made in different form factors including desired dimensions of length, width and thickness;
- easy to manufacture in a relatively cost-effective (inexpensive) manner compared to traditional printed circuit boards.

The realization of a wearable textile sensors is not a simple and obvious operation. A lot of research and studies was required to change the substrate for electronics applications: from a rigid silicon to an amorphous, complex and irregular substrate

like a textile. Nevertheless, from a technical performance perspective, a textile fabric (or clothing) is an excellent platform for the incorporation of sensors and processors while keeping its aesthetic and comfort attributes (among many other textile-unique properties).

An important and useful distinction must be done between the sensing active part and the buses connection of a sensor. To realize the sensing core of an electronic textile sensor, allowing to sense external loads, there are used different strategies: sensitive fibers woven to form fabrics, sensitive fibers integrated into commercially available textiles, such as clothes and gloves, and functional materials deposited onto commercial textiles [51]. Textile sensors can also be obtained on a large scale directly coating the fabric with conductive ink.

Furthermore, to fabricate a completely textile sensor, also data buses or pathways to carry signals must be realize with a textile connection. For instance, textile yarns, which are an integral part of the fabric, can serve as data buses or communication pathways for sensors, processors and represents the path of the signal from detection to acquisition. The placement of these data buses, can be engineered to suit the desired sensor surface distribution profile, making it a versatile technology platform for wearables. An example[52] of this buses can realize coating natural cotton fibers with gold nanoparticles or with conductive polymers like PEDOT (figure 1.8). These threads can be sewn on the fabric to realize connections providing the fabrication of whole textile-based circuits.

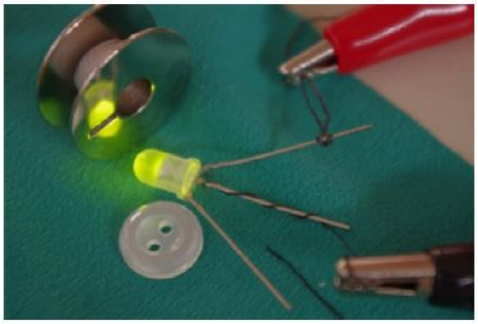

Figure 1.8: Light emitting diode (LED) biased by means of conductive cotton yarns.

There are also two main types of conductive threads available on the market: the silver-coated threads (which are nylon thread coated with silver) and stainless steel threads (there is no traditional thread core because are made entirely of stainless steel and have a reliable and low resistance)

The textiles sensors react to external deformations such as pressure and strain and, being intrinsically placed on clothes, can be exploited in several application

fields like healthcare and sports.

1.4.1 Pressure textile sensors

Several technologies have been developed to manufacture plane pressure textile sensors. These pressure sensors have the same operating principles as explained in section 1.2: resistive (piezoelectric and piezoresistive) or capacitive mode [53]. The application of an external load can cause a variation in the resistance or capacitance.

Resistive pressure sensors

Resistive pressure textile sensors can be manufactured directly on fabric substrate otherwise on fibers or yarns coated with pressure sensitive polymers and sewn to form a textile. The figure 1.9 shows the working principle of a fabric pressure sensors made by sandwiching a piece of resistive fabric strain sensing element between two tooth-structured layers of soft elastomers. After a pressure the teeth geometry of the top and bottom layers deforms the conductive elastic yarn, causing shape change and consequently an electrical resistance variation [54]. The pressure sensors are capable of measuring pressure from 0 to 2000 kPa, covering the whole human range.

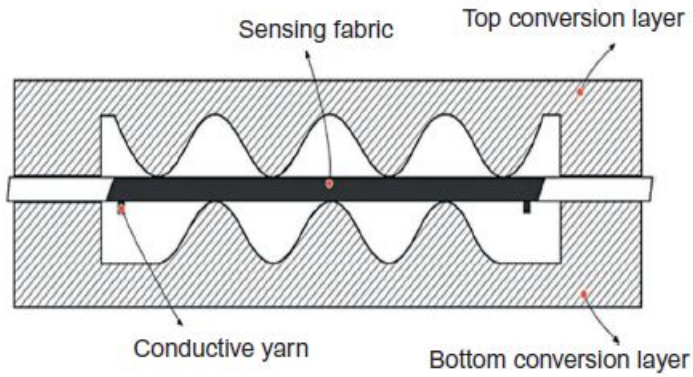

Figure 1.9: Tooth-structured resistive fabric pressure sensor[54].

It is possible realize a flexible pressure sensors also adhering conductive graphene films on the upper and bottom of a textile fabric [55]. Figure 1.10 showed the working principle of pressure sensitive sensor generated by one piece of graphene textile. The graphene are sticking on the surfaces of polyester fibers and the structure deformation of flexible textile occurred when a force is applied, resulting in an increase of contact area in the polyester fibers (structural deformation), which would cause the sensor to experience a decrease in intrinsic resistance. When the pressure is released, the polyester fiber structure could recover their initial status.

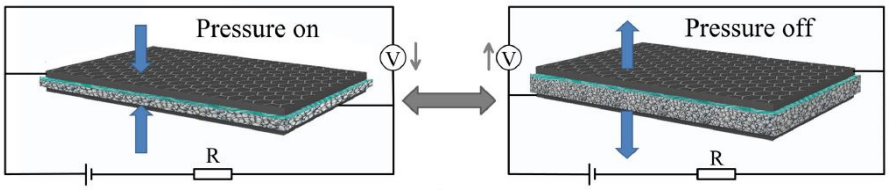

(a)

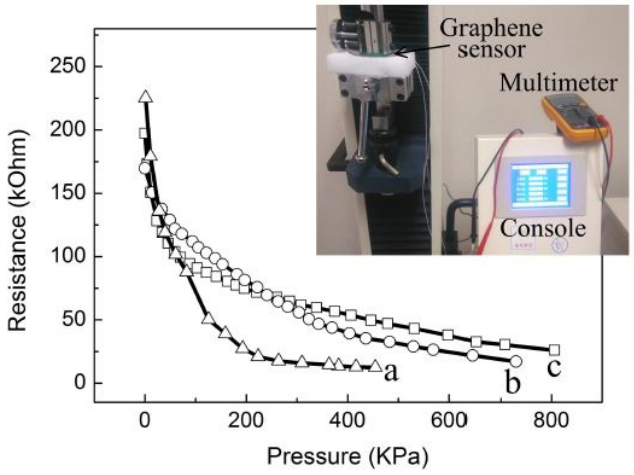

(b)

Figure 1.10: a) The working principle of pressure-sensitive graphene textile sensor. The flexible textile acts as the support substrate and graphene layers wrapped around each polyester fiber. The thickness of textile decreases with the increasing applied pressure, b) typical resistance curves of the graphene textile pressure sensors vs. applied loading. [55].

Another possible way to realize pressure textile sensors is using foams. They can become pressure sensitive coating their surface with a conducting inks which can change its conductance during a contact event.

Capacitive pressure sensors

For capacitive sensors, a pressure applied on the sensing part generates capacitance variations. Generally these sensors consist of two different electrode plates, separated by dielectric material, as shown in figure 1.11. The conductive paths on the fabric can be realize by sewing, weaving or embroidering a conductive thread, or painting, printing or screening a conductive ink. The dielectrics used are typically synthetic foams, fabric spacers or soft polymers. Furthermore, for some applications like detection of the muscle activity or analyze the sitting posture, the sensors capacitors can be place in array achieving a matrix and distributed pressure sensor.

The fabric capacitive sensors can be used to fabricate lightweight and flexible

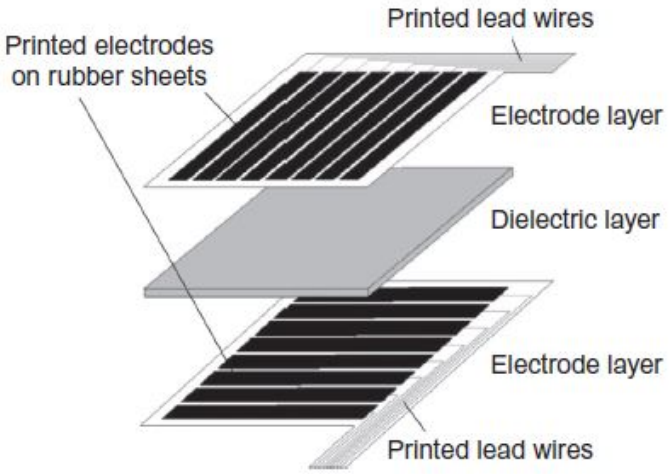

Figure 1.11: The electrodes on the two-electrode layers are oriented orthogonally and each crossing point of the two perpendicular electrode arrays makes up a capacitive sensor cell on the sheet.

wearable keyboards. For the patterning of the conducting polymer electrodes, a negative master is used and the conductive polymers solution is brush-painted on the textile [56] (figure 1.12). The capacitance sensors respond to touch by a human finger and also a pressures as small as 0,5 kPa cause an easily measurable change in capacitance.

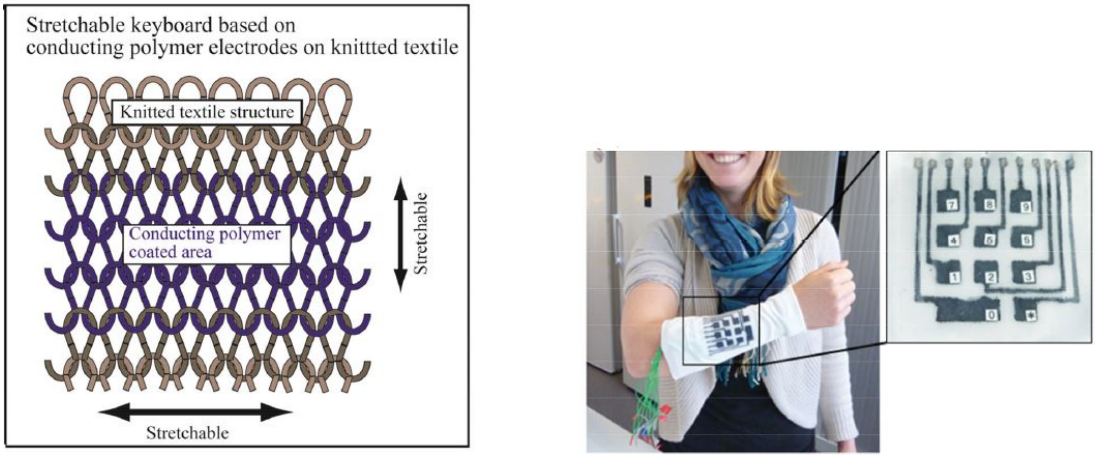

(a) (b)

Figure 1.12: a) Concept of the stretchable keyboard, showing horseshoe structures in the knitted textile and, b) the layout of a developed keyboard [56].

To solve problems encountered when trying to construct large fabric pressure sensors, it is possible utilized die-coating technique of PEDOT:PSS and Cytop (an

amorphous fluoropolymer) on polyester fibers and woven its to form a handkerchief pressure sensor fabric. The figure 1.13 report a schematic description and a picture of a large scale the capacity pressure sensor [57]. The capacitors were formed at the crossing points between the weft and warp fibers and varied according with the change in the distance between them under pressure. Its sensitivity ranged from 9.8 to 98 kPa, which is in the range of human touch, and therefore this fabric touch sensors can be used in applications from wearable keyboards to sensors embedded in beds for health care purposes.

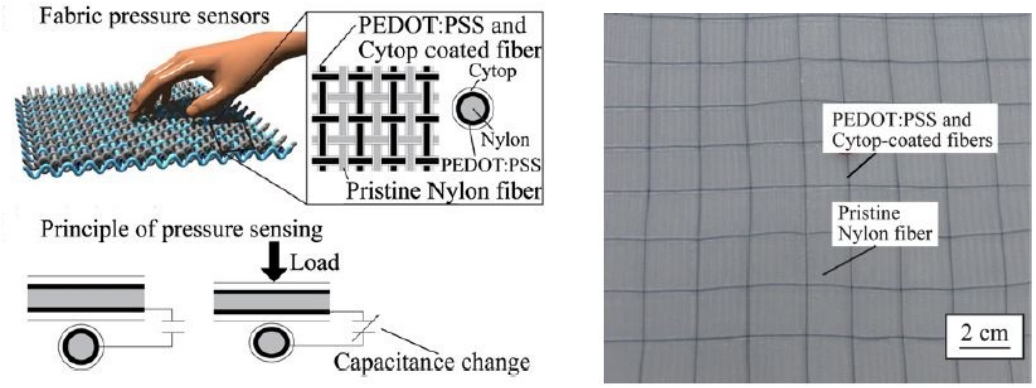

(a) (b)

Figure 1.13: a) Structure of the sensor, conductive polymer and dielectric film-coated fibers are woven as wefts and warps, forming capacitive type of pressure sensors. On the bottom the sensing mechanism, applied pressure induces capacitance change. b) Blue lines are the processed nylon fibers and white lines are pristine nylon fibers. The sensors are located at the point where blue lines are crossed [57].

1.4.2 Strain textile sensors

Strain sensors are used to monitor deformation under applied force or load and fabric strain sensors are textile structures that are able to have an electrical response after a mechanical strain. There are different techniques for the fabrication of strain sensors that involve two distinct type: textile based- and inkjet printed- strain sensors

Textile based strain sensors open new frontiers for wearable systems by integrating sensors directly into garments. Fibers that compose fabric can become strain sensitive when made out of strain sensing materials or yarns can have different topologies by interlacing sensing fibers with nonsensing fibers. Metal fibers such as stainless steel fibers can be knitted to fabricate a piezoresistive textile [58], as shown in figure 1.14. When stretched in the wale direction, a variation in the resistance of the knitted sensor is observed due to the length variation. Other mechanisms that enable

strain sensing entail inserting sensing fibers into nonconductive knits. Such is the case for a carbon knitted piezoresistive sensor and a knitted polyacrylonite based sensor [59].

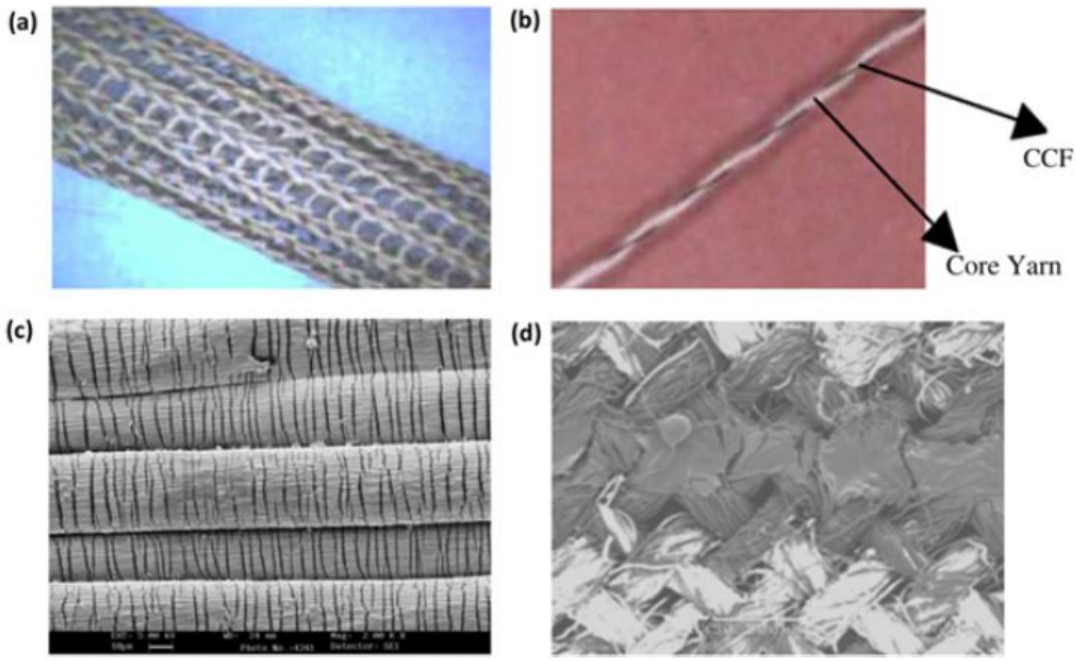

Figure 1.14: Strain fabric sensors. (s) Stainless steel knitted fabric sensors. (b)Yarn sensors composed of a single wrapping of carbon-coated fiber (CCF) with elastic fibers and polyester fibers. (c) SEM micrograph of polypyrrole Lycra fibers at 6% strain. (d) PEDOT-printed sensor on woven cotton fabric.

Applying a coating with inkjet printing with strain sensing materials or conductive inks provides low cost, efficient and rapid prototyping solution for implementation of strain sensors in wearable devices.

In term of applications, wearable strain textile sensors are mainly used for sensing and monitoring physiological signals, human activity and body parameters like heart rate, respiration and pressure blood. This is possible because the textile is in contact with the skin over a large body area. This means that the registration can take place at several locations on the body and strain textile sensors are becoming an integral part of today's wearable systems. An example of feasibility is a flexible strain sensing fabric fabricated by coating and subsequently reducing graphene oxide (r-GO) on the surface of nylon/PU (poliurethane) fabric [60]. The investigation into electromechanical performance of fabrics showed that the sensor have great sensitivity, fast response, low drift and high stability. Furthermore, the flexible

strain sensing fabrics are able to monitor the human motions in real time, including bending of finger and the flexion and rotation of wrist (figure 1.15).

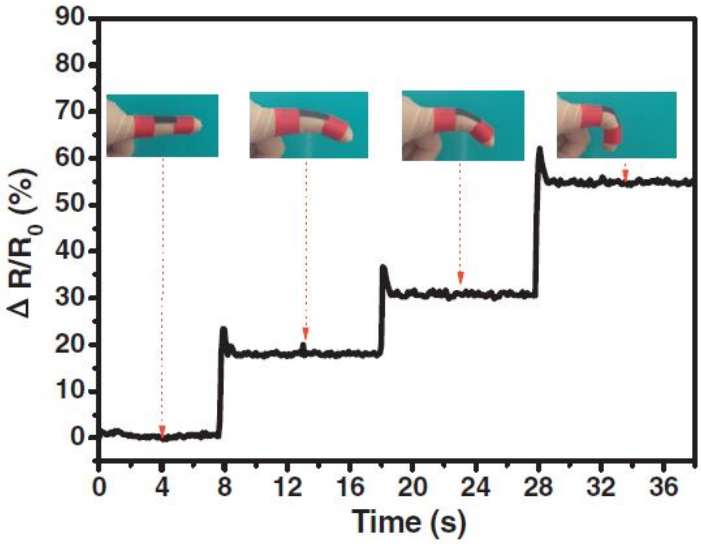

Figure 1.15: Monitoring of the finger bending motions using FSSF [60].

The realization of strain or pressure sensors require well knowledges on the electrical and mechanical properties of materials used. The realization, characterization and calibration procedures are the main steps to develop high efficient sensors. To understand the different behaviors and the electrical responses correlated with the applied load(tensile or compression) one need to separate the different contributions that come from piezoelectric or purely geometric features. The following chapters show materials, samples, instruments and methods used for study these sensors.

Chapter 2

Polymers

2.1 Introduction to polymers physics

Polymer science was born in the great industrial laboratories of the world to develop new kinds of plastics, rubber, adhesives, fibers, and coatings. The first polymers used were natural products, especially cotton, starch, proteins, and wool. Perhaps because of its origins, polymer science tends to be more interdisciplinary than most sciences, combining chemistry, chemical engineering and physics.

Organic materials are, by definition, compounds of Carbon. The main ability of this atom is to build complex molecules and macromolecules. The synthesis versatility can lead to infinite possibilities to modify chemical structures allowing change in electrical, mechanical and optical materials properties. The studies of structure-proprieties relationship is fundamental to synthesized material that meet desired requirement. Organic materials can be distinguished in two categories: molecules and polymers.

A polymer is a chemical compound or mixture of compounds formed by polymerization and consisting essentially of repeating structural units. The identical bulding blocks are called monomers[61]. The simplest polymers are chain-like molecules of the type

$$\underset{\textit{monomers}}{\mathbf{nA}} \quad \Rightarrow \quad \underset{\textit{polymer}}{\mathbf{[—A—A—A—A—\ldots]}_n}$$

where A is a small group of covalently bonded atoms and the groups are covalently linked. When the repeat unit is a single monomer the result is called homopolymer, but more often the monomers are two different unit and the result is called copolymer. There are four different categories of copolymer depending on the way to combine the based unit (figure 2.1):

- **Alternatic copolymer:** regularly alternating monomers $[ABAB...]_n$:
- **Statistical copolymer:** monomer arranged according to a known statistical rule or random;
- **Block polymer:** have two or more homopolymer subunits linked by covalent bonds;
- **Graft copolymer:** side chains whit a different composition than the main chain.

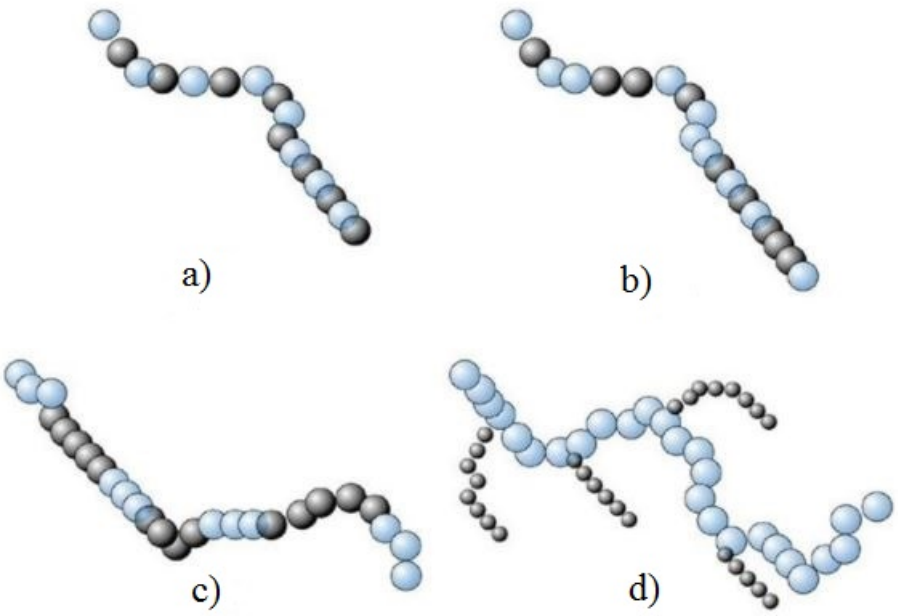

Figure 2.1: Four types of copolymers: a) alternating monomers, b) random monomers, c) block copolymers and d) grafted copolymers. Circle of different colors or sizes represent different monomers.

2.1.1 Physical properties

The subject of physical polymer science describes the interrelationships among polymer structure, morphology, physical and mechanical behavior. Physical properties of polymers include molecular weight, molar volume, density, degree of polymerization, and crystallinity of material. They are governed by the intermolecular forces (forces attracting one molecule to its neighbours): van der Waals attractions or hydrogen bonds. These two types of bonds greatly differ in energy and length.

The orientation of the molecules that compose the polymers is another crucial and complex aspect. The polymeric conformation in the solid state depends not only

to its chemical structure but also on its chain length (more precisely on the molecular weight) and the degree of crystallinity. In the case of polymers, that are a mixture of many species with different degrees of polymerization, is better to talk about the molecular weight distribution, that describes the relationship between the number of polymer molecules (N_i) and the molecular weight (M_i). Different average values can be defined to describe the distribution: number average molecular weight or M_n define as:

$$M_n = \frac{\sum M_i N_i}{\sum N_i} \tag{2.1}$$

and weight average molecular weight:

$$M_w = \frac{\sum {M_i}^2 N_i}{\sum M_i N_i} \tag{2.2}$$

The physical properties (such as transition temperature, viscosity, etc.) and mechanical properties (such as strength, stiffness, and toughness) depend on the molecular weight of polymer. The lower the molecular weight, the lower the transition temperature, the viscosity, and the mechanical performance. Due to increased entanglement of chains with increased molecular weight, the polymer gets higher viscosity in molten state, which makes the processing of polymer difficult.

The ratio of the weight-average molecular weights to the number-average molecular weights is called polydispersity index (PDI), which measures the polydispersity (namely the heterogeneity of sizes, shape and mass of molecules in the mixture) of the polymer:

$$PDI = \frac{M_w}{M_n} \tag{2.3}$$

Polymers are often described as being either "crystalline" or "amorphous" since it is actually more accurate to describe plastics by their "degree of crystallinity":

- **Cristallinity polymers:** exhibit areas of highly organized and tightly packed molecules. These polymers are rigid and have high melting point, but their impact resistance is low. Examples are polyethylene, and PET polyester.
- **Amorphous polymers:** have no patterned order between the molecules, the chain are in a irregular manner and can be likened to a bowl of wet spaghetti. However, these polymers are soft and have lower melting point. Examples are polystyrene and poly(methyl methacrylate);

A cristallinity polymer cannot be 100% crystalline and most polymers are considered semi-crystalline materials with a maximum of 80% crystallinity.

Furthermore, the thermal properties of polymers is very important to understand their behavior. There is a temperature at which the materials experience a second-order phase transition and is called the glass transition temperature T_g (it is the temperature at which the glassy state makes a transition to rubbery state). In the amorphous region of the polymer, at lower temperature than T_g, the molecules of the polymer are in frozen state, where the molecules can vibrate slightly but are not able to move significantly. This state is referred as the glassy state where the polymer is brittle, hard and rigid. When the polymer is heated, the polymer chains are able to wiggle around each other, and the polymer becomes soft and flexible. This state is called the rubbery state. The glass transition occurs only in the amorphous region, and the crystalline region remains unaffected during the glass transition in the semi-crystalline polymer.

2.1.2 Classification of polymers

There are many possible classifications of polymers according to their:

- **Origin**
  - *natural polymers*: are isolated from natural materials, e.g., cotton, silk, wool and rubber;
  - *synthetic polymers*: are synthesized from low molecular weight compounds and the majority of these are organic.
- **structure:**
  - *linear*: monomers are joined with each other and formed long and straight chain. These polymers have high melting points and high density. Examples are polythene, polyvinyl chloride and high density polythene.
  - *branch chain polymers*: monomers are joined with each other and formed long and straight chain having some branches. These polymers have low melting point and low density.
  - *cross linked or network polymers*: monomers are formed from bi-functional and tri-functional monomers and contain strong covalent bonds between various linear polymer chains. These polymers are brittle in nature. Examples are bakelite and melamine.

The structural classification of polymers are show in figure 2.2.

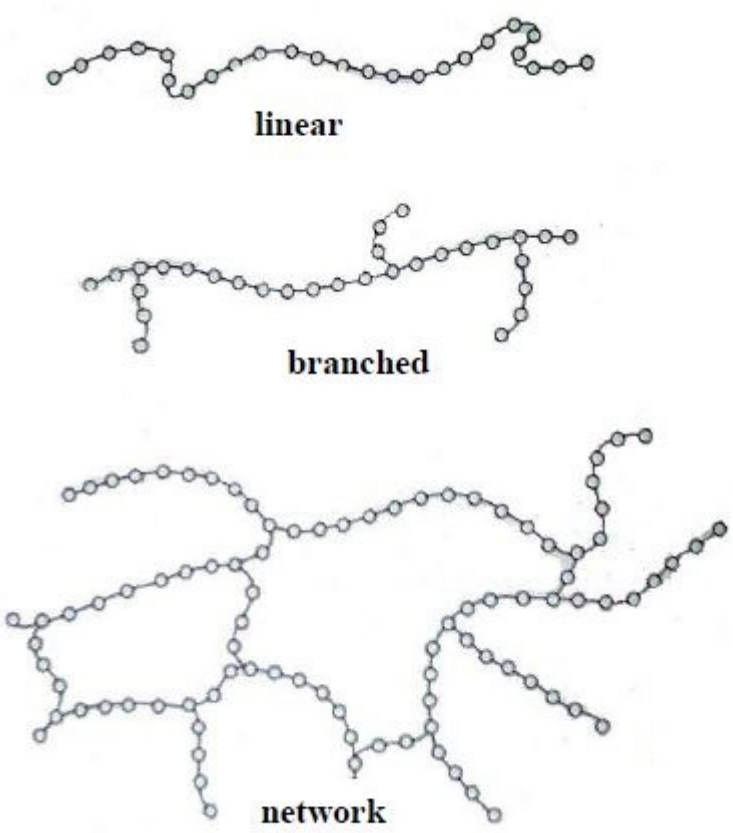

Figure 2.2: Polymers may be linear, branched or crosslinked.

- **mechanical properties:**
  - *elastomer polymers:* network polymers that are lightly cross-linked. Cause of these weak forces, the polymers can be easily stretched by applying small stress and regain their original shape when the stress is removed. They are isotropic in the undeformed state and they have the same properties in all directions. The changes of volume on deformation are very small and can be neglected.
  - *thermoplastics polymers:* linear or branched molecules held together by weak bonds. These polymers are softened when it heated and hardened when it cooled. They do not have any cross bond and they can easily convert into any shape by heating. Examples are polyetene, polystyrene, Polyvinyl chloride (PVC).
  - *thermosetting polymers*: consist of a three-dimensional network in which

the long-chain molecules are cross-linked together by small molecules via strong chemical bonds. They are normally rigid and they can not convert in other shape by heating. Examples are bakelit, melamine formaldehyde, and resin.

2.2 Conducting polymers

Usually the polymers show an insulating behavior and are used, for example, like dielectric in capacitors but, in 1977, Shirakawa, Heeger and MacDiarmid discovered a new class of polymers: conductive polymers. They found that films of polyacetylene (PAc) increase their conductivity tremendously when they are exposed to iodine vapor, from a basic value at the lower end of the semiconducting range up to values comparable to metals[62]. For this research they were awarded with the 2000 Nobel Prize in Chemistry. It is understandable that these unusual findings triggered intense activities in research and development.

One important polymer family used in this work is the conjugated polymers which shown electrical features. They are organic macromolecules that are characterized by a backbone chain of alternating double- and single-bonds that extended along all the macromolecule. Their overlapping p-orbitals create a system of delocalised π-electrons, which can result in interesting and useful optical and electronic properties.

The main proprieties of an organic semiconductor is the ability to transport charges obtained from the conjugated π molecular orbitals. To understand the physics of polymeric semiconductor is better to start from a simple molecular system. The aromatic molecule benzene (C_6H_6) is a prototypical planar conjugated molecule with an extended π electron system. The π electrons reside in the molecular orbital that are delocalized over the molecule forming a negatively charged π clouds, while in the core σ orbital the positive charged lead to a neutral molecule. As reported in figure 2.3, in comparison with the inorganic semiconductor it is possible to identify two band: the π bond energy is the HOMO (highest occupated molecular orbital) and correspond to the valence band, while the $\pi*$ bond is the LUMO (lowest unoccupated molecular orbital) and correspond to the conductive band. The energy different between this two levels is called energy gap, E_g.

This allows to understand the main features conjugated polymers. The carbon atoms typically involved in the formation of the organic polymer backbone form three contiguous sp^2 hybridized carbon centers, σ-bonds, with neighboring atoms and the remaining p orbitals — typically described as p_z orbitals — involved in the π system which is orthogonal to the other three σ-bonds[66]. If the carbon–carbon bonds were equally long, the remaining π electrons are in one half filled continuous

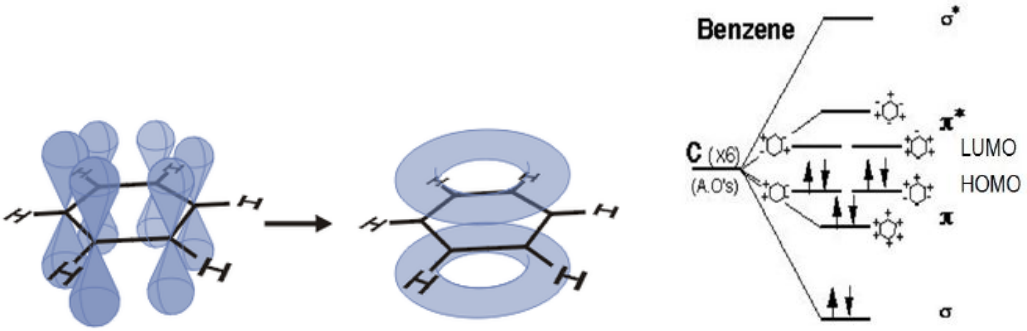

(a) (b)

Figure 2.3: Orbital distribution of benzene molecule.

band. Such a material would show metallic behavior but Peierls' theorem states that a one dimensional, equally spaced chain with one electron per ion is unstable [67]. To overcame this instability, a distortion of polymers chain reduce the symmetry of the system and the orbital levels are rearranged in a way that filled orbitals are lowered. In the case of PAc, a lattice distortion can leads to a repeat unit with two carbon atoms closer together and the next two carbon atoms further apart. For instance, the repeat unit can be described as $[—CH{=}CH—]_n$ instead of $[—CH—]_n$. This bond-alternating structure is typical for all conjugated polymers.

Intrinsically conductive polymers (ICPs) are polymers with extended π-conjugation along the molecular backbone, and their conductivity can be changed by several orders of magnitude from a semiconducting state to a metallic state by doping [63]. Usually p-doping is achieved by partial oxidation of the polymer by a chemical oxidant or an electrochemical method, and causes depopulation of the bonding π orbital HOMO with the formation of holes [64]. They can offer high electrical conductivity (from 10^{-8} to 10^{3} S/cm). The first example used to study the electrical conductivity in conjugated polymers is the polyacetilene (PAc show in figure 2.4), with molecular formula $[—CH]_n$.

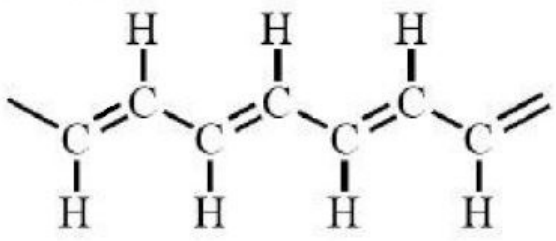

Figure 2.4: Chemical structure of polyacetilene[65].

2.2.1 Doping in conjugated polymers

A primary dopant for a conducting polymer is a substance, a relatively small quantity of which drastically changes the electronic, optical, magnetic and structural properties of the polymer and is accompanied by a large increase in conductivity. This can be brought about by a redox agent that either oxidizes (p doping) or reduces (n doping) the polymer chain. Conjugated polymers are composed by organic molecules and there are various approaches to introduce charges into these materials and to radically change their electronic properties.

As summarized in figure 2.5, reversible charge injection by doping can be accomplished in different manners [67]:

— *chemical doping by charge transfer:* it is obtained with a chemical reaction — oxidation or reduction. With this process a semiconducting material becomes conductive thanks to the creation of new electronic states. Both electron donating (n-type) and electron accepting (p-type) dopants, respectively reducing agents and oxidants, have been used to introduce charges into conjugated polymers and render them conductive. In practice, most organic conductors are doped oxidatively to give p-type materials.

— *electrochemical doping:* it attempts to obtain intermediate doping levels using an electrolytic solution (that is a substance that produces an electrically conducting solution when dissolved in a polar solvent, such as water) in which a thin film is deeped. The electrolytic solution contains free ions and with the application of an electric field the electrons could diffuse into the polymer structure. The doping level is determined by the voltage between the conducting polymer and the counter electrode (which is used to close the current circuit in the electrochemical cell); at electrochemical equilibrium the doping level is precisely defined by that voltage. Thus, doping at any level can be achieved by setting the electrochemical cell at a fixed applied voltage and simply waiting as long as necessary for the system to come to electrochemical equilibrium.

— *photo-doping:* the polymer is locally oxidized and (nearby) reduced by photoabsorption and charge separation (electron-hole pair creation and separation into free carriers).

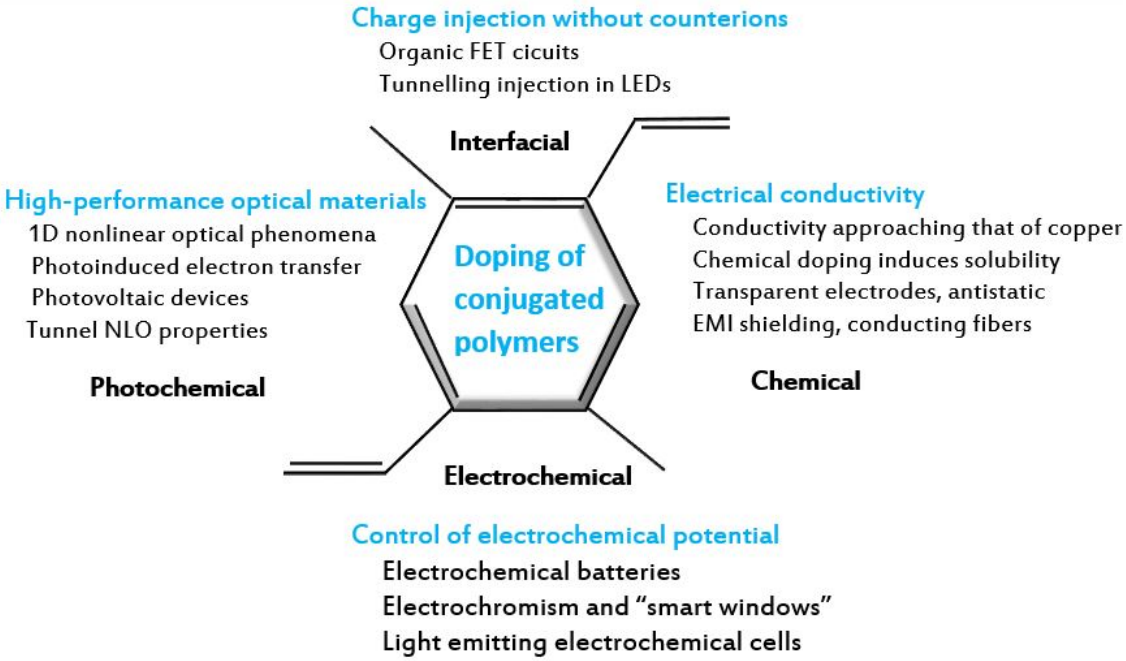

Figure 2.5: Doping mechanisms and related applications.

2.2.2 Transport properties

In general, the charge transport in a conductive polymer has to be distinguish in two contributes: the intra-chain and the inter-chain transport. The first one is defined by the conjugation length of a polymer segment. In a first approximation, it can be describe by a simple band transport model which is useful to define the energy gap and compare the energetic properties of different polymers. Unlike the inorganic semiconductor the electronic interactions between the molecular orbitals of adjacent lattice sites are weak and the resulting bands are narrow, with bandwidth below 500 meV [68]. Another difference is that in a polymer is difficult to define free charges due to the strong electron-phonon interaction. The polaron is a deformation of the latter induced by the presence of a charge in the polymer segment, and when it moves, it carries the charge associated with a structural deformation.

The second process, namely inter-chain transport, is mainly based on hopping between neighbours or multiple trapping and release mechanism. It is clear that the inter-chain transport is directly correlated with the morphology of the polymer solid state, and thus on M_w. Kline et al. [69] showed that, changing the M_w on the most popular semiconductor polymer P3HT (Poly (3-hexylthiophene-2,5-diyl)), the charge carrier mobility may vary by several orders of magnitude. Low values of M_w form highly ordered structures associated to poor connectivity between

well-defined, highly crystalline grains; however, if these crystalline zones are not electrically connected between each other, there is no charge transport. On the other hand, high values of M_w (long chains) provide electrical connectivity between more ordered regions and an efficient charge transport, with a drawback of highly disordered structures.

2.3 PEDOT: an overview

Polythiophene and its derivatives have been at the center of considerable scientific interest for their attractive and superior chemical and physical properties. Among the derivatives of polythiophene, poly(3,4-ethylenedioxythiophene) (PEDOT) is one of the most successful conducting polymers because of its low bandgap, excellent environmental stability, high electrical conductivity and transparency in thin oxidized films. PEDOT (figure 2.6) is a large molecule composed of many repeated monomer of 3,4-ethylenedioxythiophene (EDOT). Since it was first synthesized in 1989, many studies on PEDOT have been carried out. Numerous researches have been made on the syntheses of PEDOT by the electrochemical and chemical oxidative polymerizations and the more suitable process for mass production is the organic synthesis of EDOT [70].

Many applications have been reported for solid electrolytic capacitors [71], transparent electrodes in light emitting diodes [72, 73] and underlayers for the metallization of printed circuit boards.

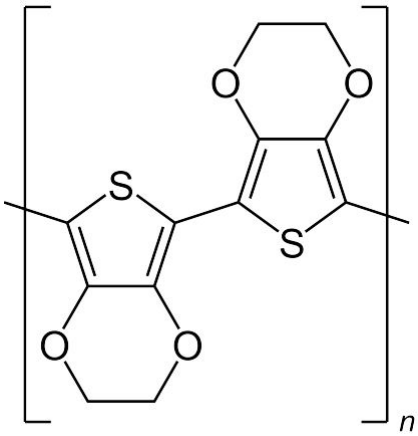

Figure 2.6: Chemical structure of poly(3,4-ethylenedioxythiophene) - PEDOT.

The big scientific interest on this highly conductive and stable polymer is documented by the continually growing number of academic publications mentioning PEDOT. It is a promising material for future applications because it exhibited some

characteristics as [74]:

Reversible doping: PEDOT can be repeatedly doped and undoped. It is almost transparent and light blue in the oxidized state and can be easily changed into opaque and dark blue appearance in the neutral state. Thus its color changes visibly when its doped state changes and may be suitable for optical applications, such as electrochromic displays[75];

Stability: PEDOT has excellent chemical and thermal stability. The studies show that degradation begins about 150°C and total decomposition at 390°C. Its stability is due to its ring geometric configuration and the effect of oxygen atoms in 3 and 4 positions, which stabilize the positive charge along the polymer chain.

High conductivity: PEDOT is a high conductivity polymer, with a low energy gap of about 1.5-1.6 eV which further reduces to 1 eV after the doping.

Electrochemical properties: compared with other conductive polymers, the electrochemical synthesized PEDOT has a very low reduction potential. This quality gives the PEDOT an exceptional stability even in the doped state.

2.3.1 PEDOT:PSS

Not mixed PEDOT is an insoluble polymer and therefore needs a counterions to become a polyelectrolytic complexes (PECs). PECs represent a special class of polymeric compounds consisting of oppositely charged polyions that can have either cationic or anionic charges. Due to their charges they are hydrophilic, normally water soluble and their solutions are electrically conductive. The first compound used to form a PEC with PEDOT was poly(styrenesulfonic acid), or PSS, which has remained the industrial standard since 1990 (figure 2.7).

The PSS is an host polyelectrolyte when is used like counterion for PEDOT, because it is always in excess. The molar ratio of thiophene groups to sulfonic acid groups in standard PEDOT:PSS dispersions is in the range of $1 : 1,9$ to $1 : 15,2$, which corresponds to a weight ratio range of 1 : 2.5 up to 1 : 20. Since only one charge is found for every three to four thiophene rings, the charge excess of PSS is between 6-fold and 46-fold. The average particle size of PEDOT:PSS dispersions is in the range of 10 nm to 1 µm and its distribution is typically non-Gaussian.

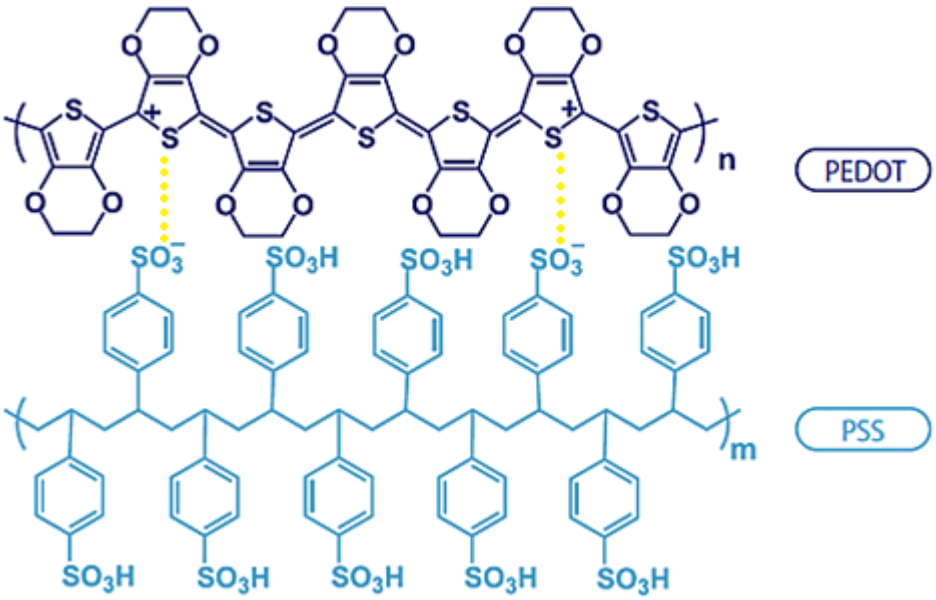

Figure 2.7: Chemical structure of PEDOT:PSS with the linking points highlighted.

Electrical properties

PEDOT:PSS is an intrinsically conducting polymer with metal-like properties and the charges transporting are caused by free charge carriers. The poly(styrenesulfonic acid) does not contributes to charge transport directly and acts only to keep the PEDOT in the dispersed state. An exhaustive theory describing the charge transport properties of strongly doped conjugated amorphous polymers is missing. Owing to its random ordering of charge transporting segments in these systems without having any translation symmetry, the quantum mechanical model of Bloch's eigenstates commonly used to explain electrical properties of crystalline semiconductors and metals are not applicable. Following the concept of charge transport in amorphous inorganic semiconductors, the conduction mechanism of conjugated polymers is commonly discussed in terms of charge hopping between adjacent sites. Explaining charge transport in molecularly doped polymers, the frequency of charge transport between adjacent sites depend on its relative energetic position, distance and the relative orientation [76].

The conductivity σ is defined by the product of elemental charge (e), charge carrier mobility (μ), and density of charge carriers (n). For hole- and electron-conducting materials, both charge carriers species contribute according to

$$\sigma = e(\mu_p n_p + \mu_n n_n).$$

In the case of PEDOT:PSS, only holes contribute to the charge transport. Injected free electrons will immediately recombine at oxidized PEDOT sites, hence the transport of electrons does therefore not contribute to the overall current.

The conductivity can be altered by various means: the modification of the ratio of PEDOT to PSS will have direct impact on the conductivity as it determines the density of charge transporting PEDOT sites. In the products usually used in scientific applications the ratio of PEDOT to PSS varies between 1:2.5 to 1:20 by weight of compounds and the conductivity changes. The conductivity σ is the inverse of resistivity ρ and the latter can be calculated by multiplying the sheet resistance R_s times the layer thickness, d, according to:

$$\rho = \sigma^{-1} = R_s \cdot d.$$

In case of two-point probe measures, special care has to be taken to distinguish between R_s and the contact resistance. Further, the conductivity of PEDOT:PSS as function of temperature have been studied and found that it increase with temperature. The explicit expression of temperature dependence of conductivity, $\sigma(T)$, is discussed using the model of variable range hopping (VRH) [77]:

$$\sigma(T) = \sigma_0 \exp\Big(-\Big(\frac{16a^3}{K_b N(E_f) T}\Big)^{\frac{1}{4}}\Big) \tag{2.4}$$

where σ_0 is the conductivity at high temperature, a is the distance from a site for the electron wave function to decay to $1/e$ of its value, often referred to as localization length and $N(E_f)$ is the density of states at the Fermi energy. The density of holes in PEDOT:PSS can simply be calculated using geometrical consideration, the knowledges of ratio of PEDOT to PSS, the solid films density and that the level of oxidatin per monomer is approximately 1 charge per 3 EDOT units. Then, its holes density can be estimated to be $n_p = 3 \cdot 10^{20}$ cm^{-3}. For highly conductive films a conductivity of 1000 S/cm has been obtained and the mobility is about $\mu_p = 20$ cm^2/Vs for the given conductivity and the estimated hole density (for silicon at room temperature the hole mobility is $\mu_p = 500$ cm^2/Vs).

Applications of PEDOT:PSS

The PEDOT:PSS, due to its properties, is used in a wide range of industrial printed electronics (thanks to the capabilities to be processed in high volume, low cost and large area) and commercial applications (figure 2.8), for instance:

- **Antistatic coatings**
  Coating with PEDOT produces surfaces with an antistatic, static dissipative,

or conductive finish with a precisely tunable sheet resistances (R_s) in the range of 10^4 – $10^10\,\Omega$/sq. With its excellent optical properties, high transmission, low haze and good durability it is a good choice to coat functional and protective films used in the LCD (liquid crystal display) industry [78].

- **Transparent Electrodes**

  Coating formulations have been optimized for individual substrates, such as PET, polycarbonate or glass for different thicknesses and surface resistivities. This, combined with the intrinsic flexible properties of organic material could permit the realization of a flexible AMOLED with an out-cell foldable touch panel based on PEDOT:PSS. In addition, transparent electrodes can be used in many applications, such as:

  – **OLED Displays and Lighting** Organic Light Emitting Diodes (OLEDs) have gained considerable momentum as a new technology for displays and lighting within the last decade. PEDOT:PSS can help to improve performance and processing of OLEDs with its function of hole-injection layer between the anode and the OLED layer stack.

  – **Organic Solar Cells**

    Organic Solar Cells (OSCs) are of growing scientific and technological interest. They have the potential to become an attractive alternative for low-cost power generation. OSCs consist of organic conductors and semiconductors applied by economic methods such as printing or coating. PEDOT:PSS can improves the processing and performance of OSCs. It can be used as an alternative to the transparent conductive oxide electrode such as ITO (indium tin oxide) and a hole transport layer facilitating the efficient extraction of charges generated in the active layer by light [79].

- **Polymer Capacitors**

  PEDOT:PSS conductive polymers are essential for low ESR (Equivalent Series Resistance) electrolytic capacitors. Because of its high conductivity and outstanding temperature stability it is widely used in the capacitor industry to manufacture polymer capacitors.

(a) Antistatic Coatings

(b) Transparent Electrodes

(c) Organic Solar Cells

(d) Printed Electronics

(e) Polymer Capacitors

Figure 2.8: Various applications based on PEDOT:PSS.

2.4 Additive to enhance conductivity

Unlike primary dopant, a secondary dopant is an apparently "inert" substance which, when applied to a primary-doped polymer, induces still further changes in the above properties including a further increase in conductivity[80]. The secondary dopant substances are widely refer as conductivity enhancement agests (CEA). PEDOT-PSS films after secondary doping with some organic inert solvents, sugars, polyols, ionic liquids, surfactants and salts (sorbitol[81, 82], NMP (1-methyl-2-pyrrolidinone), (poly)- ethylene glycol[83], dimethyl sulfoxide (DMSO)[84] and tetrahydrofuran) undergo a conductivity increase of 2-3 orders of magnitudes.

Charge hopping among the polymer chains is believed to be the dominant conduction mechanism in almost all conducting polymers. An increased interchain interaction should facilitate charge hopping among the conductive PEDOT chains. As

figure 2.9 shows, the solvent treatment significantly affects the temperature dependence of the conductivity. At room temperature the conductivity is $\sigma(295\ \mathrm{K}) = 0{,}4$, 46, 143 and 200 S/cm for the untreated, NMP (1-methyl-2-pyrrolidinone)-, DMSO- and EG-PEDOT:PSS films, respectively. When PEDOT:PSS with solvents receives a post-coating heat treatment, called annealing, an increase in electrical conductivity is obtained. The annealing process also has the effect that many of the conductivity enhancement agents are removed from the final film [81] and the reorganization of polymers chains leading a better connectivity between the conducting grains.

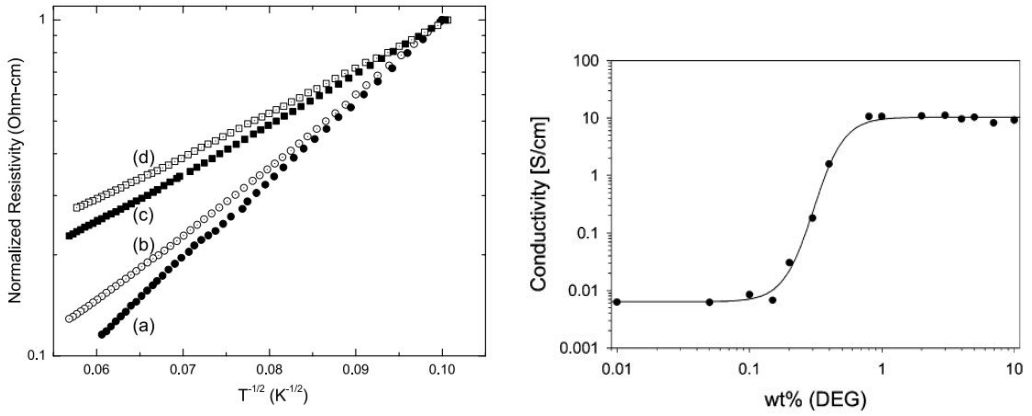

(a) (b)

Figure 2.9: **a)** Temperature dependence of the normalized resistance of PEDOT:PSS films treated with (a) untreated, (b) NMP, (c) DMSO, and (d) ethylene glycol (EG). The resistances are normalized to that at 100 K [85]; **b)** Plot of the conductivity of a films based on PEDOT:PSS versus the amount of diethylene glycol introduced to the water emulsion [87].

A morphological model of the PEDOT:PSS films before and after the addition of solvents is reported in figure 2.10. In the film without any solvent, the oblate ellipsoidal-shaped PEDOT nanocrystals, surrounded by PSS chains, are embedded in the PSS matrix with the PSS chain network largely aligned along the surface. The cores of PEDOT nanocrystal are composed of linear chain network of quionoid components and near the grain boundary regions are enclosed by randmoly oriented coil-like benziod components. When a contact is realized on the film, the higher number of PSS chains on the surface reduces the ohmic contact points to the top electrode which reduces the front surface carrier collection.

Addition of a solvent enhances the packing density of PEDOT and produces clustering with reduced PSS content at the surface. The defects generation is also suppresses at the interface because the PSS chain network is rearranged to form closely packed domains of PEDOT nanocrystal. The increase in the PEDOT nanocrystal

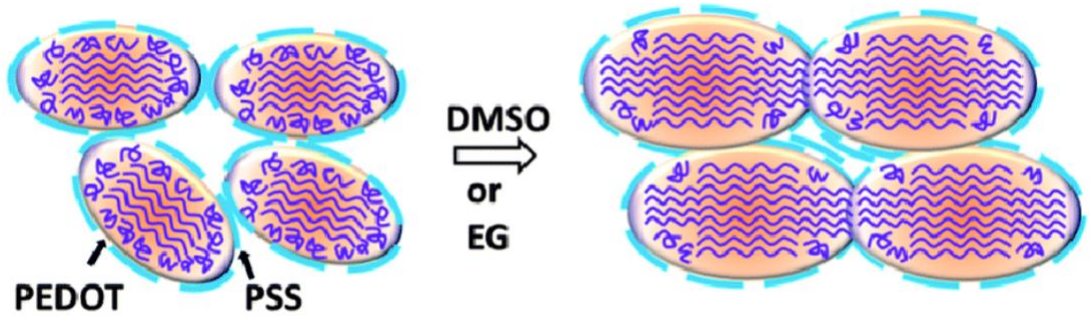

Figure 2.10: Schematic model of structural modification in PEDOT:PSS with the addition of co-solvents [86].

size upon addition of the solvent suggests an internal re-ordering inside the nanocrystals, which is likely mediated by hydrogen bond formation between the solvent and PSS. This solvent mediation stabilizes the PSS chains and realigns them along the PEDOT grain boundaries to form intermediate connection with PEDOT nanocrystals [86]. The solvent effects appear to saturate after the addition of a sufficient amount of solvent (i.e. upon reaching a certain wt%). Further addition of solvents does not contribute significantly to the internal structural re-ordering of the PEDOT:PSS possibly because of saturation of all the available bonding sites. A confermimation of this is reported by Crispin et al. [87] which found that the conductivity increase is not proportional to the additive concentration. As shown in figure 2.9 b), no effect is observed at concentrations below 0.2% diethylene glycol in the dispersion. For concentrations between 0.2% and 0.8% the doping effect becomes stronger and finally reaches a plateau for concentrations above 0.8%. Therefore, the conductivity increase is the combination of different factors such as: high solubility in water, high boiling point and a high dielectric constant that leads to a good secondary dopant for PEDOT:PSS .

A combination of all the aspects show above can give a conductivity greater than 900-1000 S/cm for the Clevios PH 1000 when DMSO or ethylene glycol are used as conductivity enhancement agent.

Chapter 3

Materials and methods

3.1 Fabric substrate

In this work will be studied pressure and strain sensors based on different woven or knitted fabric and technical textile. In this section are reported their properties and the samples fabrication methods.

3.1.1 Cotton: chemical-physical properties

Cotton has worldwide popularity for its variety of use. Cotton fibers is the most used fibers for producing various types of fabric and the cotton fabrics are comfortable to wear than other fibers product. The realization of sensors directly on it represent a novelty in the wearable electronics field and can lead to develop new wearable devices. Like all the textile fibers, cotton has its own physical and chemical properties which are require to know for better use this materials in the electronic world.

Chemical properties

Cotton is a linear cellulose polymer and consist of glucose ($C_6H_{12}O_6$) linked together to form the cellulose chain molecule. The structural formula of the cellulose chain molecule is shown in figure 3.1 with the repeating unit called cellobiose [88]. Each glucose molecule added to the repeating unit of the molecule chain is rotated 180°C. The number of the glucose monomers ($C_6H_10O_5$) in the cellulose chain is called the degree of the polymerization and in cotton it is about 5000[89].

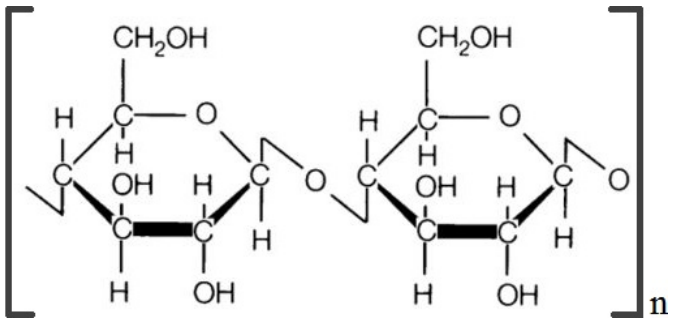

Figure 3.1: The structural formula of cellulose which forms cotton fibers [88].

Physical properties

Cotton in moderately strong fibers, it has a tenacity of 3 - 5 gm/den and it is due to the 70% crystallinity of its long fiber. It is one of the few fibers which gains strength when wet because the polymer chains in the amorphous regions temporary improve their alignment. This affect increase the number of hydrogen bonds, with an approximate 5% increase in fiber tenacity. The hygroscopic nature of cotton fiber is due to countless polar *OH* groups present in its polymers and water molecule can only enter the polymer system through its amorphous regions. Cotton does not stress easily and it has an elongation at break of 5 - 10 %. It has an excellent resistance to degradation by heat and can conduct heat energy. It begin to turn yellow color after several hours at 120°C and decomposition happens at 150°C. For the purpose of this work, the cotton are heated at a temperature low enough to avoid this effect. The woven cotton (0,32 ± 0,05 mm) used is a commercial fabric bought in local market and show in figure 3.2 a).

3.1.2 Elastic fabric

Others useful textile materials used in the world of wearable electronic show a greater elastic behavior. Stretchable fabric is usually a synthetic fabric which stretches under a tensile load and are either 2-way or 4-way stretch depending on the deformation directions. *2-way stretch fabrics* stretches in one direction and *4-way stretch fabrics* stretches in both directions, crosswise and lengthwise. Elasticity is the property of material to deform (usually to elongate) in proportion to the load applied and to recover its original shape when the load is release. This is the property of a material by virtue of which it tends to recover its original size and shape immediately after removal of the force causing deformation. The textile in figure 3.2 b), with a thickness of (0,45 ± 0,05) mm, will be use to realize a new kind of strain sensors and its mechanical properties will be show in chapter 5.

(a) (b)

Figure 3.2: a) The woven cotton used to realize wearable devices; b) elastic fabric used to realize the strain sensors.

3.1.3 High performance sports technical fabric

An interesting textile used in the world of sport is shown in figure 3.3 a) and is produced by an Italian company. For its specific application for cyclist suits, this fabric can be used as substrate for innovative and wearable pressure sensors. The fabric is composed with two layers one on top the other (20% elastan and 80% poliamide) with a density of 60 kg/m^3 and is a high performance sport technical fabric (*HP - STF*). The figure 3.3 b) report this specific textile with the addition of a special polyurethane padding for improved biker comfort during cycling.

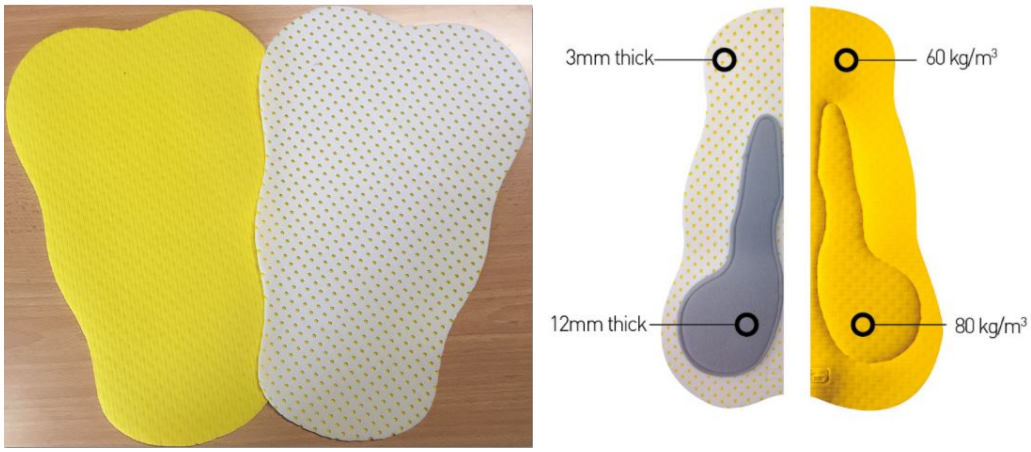

(a) (b)

Figure 3.3: a) Composite elastic material with two layers structure to facilitate the absorption and outside damp transport. The covered with holes weft increase breathability of material. b) The same fabric with the addition of special polyurethane padding.

3.2 Conductive polymers as active layer

The polymer used in this work have a wide areas of applications because they can be deposited as thin film on flexible and stretchable plastic substrate using suitable low cost fabrication process at room temperature.

PEDOT:PSS represent the active layer of the sensors realized in this work. PEDOT:PSS dispersions are commercially available from *Heraeus Deutschland GmbH & CO. KG, Leverkusen* under the trade name Clevios™ and the table 3.1 summarizes the properties of the more common products.

Table 3.1: Typical values for solids content, PEDOT:PSS ratio, viscosity, particle size and conductivity of commercial PEDOT:PSS dispersions.

Trade name	**% Solid content in water (w/w)**	**PEDOT:PSS ratio(w/w)**	**Viscosity at 20°C (mPas)**	**Average particle size (nm)**	**Conductivity in S/cm†**
Clevios P	1.3	1: 2.5	80	90	80
Clevios PH	1.3	1: 2.5	25	30	30
Clevios PH500	1.1	1: 2.5	25	30	500
Clevios PH750	1.1	1: 2.5	25	30	750
Clevios PH1000	1.1	1: 2.5	30	30	1000

† Values for conductivities were measured in the presence of 5% (w/w) dimethyl sulfoxide.

For the purposes of the present case the Clevios P and Clevios PH1000 are used to realize the conductive layer on the textile sensors. The former is in isopropanol dispersion and the latter is in aqueous dispersion. Both of them are odorless, dark blue color and with a density of about 1 g/cm^3 at 20°C. The products are sensitive to frost and should therefore not be stored at temperatures below than 5°C.

3.2.1 Chemical additives

The commercial suspension of conductive polymer (PEDOT:PSS), which functionalized the textiles, is usually mixed with an organic solvent, called secondary dopant, in order to increase its electrical conductivity. In this work, the ethylen glycol has this function. Other chemical compounds can be added to the suspension to endow with specific features the conductive polymer layer.

Ethylene glycol

Ethylene glycol (IUPAC name: ethane-1,2-diol) is an organic compound with molecular formula $C_2H_6O_2$, figure 3.4. It is produced from ethylene, via the intermediate ethylene oxide and a successive reaction with water. It is colorless, odorless,

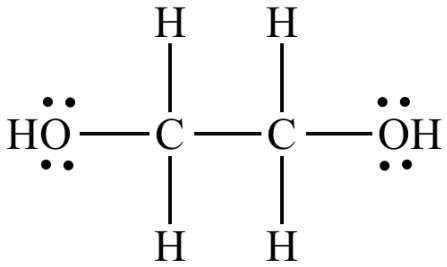

Figure 3.4: Structural formula of ethylen glycol.

viscous and moderately toxic. It has a density of 1,11 g/cm^3 with a melting and boiling points respectively of -12,9 °C and 197,3 °C. Ethylene glycol is the most important glycol commercially available and is used as an conductive enhancement agent in conductive polymers solution

Surfactants compounds

Surfactants are compounds that lower the surface tension (or interfacial tension) between two liquids or between a liquid and a solid. They are usually organic compounds that contain both hydrophobic groups and hydrophilic groups. Surfactants may act as detergents, wetting agents, emulsifiers, foaming agents, and dispersants.

Triton X Incorporating plasticizers such as Triton X enable the stretching of PEDOT:PSS. It is a surfactant and has a dramatic plasticizing effect on PEDOT:PSS film, like the decrease in tensile modulus and increase the ductility, which is manifested by an increase in the crack-onset strain[90].

DBSA The surfactant dodecyl benzene sulfonic acid (DBSA) is widely used as an additive (surfactant) to facilitate film processing from PEDOT:PSS suspensions. The DBSA can also enhance the electrical conductivity of PEDOT:PSS films, (inset of figure 3.5). The highest conductivity (500 S cm) is observed for a mixture containing 2 % DBSA [91]. However, a concentration of DBSA higher than ca. 0.5% induces a phase separation in the mixture, which makes processing by spin coating more difficult and results in a poor film quality. Therefore, for the future studies, the DBSA concentration will be kept very low and conductivity enhancing agents, such as EG, shall be used to achieve high film conductivity.

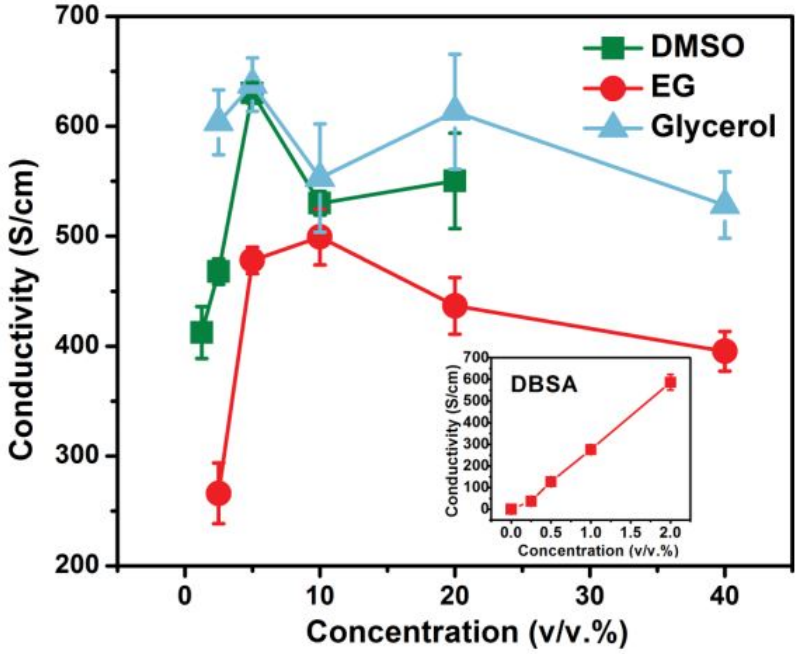

Figure 3.5: Electrical conductivity of PEDOT:PSS films processed from mixtures containing Clevios PH1000, 0.5% DBSA, and different % concentrations of conductivity enhancing agents (DMSO, EG, glycerol). The inset shows the electrical conductivity variation versus increasing DBSA concentrations in absence of conductivity enhancing agents [91].

3.3 Deposition methods

The active layer for the wearable pressure and strain sensors, and the thin film used for the electrical characterization of conductive polymer compounds, have been realized with different deposition and patterning techniques. The deposition methods used can be divided in: *coating* and *printing* methods. The difference between them lays on the fact that the former technique covers all the available surface, while the latter method transfers the ink (namely the conductive solution) only over a predefined pattern. The most important coating methods are drop casting, spin coating, dip coating and spray coating, while for printing are screen printing, pad printing, ink-jet printing and nozzle printing. The most suitable deposition technique would be chosen taking account of some factors: the shape, dimension and surface features (roughness and wettability) of the substrate; the solubility, polarity and nature of deposited material; the uniformity and thickness chosen for the final layer. Here is reported only a description of the methods used in this project.

3.3.1 Coating methods

Spin coating method

The spin coating method is used to fabricate thin films of PEDOT:PSS.

In the spin coating process, the substrate spins around an axis which is perpendicular to the coating area. The spinner is designed to coat thin films of liquids on the substrate surface. The thickness of layer is controlled by spin speed, spin time and viscosity of the solution. The spin coating process involves the four stages as shown in figure 3.6. These stages include deposition, spin up, spin off and evaporation.

In the deposition process, an excessive amount of fluid is deposited at the center of the substrate. In the spin up process, the substrate is accelerated to its final spin speed. In liquid, rotational forces are exerted on the upward direction causing formation of a wave front. This wave front flows to the substrate edge by the centrifugal force and hence results in a uniform layer. The spin off stage is the spin coating stage where the excess solvent is removed from the substrate surface. In spin coating process, evaporation is the complex process by which a portion of the excess solvent is absorbed into the atmosphere.

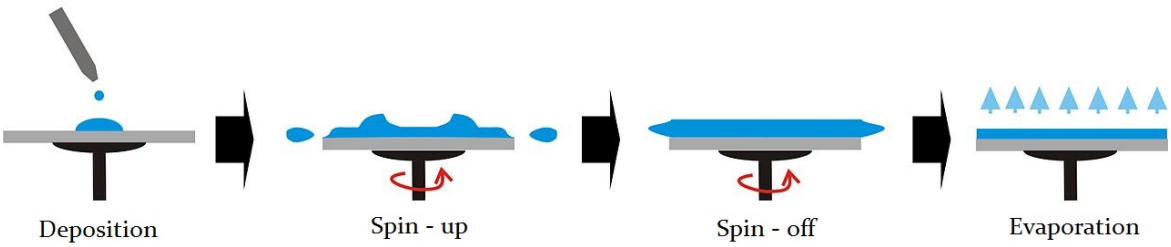

Figure 3.6: Process of Spin Coating.

The advantages of this technique are:

— thickness of the film can easily be changed by varying the spin speed or using different viscosity solution

— films of highly uniform thickness can be obtained

The disadvantages are:

— large substrates cannot be spun at a sufficiently high rate;

— greater waste of material;

— film dries fast providing less time for molecular ordering.

Drop casting method

The solution dropping on the target substrate and spontaneous solvent evaporates. If the solution used is conductive, the samples, after deposition, are dried in an oven to evaporate the solvents and improve the conductivity. This procedure is very simple and there is low waste of material. The disadvantage is that it is not easy to get a uniform and large area coating and thickness is hard to control. In the present work, this technique is very useful and is used to fabricate pressure sensing layer on a fabric substrate. The hydrophillic behavior of cotton fabric, and the solvent in the polymeric solution, allows the fabrication of conductive regions on it.

3.3.2 Printing method: screen printing

The screen printing technique, for the fabrication of wearable pressure and strain sensors, can be divided in two cases according to the frame used. This procedure is based on a stencil process; a silk screen frame or an open mask can be used to realize a conductive design on the fabric. The conductive paste based on PEDOT:PSS and ethylene glycol solution require to be thickened evaporating solvents in the solution. Usually, the solution mass is reduced by an half to spread better the paste on fabric substrate (figure 3.7).

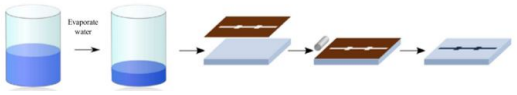

Figure 3.7: Formulation preparation and screen printing.

The first uses a frame reported in figure 3.8, where the viscous conductive polymers paste is squeezed by a moving blade. This technique is also called *serigraphy* and the steps to print with the silk screen frame are reported in figure 3.8 b).

The screen is formed by a monofilament polyester mesh which has a low-elongation, precision bore, and high stability. The solution passes through the interlocked mesh and the conductive pattern does not penetrate to the bottom side of the textile. The realization of strain sensors realized in this work uses this deposition method.

The other technique not require a frame, but uses only an open mask of plastic sheet with opportune geometry fabricated homemade (figure 3.9). This mask has parts cut from it in order to produce patterns on an underlying substrate. This

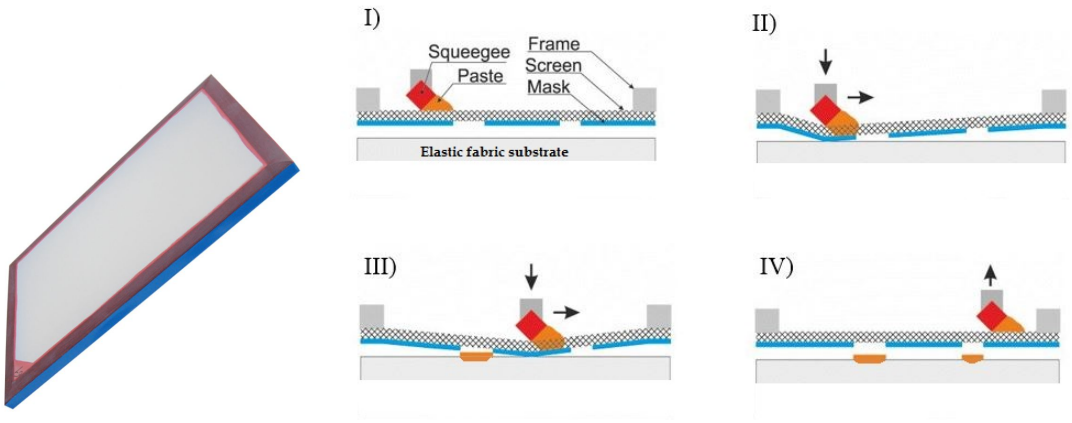

(a) (b)

Figure 3.8: a) Silk screen frame used to patterning the fabric substrate to realize strain sensors, b) sequence of steps in the serigraphy printing.

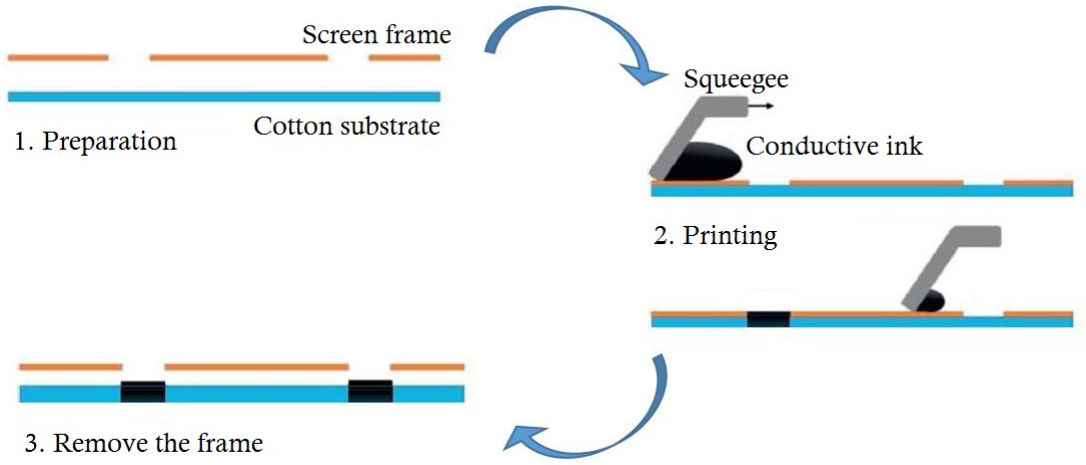

Figure 3.9: Screen printing steps; the cotton hydrophilicity and the absence of a mesh in the screen allow the conductive ink to penetrate from top to bottom.

allows the conductive ink to develop a thick pattern from paste-like material. By applying a viscous paste through the cut-out holes in the sheet, the paste can be deposited over the substrate surface, soaking the fabric from top to bottom. This method is simple but have a limited thickness resolution, a great waste of material and require only viscous solutions.

3.4 Morphological characterization

3.4.1 Atomic force microscopy

The atomic force microscopy (AFM) is a very-high-resolution type of scanning probe microscopy. In the AFM, the sample surface is scanned with a probe consisting of a microscopic tip situated at the end of a cantilever. The bending of the cantilever (contact mode) or damping of its oscillation amplitude (tapping mode) in response to the repulsive or attractive forces between the sample and the tip is monitored by an optical lever. The bending deflection, bending oscillation, and torsion of the cantilever is detected using a laser beam focused onto the end of the cantilever and monitored it reflection by a position sensitive detector (PSD) composed by four-quadrant photodetector. The sample is moved under the tip by the piezoelectric drive in a horizontal plane, while the vertical motion is controlled by a feedback mechanism (figure 3.10). The deflection of the cantilever measures the the force

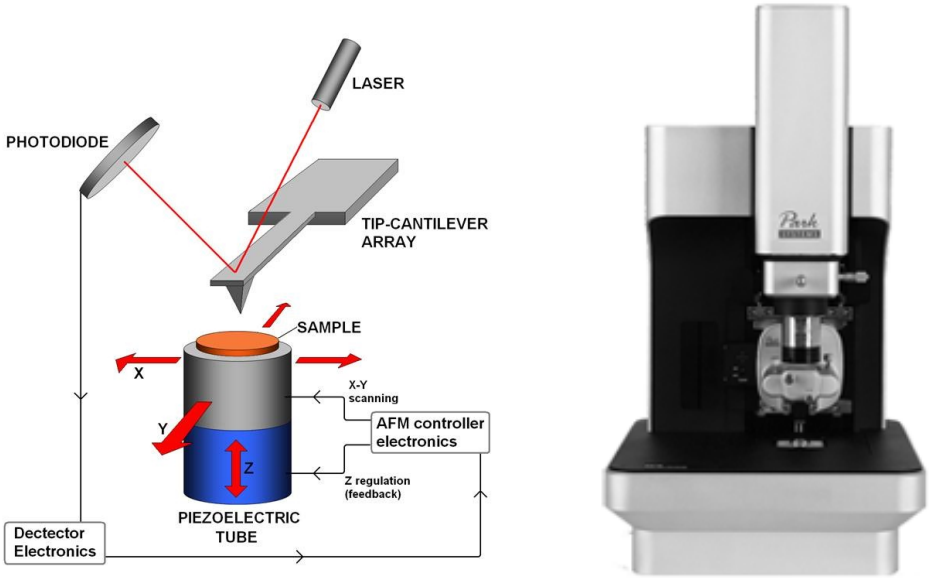

(a) (b)

Figure 3.10: a) Working principles of AFM, b) Atomic force microscopy Park System NX10 used in this work.

between the tip and the sample. Plotting the deflection of the cantilever versus its position on the sample, a topographic image of the sample is obtained. In a different manner, it is possible to plot the height position of the translation stage. This height is controlled by a feedback loop, which maintains a constant force between tip and sample. To create the height image, the variations of the z-position of the sample during scanning are plotted as a function of the x,y position of the tip. The

mechanical properties of cantilevers are characterized by the spring constant k_c and the resonance frequency ω_0.

A good cantilever should have a high sensitivity, that can be achieved with low spring constants. Hence, in order to have a large deflection at small force cantilevers should be long and thin.

In AFM applications on soft materials, such as polymers and biological samples, it was found that high tip-to-sample forces in the contact mode often led to mechanical deformation of the surface. For this reason, organic thin films are investigated with the no-contact mode or tapping mode. In tapping mode, tip-to-sample repulsive interactions reduced the oscillation amplitude from the freely oscillating probe (A_0). The oscillation amplitude is kept at the set-point value (A_{sp}) by adjusting the vertical (z-axis) position of the sample with the piezoelectric drive. Such operation modes, called constant force, are the most common in AFM and the cantilever tip hovers about 5-15 nm above the sample surface to detect the attractive van der Waals forces acting between the tip and the sample. In the thin films, the AFM is a useful tools in order to investigate the nanomorphologies of the active layer. Thus AFM images can give qualitative informations about the active layer morphology.

Besides a qualitative analysis, a rough quantitative analysis can be carried out. The main parameter that allows to compare images of different blend is the Means Square Roughness (RMS). In statistical terms, it is defined in the same ways as the standard deviation. It is calculated as a square root of the mean of the squares of deviations from the mean[93]:

$$RMS = \sum_{i=1}^{N} \Big[\frac{(z_i - \bar{z})^2}{N} \Big]^{1/2} \tag{3.1}$$

where z_i represents the surface height at each data point on the surface profile, z represents the average height of the surface profile, and N is the number of data points.

3.4.2 Scanning Electron Microscope

A scanning electron microscopy (SEM) has been used to study the morphology of the fabric fibers soaked with the conductive solutions of PEDOT:PSS.

SEM is a microscopy which has the aims to provide a topographic image of the objects, at a nanometric scale, rebuilding a signal product by the interaction of an electronic beam with the target. SEM used for the analisys in this work is called "thermionic emission", because the beam has reached by the overheating of a filament (generally tungsten) through the use of an electric current; the beam undergoes an

acceleration to the target by a potential difference (approximately 40 kV) and focused by a system of magnetic lenses. The model used is the *Cambridge Stereoscan 360*. An electronic microscopic permit to analyze three kinds of signal: Back Scattered Electrons (BSE), Secondary Electrons (SE) and X-ray. Figure 3.11 a) shows a section of interaction's volume between the electronic beam and the object to analyze, and the different zones of origin the signals.

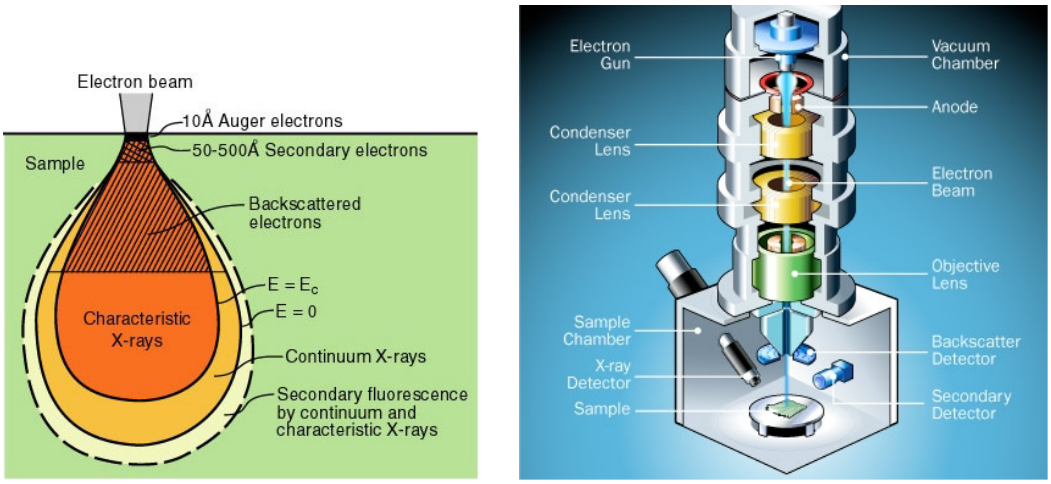

(a) (b)

Figure 3.11: a) Section of interaction's volume between the electronic beam and the sample, b) internal pattern of a SEM.

BSE are characterized by an energy range between 50 eV and the beam's energy. Is important point out that those electrons are not emitted by the target, but they are always the original one that has been scattered (elastic scatter) with an angle of almost 180 degrees. BSE signal is proportional to the atomic number of the object to analyze, this permit to map the compositional information of the target. The high energy of electrons allows a penetration around 1 µm, so it returns information about the internal structure loosing the external one.

SE are the product of the interaction between beam and valence's electrons of external atoms; those are called secondary because they are the product of the interaction. It is possible detect just the electrons that had been subjected recombination processes, so that came from by the external surface (impossible more than 5 nm). Their energy, consequently, is lower compared with BSE. SE give an external morphology, with an higher resolution of the BSE.

X-rays are product by the loss of energy of atoms after the ionization caused by the impact of primary beam's electrons with core atom's one. The ionized core electron create a hole that is fill by an electron of a more external shell; this transition

de-energizied the atom that emit energy in X-ray form. In figure 3.11 b) is shown the internal pattern of a SEM.

3.5 Electrical characterization

For the electrical characterization of thin films and conductive layers deposited over cotton fabric, the resistance is measured with the Van der Pauw method [92]. It is a technique commonly used to measure the resistivity of a planar material with an arbitrary contour, and the electrodes are placed on its perimeter. The Van der Pauw method employs a four-point probe placed in the four corners of a squared sample and the small electric contacts (approximately triangle-shaped) are realized with a silver conductive paste. Taking a measurement (3.12 a), a current flows along one edge of the sample (for instance, I_{12}) and the voltage across the opposite edge (in this case, V_{34}) is measured.

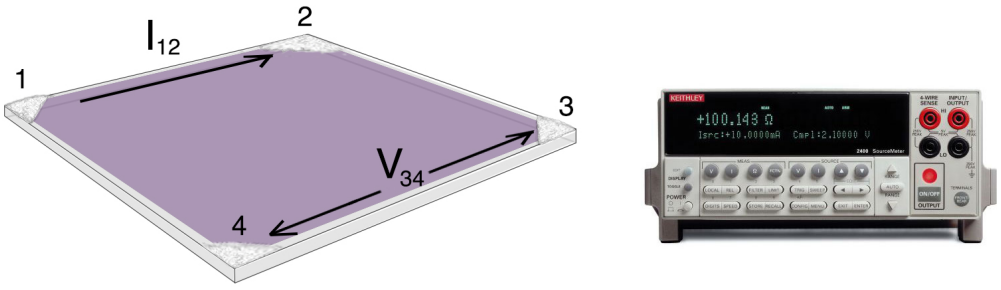

(a) (b)

Figure 3.12: a) Conductive contacts on a thin film to realize a Van der Pauw measurement; b) *keithley 2400 Source Meter* used to electrical characterization.

From these values, using Ohm's law, it is calculated a resistance as $R_{12,34} = \frac{V_{34}}{I_{12}}$. Then, exchange the contacts from I_{12} to I_{34} and V_{34} to V_{12} it has been obtained the reciprocal value $R_{34,12}$. To obtain a more precise value, these two values of resistance are averaged. The resistance along the other direction is overlooked at this level.

The current flow and potential difference on the surface layer are measured with the *Keithley 2400 Source Meter* 3.12 b). It is a source measurement unit (SMU) instrument designed specifically for test applications that demand tightly coupled sourcing and measurement. In operation, these instruments can act as a voltage source, a current source, a voltage meter, a current meter, and an ohmmeter. It provide four-quadrant operation. In the first and third quadrants it operates as a source, delivering power to a load. In the second and fourth quadrants it operates as a sink, dissipating power internally. Voltage, current, and resistance can be measured

during source or sink operation. *Keithley 2400* have two channels and can supply voltage from 100 nV to 200 V, current from 1 pA to 1 A and a maxim power of 20 W[94].

3.6 Mechanical characterization

3.6.1 Dynamic Mechanical Analysis

Dynamic Mechanical Analysis, otherwise known as DMA, is a technique where a small deformation is applied to a sample in a cyclic manner and measures the sample mechanical response to study composition and viscoelastic properties. The response to the deformation can be monitored as a function of temperature or time. It allows characterization of composition and viscoelastic properties.

DMA works by applying an oscillatory (sinusoidal) deformation to a sample of known geometry. The sample can be subjected by a controlled stress or a controlled strain. Where a stress is applied, the sample will deform a certain amount and it is measured. A force motor generates the sinusoidal stress wave and this is transmitted to the sample via a drive shaft. Applying a sinusoidal force, the stress in a dynamic experiment is a complex stress $\sigma*$ and can be separated into two components (with phase angle δ, the difference between deformation and response):

real part $\sigma' = \sigma^* \cos\delta$, is the degree to which materials behaves like an elastic solid;

imaginary part $\sigma'' = \sigma^* \sin\delta$, is the degree to which behaves like an ideal liquid.

In same way, the modulus can be expressed as an in-phase component, the elastic (storage) modulus E', and an out-phase component, the viscous (loss) modulus E'' (figure 3.13).

The storage modulus E' is the measure of the sample's elastic behavior and the ability of the material to store energy. The ratio of the loss to the storage modulus is the $tan\,\delta = E''/E'$ and it is often called damping. It is a measure of the dissipation energy of a material under cyclic load and it indicate how well a material can get rid of energy.

3.6.2 TA Instrument DMA Q800

For the analysis and tests on the textile materials the TA Instrument DMA Q800 has been employed. The Q800 utilizes non-contact, linear drive technology to provide precise control of stress, and air bearings for low friction support. Optical encoder technology measures strain and it provides unmatched sensitivity and resolution.

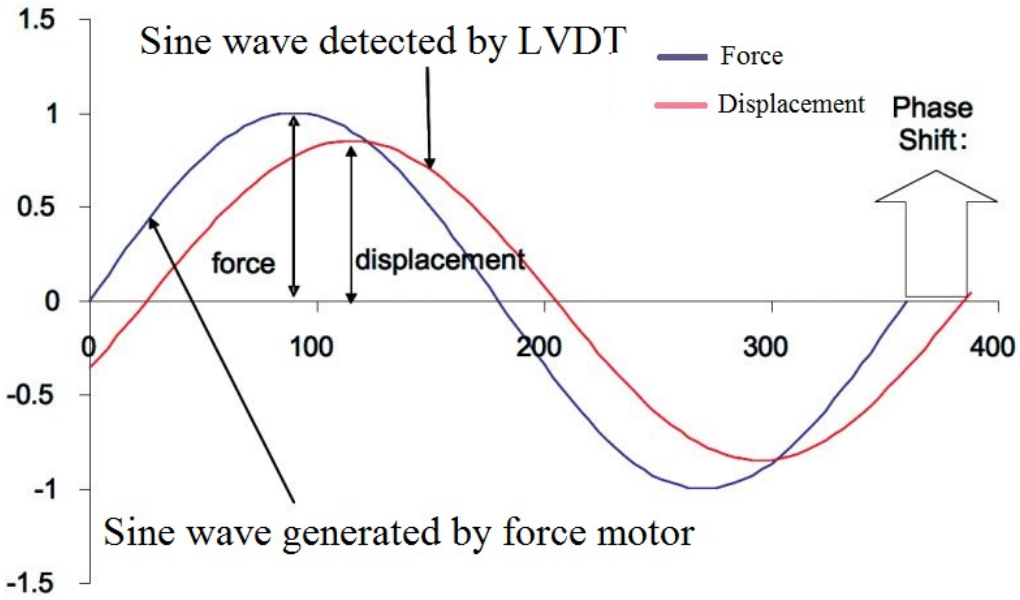

Figure 3.13: Schematically representation of the oscillatory (sinusoidal) force applied to a sample and the corresponding deformation response.

In figure 3.14 is reported the different parts that compose the *DMA Q800*. The motor is formed of high performance composites that ensure low compliance. It is thermostated to eliminate heat build-up even when using large oscillation amplitudes and high deformation forces. Sophisticated electronics enable the motor current to be rapidly adjusted in small increments. The motor can deliver reproducible forces from $0,1 \cdot 10^{-3}$ N to 18 N and the force can be changed rapidly, up to 200 Hz. This motor transmits force directly to a rectangular air bearing slide (that connects to the drive shaft and sample clamp), and pressurized air flows to the bearings forming a frictionless surface that permits the slide to "float." A high-resolution linear optical encoder is used to measure displacement and it is based on diffraction patterns of light through gratings (one moveable and one stationary). Due to the excellent 1 nanometer resolution of the optical encoder, very small amplitudes can be measured precisely.

The Q800 features a variety of sample clamps that provide for multiple modes of deformation. The clamps have an high stiffness, low mass, and each one is individually calibrated to ensure data accuracy. The high stiffness minimizes clamp compliance, and the low mass ensures rapid temperature equilibration. There are different modes of deformation that needed a specific clamp for each of them: dual/single cantilever, 3-Point bending, shear sandwich, compression and tension mode. In compression mode, the sample is placed on a fixed flat surface and an oscillating plate

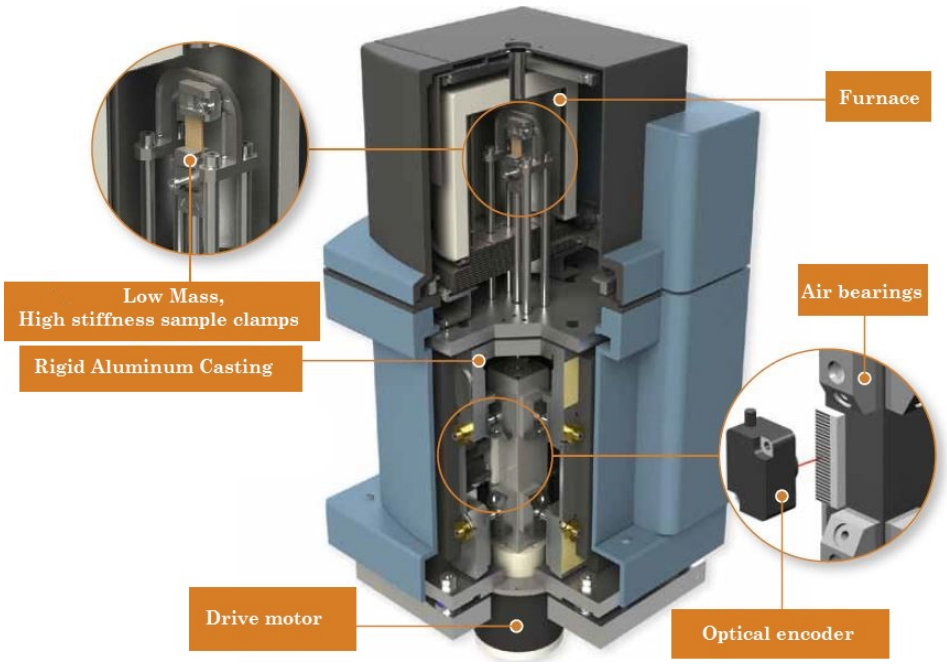

Figure 3.14: Illustration of the most important part of TA Instrument DMA Q800

applies force, while, in tension mode, the sample is placed in tension between a fixed and moveable clamp (figure 3.15). These two modes are used to study the response of pressure and strain sensors, and the mechanical properties of textiles.

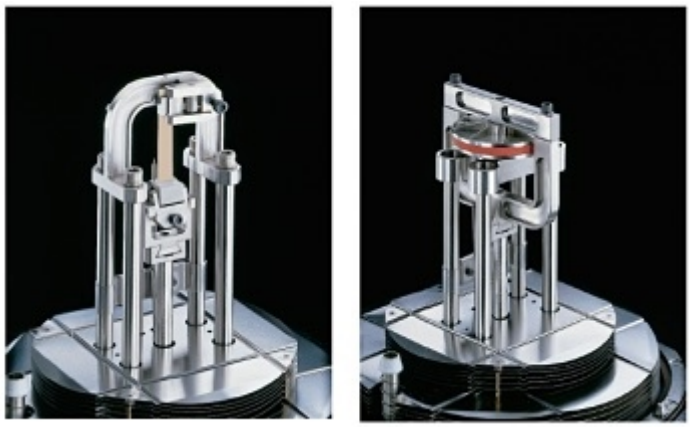

Figure 3.15: Tension and compression clamps for TA Instrument *DMA Q800*. The automatic mass, zero and compliance calibration for each clamp is possible with a proper software.

Chapter 4

Electrical characterization

PEDOT:PSS in the form of Clevios P and Clevios PH1000, is the main compound of the conductive solutions used to realize the sensitive parts on the textile sensors. Various formulation of PEDOT:PSS can be obtained adding the ethylene glycol as conductive enhancement agent. In this chapter, a comparison between electrical properties of the different formulations deposited over cotton fabric and the corresponding thin films on glass substrate is performed. It have been realized six different PEDOT:PSS formulations:

Clevios P	pristine LC MC HC	**Clevios PH1000**	Pristine HC

The words LC, MC and HC indicate low concentration, medium concentration and high concentration of ethylene glycol respectively.

4.1 PEDOT:PSS thin film

4.1.1 Fabrication

To discover and investigate the intrinsic properties of conductive material, thin films of various formulation have been fabricated. The first step for the realization of thin films is the washing of the glass substrate. They are put in a tank with acetone inside an ultrasonic probe for 15 min. Te same process are performed using isopropanol to clear the surface. Also the polymer dispersion is place in a ultrasonic

probe for 15 min before and after the addition of the additive (EG). The solution is deposited homogeneously onto the glass substrate using a syringe and the thin films are realized with **SCS 6800** Spin Coater Series with a ramp of one second, spinning speed of 1500 rmp and a duell time of 20 seconds. Two drops of DBSA surfactant is added to the conductive solution to improve adhesion with the glass substrate and achieve homogeneous thin films (figure 4.1).

(a)

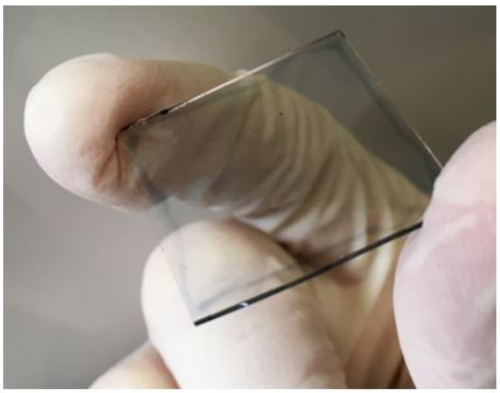

(b)

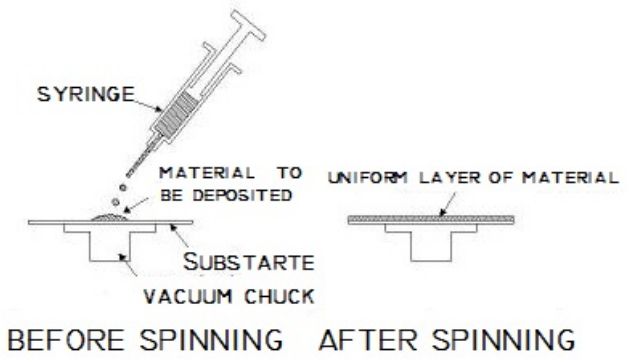

(c)

Figure 4.1: a) Spin coater **SCS 6800**; b) thin film of Clevios P; c) steps of spin coating procedure to realize thin film.

4.1.2 Morphology characterization

The atomic force microscopy is used to study the morphology of the thin film surfaces, compute their thickness and calculate the RMS, which gives information about surface roughness. Table 4.1 shows these values and figure 4.2 reports the AFM images of Clevios P, Clevios P + HC, Clevios PH1000 and CLevios PH1000 + HC.

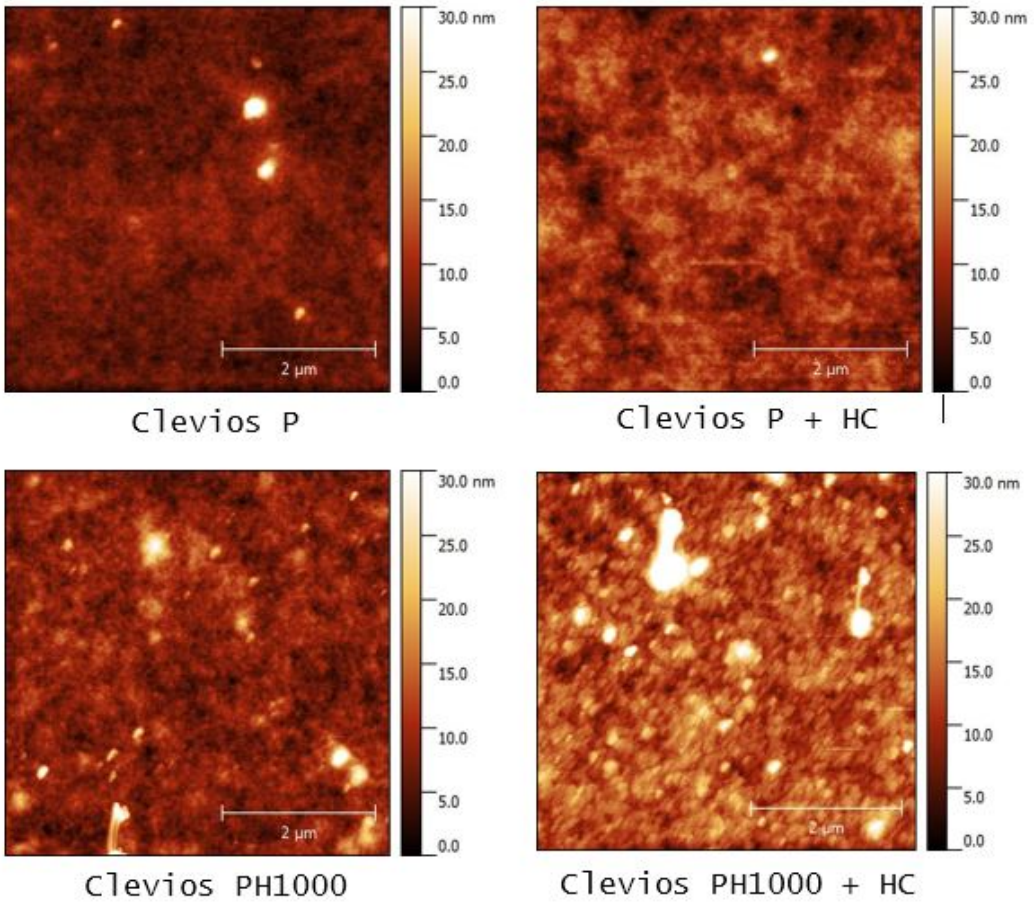

(a)

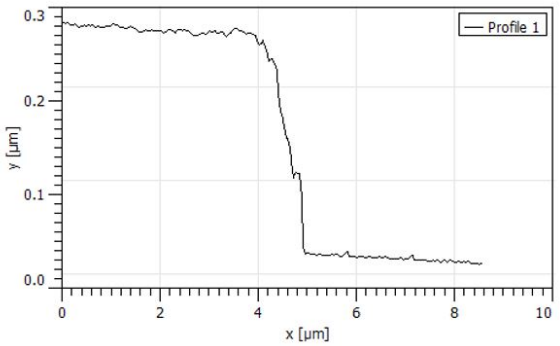

(b)

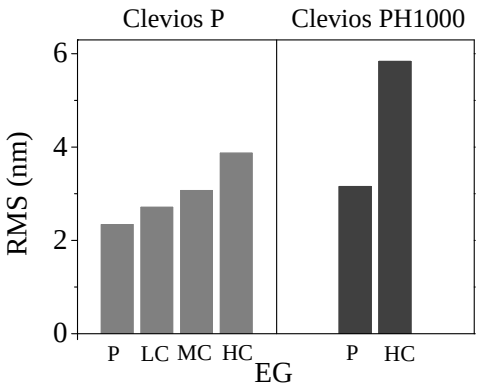

(c)

Figure 4.2: a) AFM photographs realized with Park System NX10, b) typical graph to calculate the sample thickness; c) RMS values.

Formulation		**t** (nm)	**RMS** (nm)
Clevios P	pristine	125	2,34
	LC	150	3,81
	MC	100	3,07
	HC	180	3.87
Clevios PH1000	Pristine	250	3,15
	HC	170	5,83

Table 4.1: Thickness and roughness mean square for the six thin film samples.

4.1.3 Resistance: Van der Pauw method

The electrical conductivity properties of the thin films depend on the chemical and physical properties of the solution, the homogeneity of the deposited layer structure and geometry (e.g.,thickness, edge definition, surface morphology, etc.) and the interfacial properties between the different materials. Electrical conductivity measurements of the thin films are performed based on the Van der Pauw technique. Square specimens are used and four very small ohmic contacts were placed in its corners, and subsequently the resistance are measured, namely the thin film resistance (R_{Tf}). The resistance measurements of thin films deposited on glass substrate has been carried out for all formulations of PEDOT:PSS to allow electrical characterization. These results will be used to compare the behavior of PEDOT:PSS when it is deposited on a textile substrate. Therefore, for each of the six thin film samples, two resistances have been calculated performing a current-voltage characteristic with the *Keithley 2400 Source Meter* in 4-wire sensing mode. The instrument is controlled by a LabView program, specifically developed for this purpose. This is a measure of the bulk resistance and the four electrodes on the corner remove the contact resistances.

4.1.4 Results

The results for resistance measurements for the different conductive thin films are summarized in table 4.2 and shown in figure 4.3. In 4-wire sensing mode, the suitable current range is selected. When the voltage reaches values greater than ~ 5 V the linear trend turn into an S-shaped current–voltage characteristics, typical for some organic materials [95].

As expected, the increase of additive improve the conductivity and a decrease in the resistance is observed. These results represents a starting point for electrical characterization of the conductive solutions and they are useful to compare the behaviors of conductive layers when they are deposited on cotton fabric substrate.

Formulation		R_{Tf}(kΩ)	G(mS)
Clevios P	pristine	160 ± 10	$(6{,}3 \pm 0{,}5)\cdot 10^{-3}$
	LC	23 ± 2	0,040 ± 0,004
	MC	0,30 ± 0,03	3,3 ± 0,3
	HC	0,19 ± 0,01	5,3 ± 0,3
Clevios PH1000	Pristine	5,0 ± 0,2	0,20 ± 0,01
	HC	0,025 ± 0,001	40 ± 2

Table 4.2: Electrical properties of thin films with various PEDOT:PSS solution formulation.

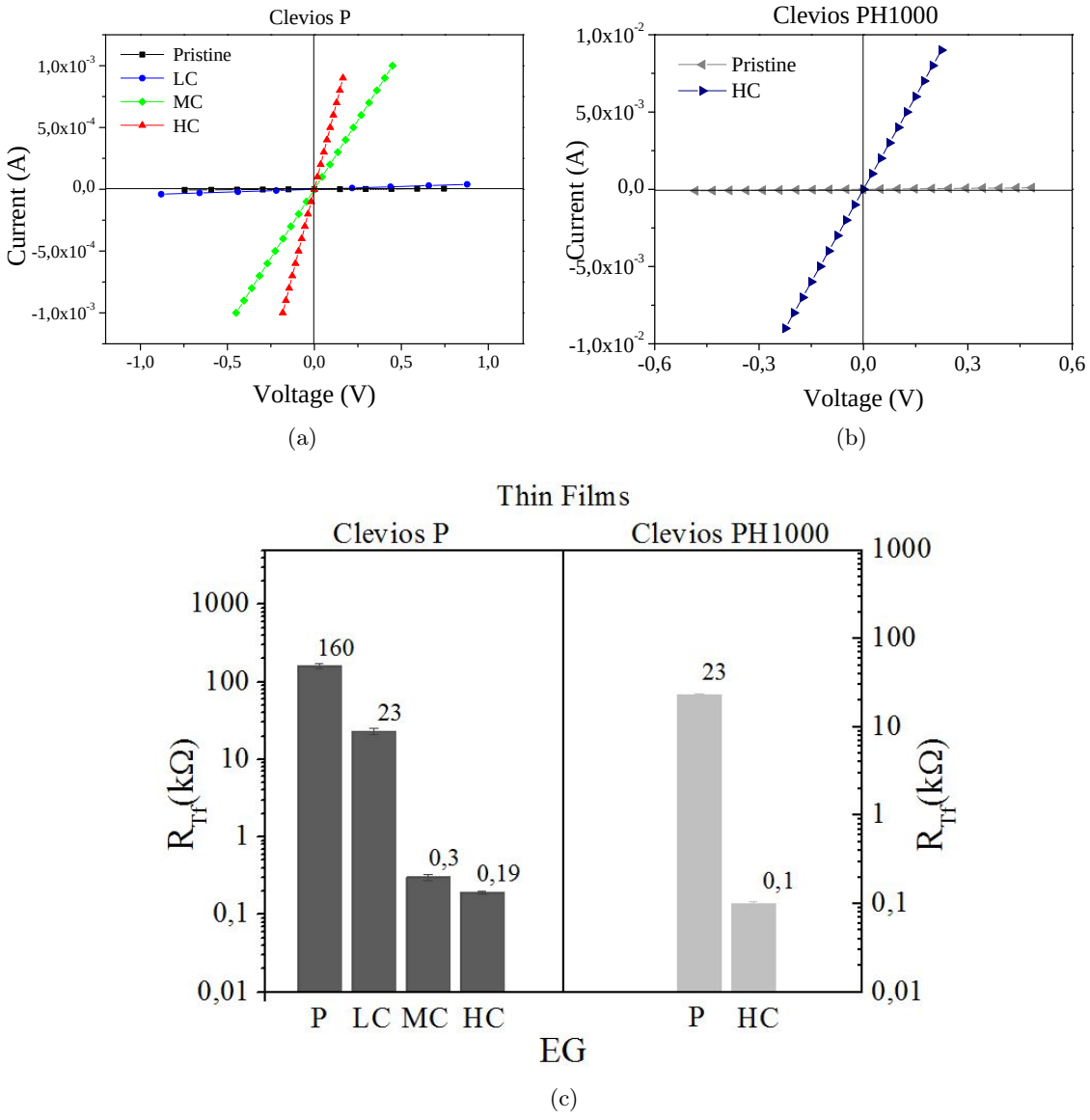

(a) (b) (c)

Figure 4.3: Current-voltage characteristics of Clevios P formulation (a) and Clevios PH1000 formulation (b); c) the resistance of the different thin films.

4.2 PEDOT:PSS coated cotton fabric

The pressure sensors developed in this thesis is fabricated on cotton fabric or a HP-STF as substrate. Before studies their responses, it is important to know the electrical features such as In-plane resistance and vertical resistance. In this section will be investigate the features of the conductive solution when it is deposited onto cotton fabric. Those two characterization use circular pixel of conductive ink deposited by drop casting method on cotton. The six different PEDOT:PSS formulations are prepared using Clevios P, Clevios PH 1000 and ethylene glycol as described before. After 15 min in the ultrasonic probe, a solution's drop of 5 µL is deposited on the cotton fabric with the Ripette®pro pipette. Thanks to the hydrophilic property of cotton, the drop casting method is the most appropriate mode to create conductive pixels. The cotton fabric samples dry in a oven for 15 min at 70 °C. For each formulations, four conductive pixels are realized to allow statistical analysis.

4.2.1 Morphological properties

The morphology of cotton fabric treated with the different formulations of PEDOT:PSS can be investigated with a scanning electron microscopy. The conductive solutions of Clevios P and Clevios PH 1000 with the addition of ethylene glycol are deposited over cotton fabric by drop casting. Figure 4.4 shows the difference between a treated and an untreated cotton fabric.

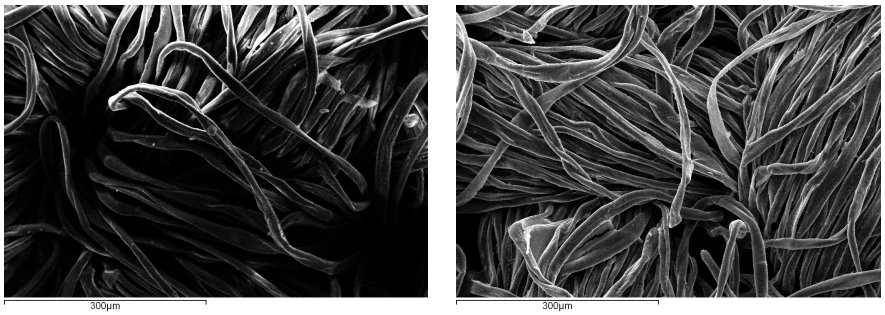

(a) (b)

Figure 4.4: SEM images of an (a) untreated and (b) coated PEDOT:PSS coated cotton fabric.

With this deposition method all fibers that compose the textile are interested and uniformly coated. The pristine solutions (namely those without the conductive enhancement agent) have the same PEDOT:PSS ratio but are dispersed in different solvents. The Clevios P is in isopropanol while the Clevios PH1000 is in water. This difference causes a different deposition on the cotton due to its hydrophilic

behavior(figure 4.5).

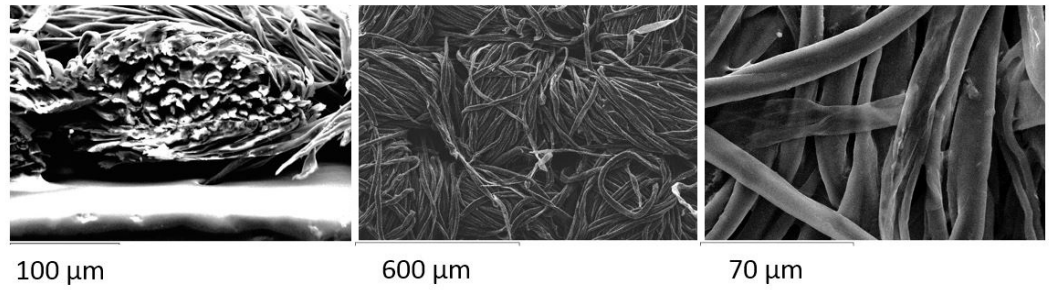

(a) Clevios P

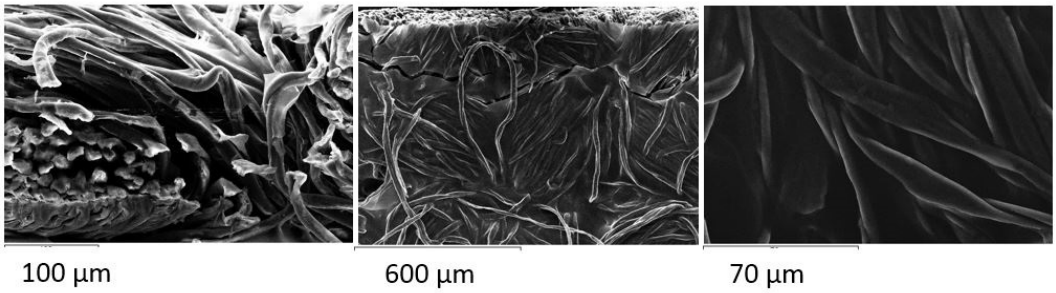

(b) Clevios PH1000

Figure 4.5: Cross section, top view and zoom in view of a cotton fabric coated with (a) Clevios P and (b) Clevios PH1000.

Figure 4.6 reports some SEM imagines of treated cotton fabric with high concentration of additive. The ethylene glycol allows an homogeneous coating along the vertical direction of fabric justifying its use as pressure sensor .

The images show that the Clevios PH1000 forms a compact layer connecting together the various cotton fibers (see cross section images). Conversely, the images of Clevios P show that the PEDOT:PSS is uniformly deposited on the fiber surface, however leaving it separate. This can be justified by the high cotton hydrophilicity: the formulation dispersed in water is completely absorbed by the cotton, while the one in isopropanol is deposited only on the surface.

4.2.2 In-plane resistance

The Van der Pauw method has been used to measure the conductive pixel In-plane resistance on cotton fabric. The silver conductive paste and copper wires are used to realize the electric contact on the pixel. The four contacts on each pixel allows an 4-wire sensing mode with the *Keithley 2400 Source Meter*. For each pixel, two resistance measurements have been done inverting the electrodes and averaging the results (figure 4.7). Typically, these two values do not differ more than 5%. Four

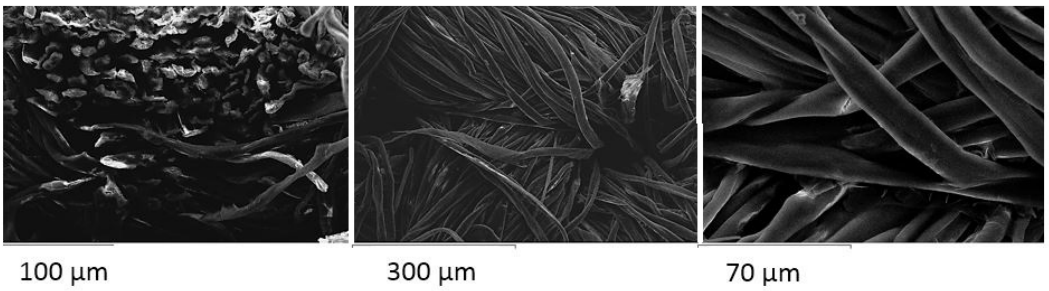

(a) Clevios P + HC

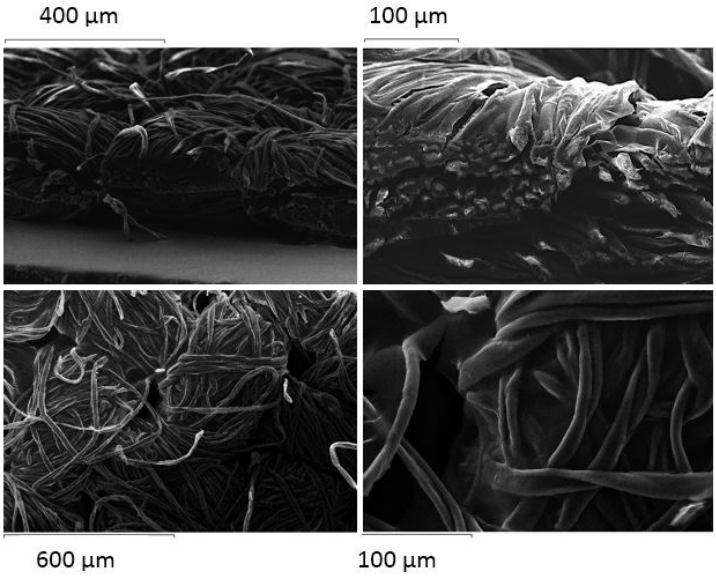

(b) Clevios PH1000 + HC

Figure 4.6: Cross section, top view and zoom in view of a cotton fabric coated with (a) Clevios P + HC and (b) Clevios PH1000 + HC.

pixel for each formulation are investigated and the results are shown in table 4.3 and figure 4.8 a).

Formulation		$\boldsymbol{R_{Ip}}$ (kΩ)	**Area** (cm^2)	$\boldsymbol{R_{Ip}/A}$ (kΩ/cm^2)
Clevios P	pristine	740 ± 160	0,5 ± 0,1	1500 ± 400
	LC	520 ± 90	0,4 ± 0,1	117± 340
	MC	370 ± 60	0,6 ± 0,1	650 ± 160
	HC	80 ± 20	0,6 ± 0,1	126 ± 40
Clevios PH1000	Pristine	4,0 ± 1	0,20 ± 0,07	20 ± 10
	HC	0,6 ± 0,2	0,23 ± 0,09	2,5 ± 1,0

Table 4.3: Electrical properties of conductive pixel on cotton fabric: In-plane resistance and pixel's area.

The range current sets up for the experiments is from −1 µA to 1 µA and figure

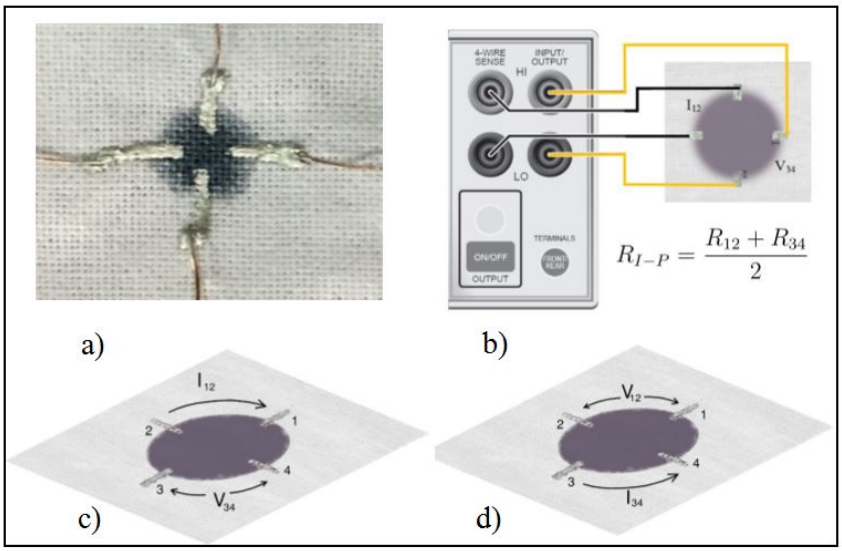

Figure 4.7: a) Photograph of conductive pixel with silver paste contacts, b) connections with *Keithley 2400 Source Meter* to measure R_{Ip}, c) and d) schematic view of conductive pixel with switching step.

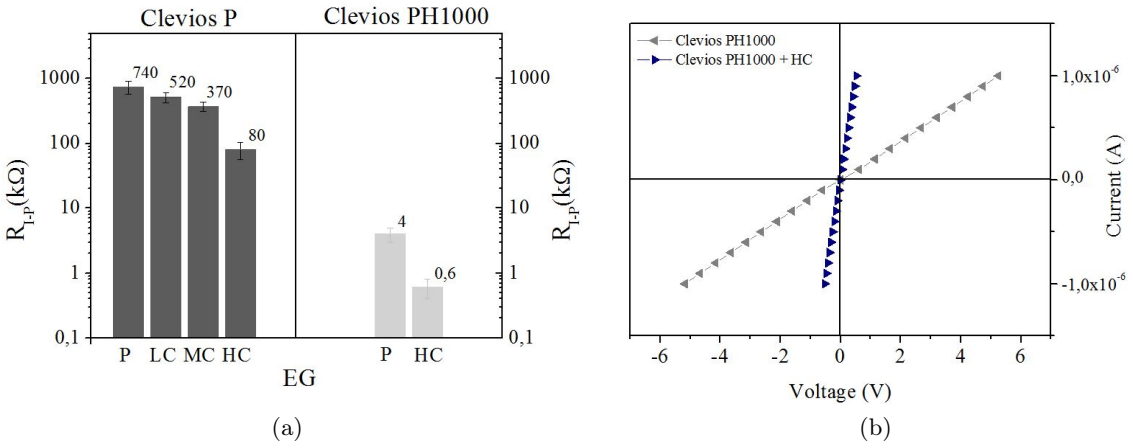

Figure 4.8: a) In-plane resistance for different formulations of Clevios P and Clevios PH1000, b) *I-V* characteristic of one pixel for Clevios PH1000 pristine and with HC.

4.8 b) shows the *I-V* characteristics of pixel one for Clevios PH1000 and Clevious PH1000+ HC samples. The slope of the curves is the conductance of the samples ($G = \frac{1}{R}$) and, for every formulation, the final In-plane resistance is found averaging four results.

4.2.3 Vertical resistance

Drop cast deposition method allows the conductive ink to soak the cotton fabric from top to bottom. Therefore, the vertical resistance of the conductive pixels is a fundamental aspect for the pressure sensors because it is the main parameter that change as a result of an applied pressure. The electrical contacts needed to supply voltage and measuring current are realized with the conductive silver paste as shown in figure 4.9. The tracks on top and bottom sides on the active layer are not in contact to avoid a short circuit and they are 3 mm in length. For each formulation,

Figure 4.9: Top-bottom contacts to measure R_V resistance.

the vertical resistance value of each formulation is calculated averaging the resistances of four different pixels. The R_V of a single pixel is the mean of two measurements obtained switching the electric contacts. Figure 4.10 shows I-V characteristics only for one pixel of each formulation of Clevios P and the R_V values.

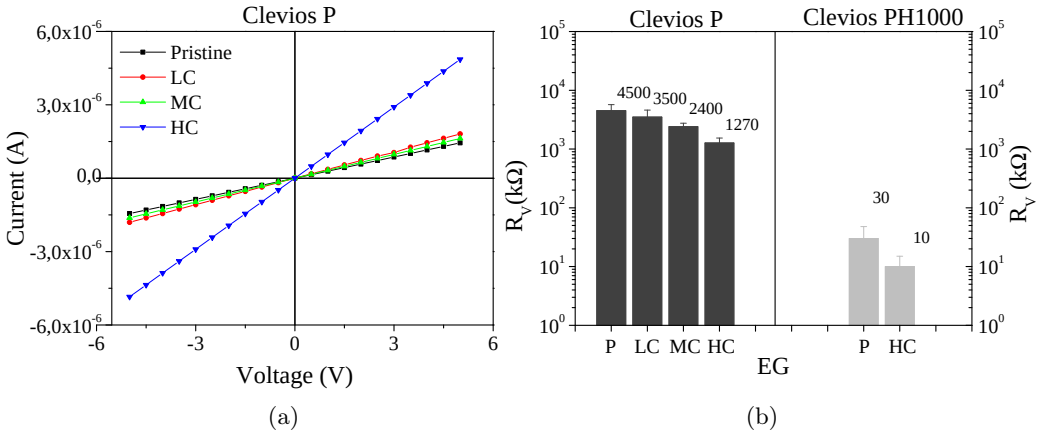

(a) (b)

Figure 4.10: a) I-V characteristics of one pixel for all formulation of Clevios P, b) comparison of vertical resistance.

As expected, the presence of additive changes the electrical properties of PEDOT:PSS and, even at low concentration, the conductance increase of 20 % respect to the pristine state. The high concentration formulation reaches a conductance value greater than tree times respect to the formulation without additive. The vertical resistances are significantly larger than the other resistances, though the effect

of ethylene glycol is always present but with a less relevance.

4.3 Comparison

In this chapter has been discussed the electrical properties of the various formulations of Clevios P and Clevios PH1000 that will be use to realize textile pressure sensors. Table 4.4 and figure 4.11 resume all the electrical characterization results. Since in the In-plane resistance measure the contacts are all in the same position respect the center of the pixel and the silver tracks on cotton have the same length, the resistance values are not normalized. The same happens for vertical resistance, because the thickness of various sample is constant and the contacts have been done all in the same way.

Formulation		R_{Tf} (kΩ)	R_{Ip} (kΩ)	R_V (kΩ)
Clevios P	pristine	160 ± 10	740 ± 160	4500 ± 1200
	LC	23 ± 2	520 ± 90	3500 ± 1100
	MC	0,30 ± 0,03	370 ± 60	2400 ± 350
	HC	0,19 ± 0,01	80 ± 20	1270 ± 270
Clevios PH1000	Pristine	5,0 ± 0,2	4,0 ± 1	30 ± 18
	HC	0,025 ± 0,001	0,6 ± 0,2	10 ± 5

Table 4.4: Summary of resistance measurements: thin film resistance R_{Tf} of PEDOT:PSS thin film, In-plane resistance and vertical resistance of conductive pixel on cotton fabric.

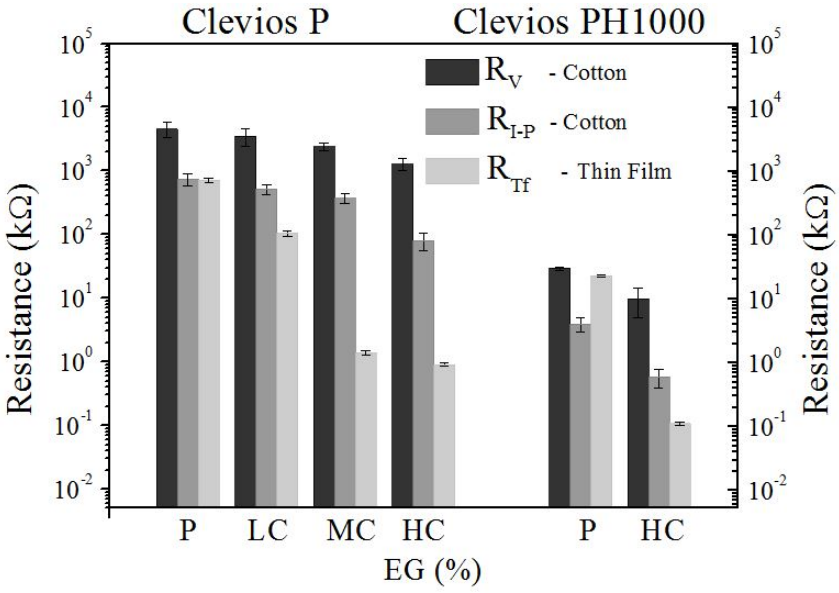

Figure 4.11: Comparison of resistance measurements.

The addition of ethylene glycol causes an increase in the conductance both in PEDOT:PSS thin films (on glass substrate) and in the active layers on cotton fabric. The resistance variation with the increase of EG concentration is greater when the solution is deposited onto glass substrate than in cotton fabric. According to the very different nature of the substrates, the differences between the In-plane and vertical resistance of Clevios P and Clevios PH1000 (in pristine state) are greater than the difference between thin film resistance of Clevios P and Clevios PH1000. The Clevios PH1000 is dispersed in water and the hydrophilic feature of cotton allows a better fibers coating. The EG effect is greater in the thin films sample than in cotton fabric due to the complex structure of textile. It can also be noted that, when the EG is added to solution, the Clevios P became conductive as the Clevios PH1000 in the thin film samples while, in the cotton fabric, this behavior is not reached because, as has been seen, the fibers get soaked in different way.

Chapter 5

Mechanical properties of fabrics

For the realization of a wearable sensor device the mechanical properties of fabric used is one of the most important parameters that developers must take into account. The fabrics have many different features, for instance flexibility, strength, recovery ect., that a mechanical analysis can discover. These behaviors affect the development of the sensors because they are integral part of it. The textile response depends on the material properties, the way of load and its ability to be molded in suitable shape. Numerous parameters influence the mechanical properties of woven fabrics, such as fibers structure, the warp and weft density and weaving conditions.

Before describing the specific fabrics used in this work, an excursus in rheology theory is needed to understand the different ways and methods necessary to find mechanical properties.

5.1 Force, stress and deformation

When a force is applied to a sample it gets a deformation, but the force is an inexact way of measuring the cause of this distortion. The force exerted by a probe equals the mass of the probe m times its acceleration a. However, force gives an incomplete picture since, for example, the effects produced by two objects that hit a wall with the same force depend on the area of impact. Usually, if one object is harder than the other, one expects that the impact of the former is going to do more damage. This damage is called a deformation and is related to the impact area A. The ratio of a force F to an area A is a stress, $\sigma = \frac{F}{A}$ and it is a pressure normally given in Pa. The deformation caused by an applied stress is called strain, ϵ, and it is calculated as $\epsilon = \frac{\Delta L}{L}$, where L is the original sample dimension and ΔL is the change in that dimension under stress.

The engineering stress and strain use fixed and undeformed cross-sectional area

in the calculations, while the true stress and strain take into account the changes in cross-sectional area by using the instantaneous values for the area. The engineering stress-strain plot gives an easier but not true indication of the deformation characteristics because it is based entirely on the original dimensions of the specimen, and these dimensions change continuously during the testing. In order to study the mechanical features of the fabrics, the engineering stress and strain will be used in this work. There are different ways to apply the stress that can also affect the deformation of the material. The main ways of applying a static stress are: increasing the applied stress σ over time at constant rate (stress–strain curve is generated tracking the change in strain as a function of stress), applying instantaneously a constant stress to the sample (monitor the material deformation under that load) or applying a constant stress varying the temperature to supervise the material change.

5.1.1 Creep-recovery and stress relaxation experiment

For the characterization of textile materials and for the next studies on wearable sensors response, a description of creep, recovery and stress relaxation testing is needed. Creep testing is a basic probe of polymers behaviors and involves loading a sample with a set force and watching the strain change over time. Recovery tests look at how the material relaxes once the load is removed. The tests can be done separately but they are most useful together.

Stress relaxation is the inverse of creep: a sample is pulled to a set length, held there, and the force necessary to maintain that strain is measured. These are shown schematically in figure 5.1.

Creep–Recovery Testing

In a creep-recovery experiment, the sample is loaded with a very low stress level, just enough to hold it in place, and allowed to stabilize. The testing stress is then applied very quickly and the changes in the material response are recorded as percent strain. The material is then held at this stress for a period of time until the material reaches equilibrium.

To examine a creep–recovery curve, there are different options in interpreting the results: plot strain versus time or plot creep compliance, $J = \frac{\epsilon}{\sigma}$, versus time. The former method of analysis, shown in figure 5.2 a), is more suitable to the real world. In the figure reported below, the slope of the equilibrium region of the creep curve gives a strain rate, $\dot{\epsilon}$, and it is possible to estimate the initial strain, ϵ_0, equilibrium strain ϵ_e, and the recoverable strain, ϵ_r. The modulus (σ/ϵ) and the viscosity $(\sigma/\dot{\epsilon})$ can be calculated because stress and strain are known for each point on the curve.

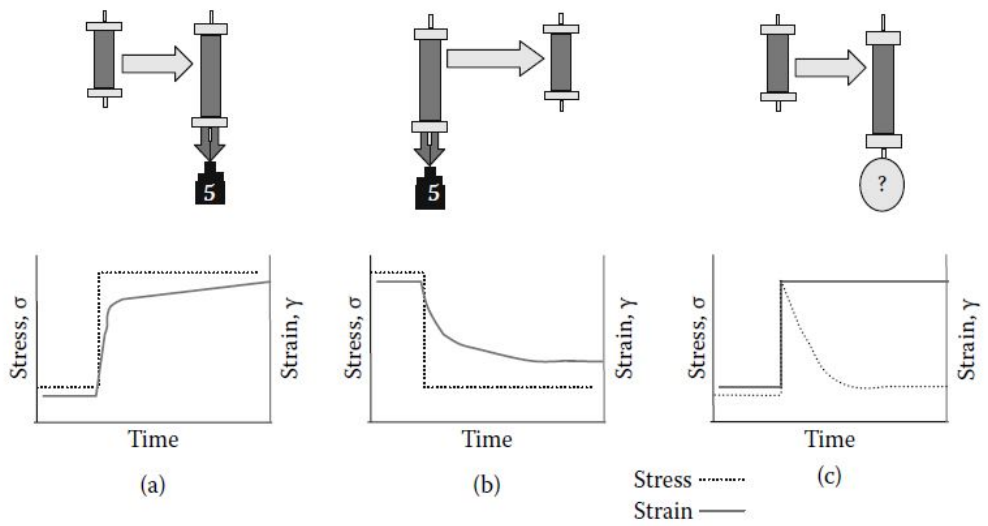

Figure 5.1: Creep, recovery, and stress relaxation tests. (a) Creep testing is preformed by applying a load or stress to a sample. (b) When the stress is removed and the material is allowed to recover, this is called a recovery test. (c) Stress relaxation is the reverse of creep. Holding a sample at a set length, the change in stress as a function of time or temperature is recorded.

Some parameters can be calculated to quantify the recovery curve: percent recovery is simply how much the material comes back after the stress is released and the relaxation time is the amount of time required for the strain to recover to 36.79% (or 1/e) of its original value.

Another method of analysis is to plot creep compliance against time (figure 5.2 b), where various compliance values can be calculated (compliance is the willingness of the material to deform and is the inverse of elastic modulus). In this case, the linear trend of creep compliance means that the material does not reach an equilibrium condition, typical of elastic materials, but has a viscoelastic liquid trend. The slope of this region is equal to $1/\eta$. The recovery curve can be used to independently calculate J_e (equilibrium compliance) because the recoverable creep compliance, $J_r(t)$, gives information about the strain recovered. A constant trend of $J_r(t)$ means that the material has recovered anything it could have recovered. Since it is known that:

$$\lim_{t\to\infty} J_r(t) = J_e \quad for \quad \dot{\epsilon}(t) = \dot{\epsilon}_\infty \tag{5.1}$$

with $J_r(t) = \frac{[\epsilon_u - \epsilon(t)]}{\sigma}$ and ϵ_u the strain at unloading and $\epsilon(t)$ time dependent recoverable strain. If $J_r(\infty)$ is different from J_e, the sample was permanent deformed.

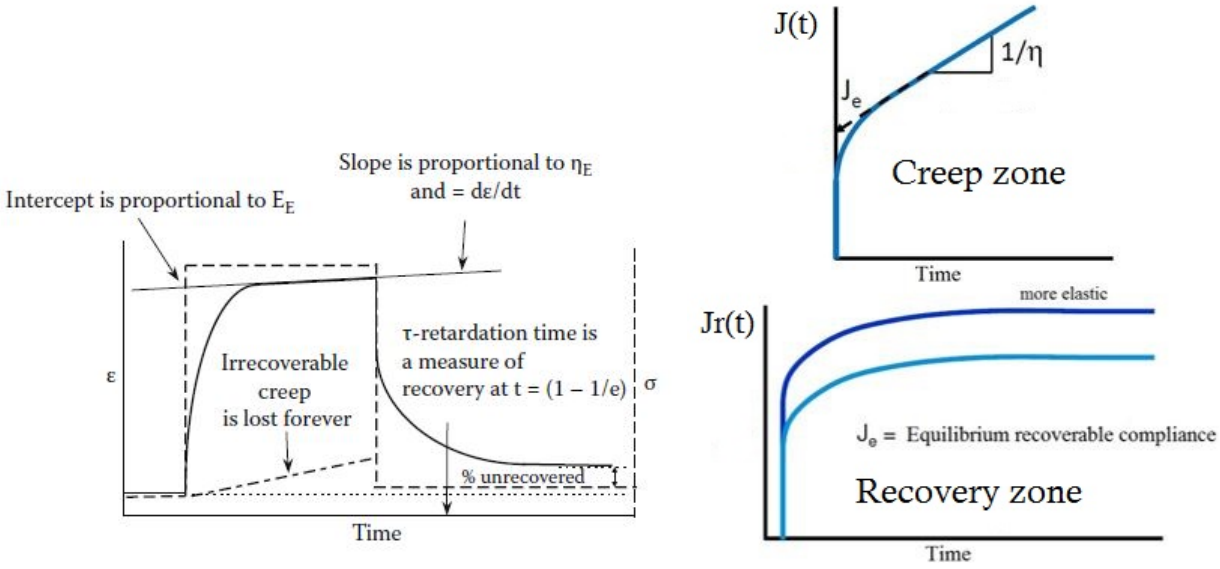

(a) *Creep recovery experiment.* (b) *Creep compliances versus time.*

Figure 5.2: a) Representation of the main informations which are extractable from a creep recovery testing: strain rate $\dot{\epsilon}$, recoverable strain ϵ_r, equilibrium modulus E_e and relaxation time τ; b) creep and recoverable compliance plotted against time: it is useful to extrapolate information about the elastic, viscous or viscoelastic behavior of tested material.

Stress relaxation experiment

The conceptual inverse of a creep testing is the stress relaxation experiment (figure 5.3), in which the relaxation modulus can calculated as:

$$E_r(t) = \frac{\sigma(t)}{\epsilon} \tag{5.2}$$

where $\sigma(t)$ is the stress at time t, and ϵ is the constant strain. Stress relaxation tests are of interest because they generate some very useful data about a polymer's real-world behavior. The data from a true stress relaxation test provides some very useful information that complements the more commonly available creep data. Creep data and stress relaxation data can be treated as reciprocal and roughly related as

$$(\epsilon(t)/\epsilon_0)_{creep} = (\sigma_0/\sigma(t))_{stress-relax}$$

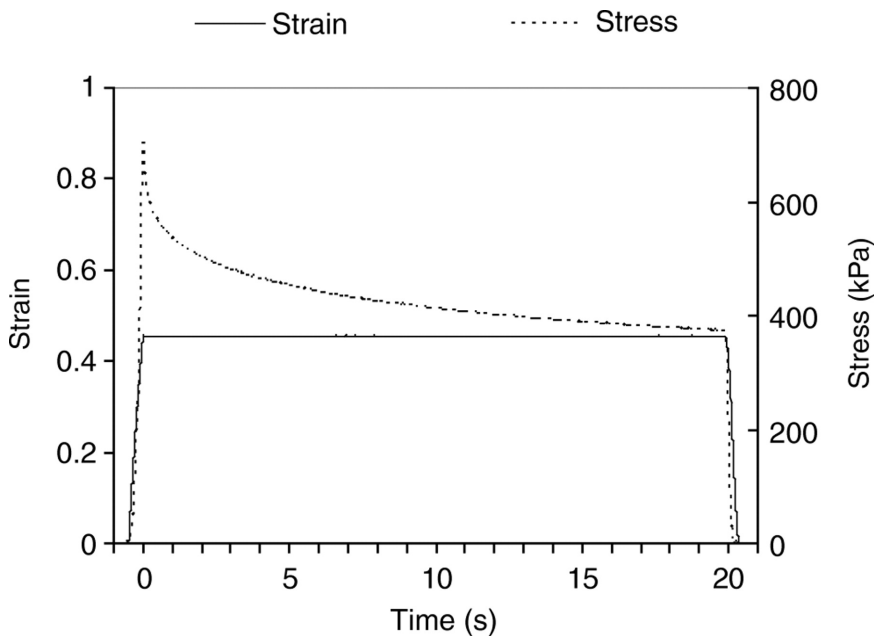

Figure 5.3: Stress relaxation experiments. Analysis of a classical stress relaxation experiment where the sample is held at length, l, and the stress changes are recorded.

5.1.2 Elastic and plastic response

Material properties can be conceived as being between two limiting extremes: elastic (or Hookean) and viscous (or Newtonian) behavior. The stress-strain curve relates the applied stress to the resulting strain and each material has its own unique stress-strain curve. A typical engineering stress-strain curve is shown below in figure 5.4 a).

It can be seen in the figure that the stress and the strain have initially an increasing linear relationship. This is the linear-elastic portion of the curve and it indicates that no plastic deformation has occurred. In this region of the curve, when the stress is reduced, the material will return to its original shape. The model used to describe this behavior is the spring and Hooke's law relates the stress to the strain of a spring by a constant, $E = \frac{\sigma}{\epsilon}$.

The modulus of elasticity (E) defines the properties of a material such as its stiffness and it is important to know how much stress is needed to deform the material. This is the yield point, where the stress-strain curve deviates from the straight-line relationship. From this point on in the test, some permanent deformations occur in the specimen and the material reacts plastically to any further increase in stress. The material will not return to its original, unstressed condition when the load is removed.

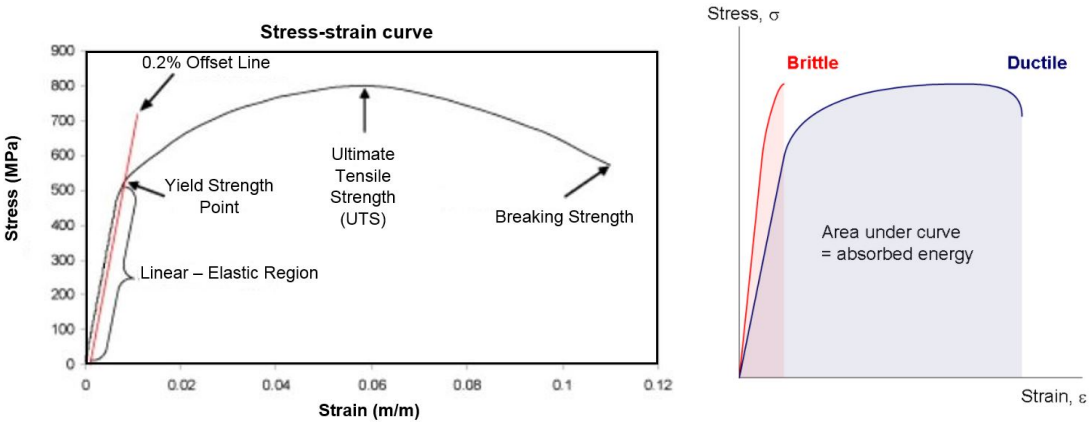

(a) (b)

Figure 5.4: a)A typical engineering stress-strain curves for polymer film undergoing tensile strain testing showing linear elastic region, material's yield strength, tensile strength and breaking strength; b) behavior of brittle and ductile materials under an applied stress. The UTS points are found in different place in the curve.

The maximum engineering stress level reachable in a tension test is the ultimate tensile strength, *UTS*. The strength of a material is its ability to withstand external forces without breaking. In brittle materials, the *UTS* is at the end of the linear-elastic portion of the stress-strain curve, or close to the elastic limit. In ductile materials, the *UTS* is outside the plastic portion of the stress-strain curve (figure 5.4). Finally, the area under the curve is proportional to the energy needed to break the sample.

5.2 Mechanical features of tested materials

The performance of fabric is affected by chemical, physical and mechanical properties of its constituent fibers and yarns. Fabrics fall into two basic categories: knits and wovens. In knit fabric, one continuous yarn is looped repeatedly to create what looks like tiny rows of braids. In woven fabric, multiple yarns cross each other at right angles to form the grain, like a basket. The mechanical properties of woven fabrics are influenced by the direction and type of the applied load (tension or compression), fiber length, yarns spinning, warp and weft density and the weave method.

Strength and elongation of woven fabrics are the most important features governing their performance. Any slight deformation of the fabric gives rise to complex movements of the fibers and yarns that formed the woven fabric. When the load is sufficiently increased, a plastic deformation of the material occurs until it reaches a final break. The work of rupture gives a measure of the ability of the material to

withstand sudden shocks of a given energy and it is called toughness.

5.2.1 Cotton fabric

Compression mode

The creep recovery behavior of cotton fabric, subjected to a compression load, is reported in figure 5.5, in which are studied three different square (20 x 20 mm^2) cotton samples with an initial thickness of $0,32 \pm 0,05$ mm. The values are obtained

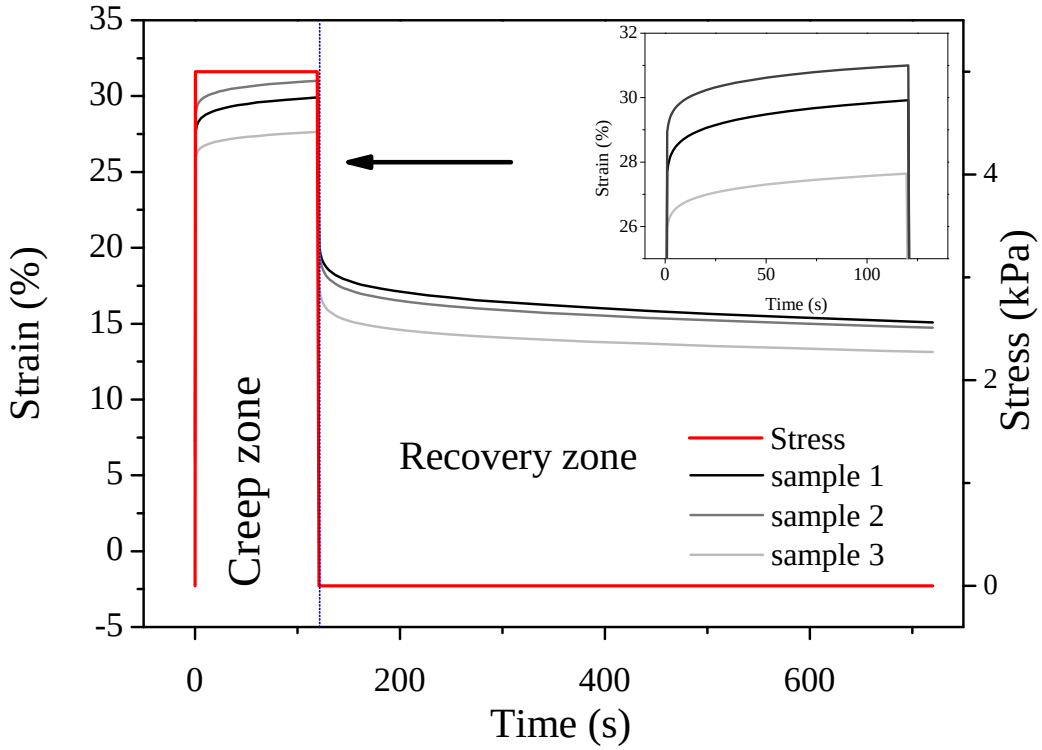

Figure 5.5: Strain against time for three different cotton fabrics during creep and recovery when a compression load is applied. The red curve is the constant stress of 5 kPa. A zoom of a creep zone is reported in the inset plot.

with the DMA Q800 and the samples are loaded with a constant stress of 5 kPa. During the load, the materials are deformed until 30% and, after 10 minutes without force, they recover until 15% of strain. All this measures have been done at constant temperature of 35 °C. This test is useful to know the fabric response when it is continuously compressed for a long period, and also the resulting thickness after the application of the load.

Tension mode

Other important characteristics of cotton can be discovered applying a tensile stress to a rectangular (20 x 7,3 mm^2) sample of cotton. The creep recovery test with tension load requires a larger stress than the test with compression load, implying that cotton is harder to stretch. The pre-load force applied before the start of the test is 0,01 N and it is used to measure the length (∼15,10 mm) of the stretched sample. In figure 5.6 the experiment results after a load of 3 MPa for 10 min and 20 min of recovery are reported. Furthermore, the small strain reached by the sample, although

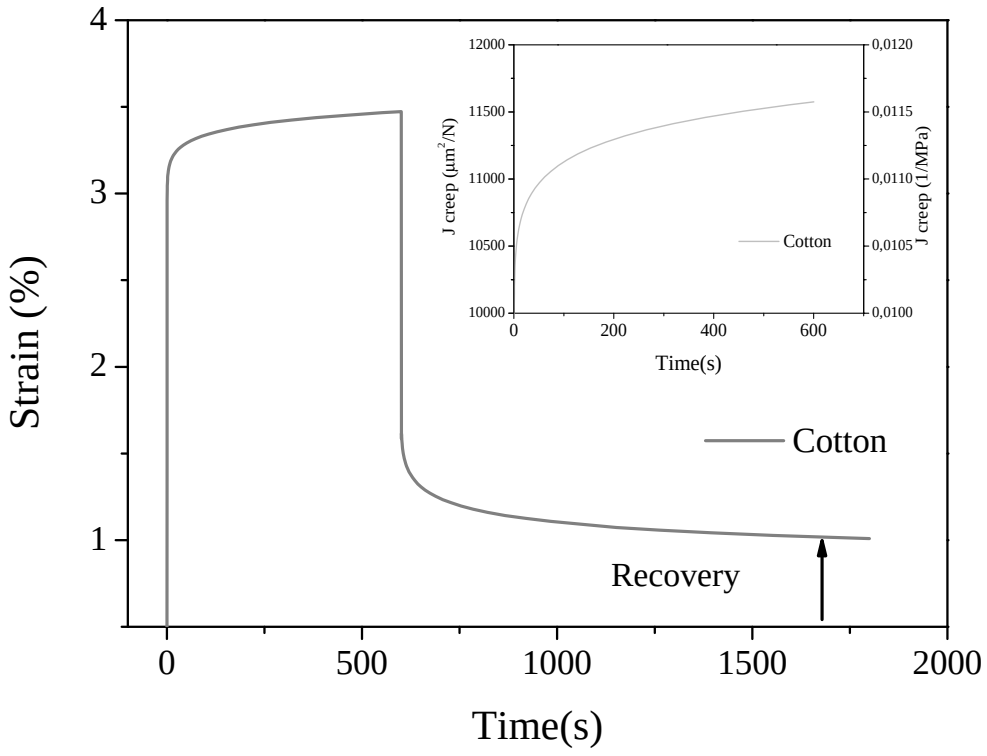

Figure 5.6: Strain against time of a cotton fabric during creep and recovery when a constant tensile load of 3MPa is applied. In the inset plot is represented the creep compliance versus time.

the applied tensile stress is high, is due to the fact that tensile elastic modulus ($\sim 0,1$ kPa^{-1}) is lesser than compressive elastic modulus ($\sim 1 \cdot 10^{-5}$ kPa^{-1}). During the recovery time, the sample recovers most of strain, up to 1%. The linear region in the creep compliance graph means that in 10 min the equilibrium deformation condition has not been reached. A linear fit on the linear region of the graph provides a strain rate of (0,013 ± 0,001) %/min.

In figure 5.7 a) the stress relaxation is observed keeping the structure in a strained condition for a finite interval of time. The sample is subjected to 4% strain for 10 min at a constant temperature of 30 °C. The non-material parameters like magnitude of initial loading, speed of loading, temperature, loading medium and friction affect stress relaxation in polymer materials. One may plot the *relaxation modulus*, defined as $G(t) = \sigma(t)/\epsilon_0$, against log time (inset of figure 5.7 a).

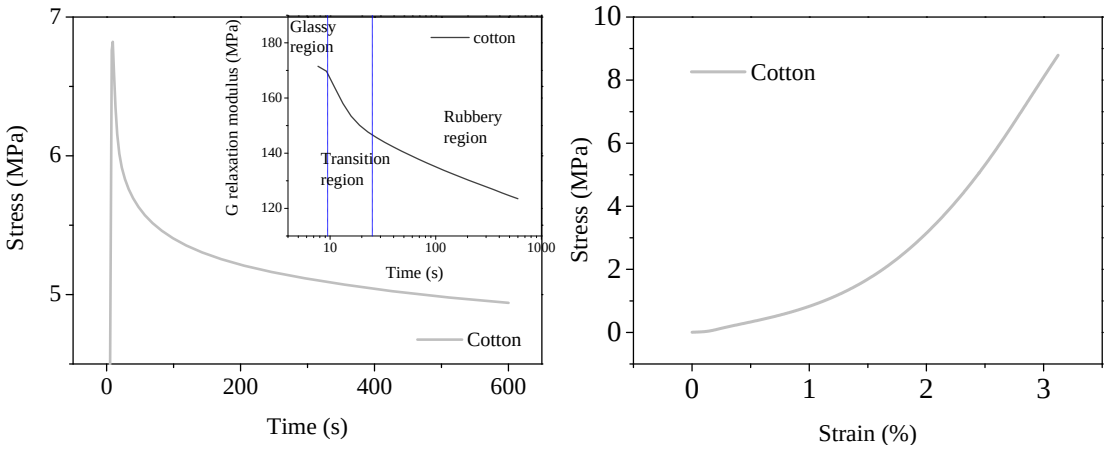

Figure 5.7: a) Stress against time trend when a constant strain of 4% is applied. In the inset graph is reported the stress relaxation modulus, $G(t)$, with respective glassy, transition and rubbery regions; b) stress strain curve for cotton fabric under a tensile stress. The behavior is soft rubbery like. The strain speed is of $0,45\%/min$. The temperature has been maintained constant during the measurement at 35 °C .

At short times, the stress is at an high plateau corresponding to a "glassy" modulus E_g of about 170 MPa, and then it falls towards a lower equilibrium "rubbery" modulus as the polymer molecules gradually adapt to the strain. Finally, the stress-strain curve reveals the J-shaped behavior of cotton fabric at small strain. The maximum value achievable with the DMA Q800 is 4,5% after that the instrument reaches the limit of the static force (18 N). The following type of stress-strain curve, figure 5.7 b), is common for many biomaterials and for textile.

Knitted and woven fabrics have J-shaped curves and the former fabric usually fails by unravelling and not by ripping, while the latter tear usually along the warp and weft directions.The curve shows that initially, small increases in stress give large extensions; however, at larger extensions, the material becomes stiffer and more difficult to extend. J-shaped stress-strain curves cause the materials to be extremely tough, even though their fracture energy is not particularly high. This toughness arises for the following reason: the lower part of the J-shaped curve gives very large

extension for low applied stress, so the modulus in this region is very low.Since the J-shaped curve is concave, the area under the curve up to a given extension is far lower than the one for the equivalent Hookean curve. This means that the energy released to fracture a material with a J-shaped stress-strain curve is far lower than the energy released when an equivalent Hookean material fails. Given that the energy release drives the crack propagation, a material that releases less energy on fracture is tougher.

5.2.2 Elastic fabric

Tension mode

The elastic fabric (EF) used in this work for the realization of strain sensors has some interesting features that were examined with the *DMA Q800* in the tension mode. The EF has a different behaviors according to the stretch direction: one of *greater* elongation and one of *minor* elongation, perpendicular to each other, can be identified. The elastic sample has a rectangular geometry (25,0 ± 0,5 x 7,0 ± 0,5) mm^2 with a thickness of (0,45 ± 0,05) mm and it is subjected to a tensile stress of 30 kPa for 10 min with a recovery time of 20 min. The figure 5.8 reports the main features of the EF studied.

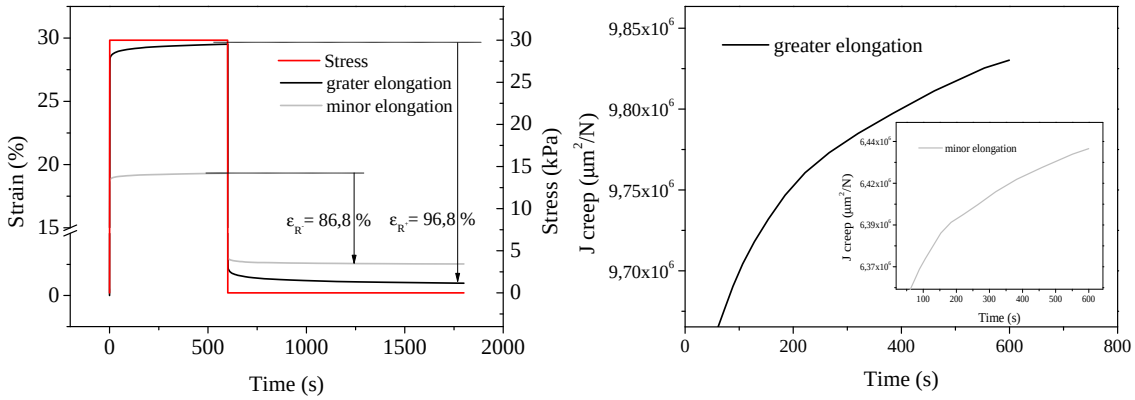

(a) *Creep recovery experiment.* (b) *Creep compliance against time.*

Figure 5.8: a) Different behavior of elastic material depends on stretch direction. Strain rate decreases with time in the creep zone, until it reaches a steady state. In the recovery zone, the viscoelastic fluid recoils, reaching an equilibrium; b) creep compliance trend along the greater and minor directions.

When the material is stretched along the greater elongation direction, it reaches a strain of about 30% recovering much of the deformation ($\epsilon_R = 96,8\%$), while when it is stretched along the minor elongation direction with the same stress it reaches

a strain of about 20% recovering less deformation (in this case the material stores more energy).

One can notice that the material behaves in a viscoelastic liquid manner because it does not reach an equilibrium deformation in creep zone but there is a linearly increasing deformation with time (figure 5.8 b). For this reason, when the load is removed at a time t before the strain reaches its equilibrium value ($\epsilon(\infty) = \sigma_0 J_e$), the course of recovery will not be a simple mirror image of the creep curve.

The stress relaxation experiment performed along the different directions is showed in figure 5.9. The samples are subject to a constant strain of 30 % and, as expected, the required stress along the greater elongation direction is lower than the stress along the minor elongation direction. After 10 min, the stress needed to maintain the wanted strain decrease of about 11 % for the first and of 16 % for the second sample. This means that the fabric along the minor elongation direction is affected to a permanent deformation. Along the more elastic orientation, the tensile stress is less reduced over time because the fabric offers a greater resistance to a permanent deformation and tends to return to the initial conditions.

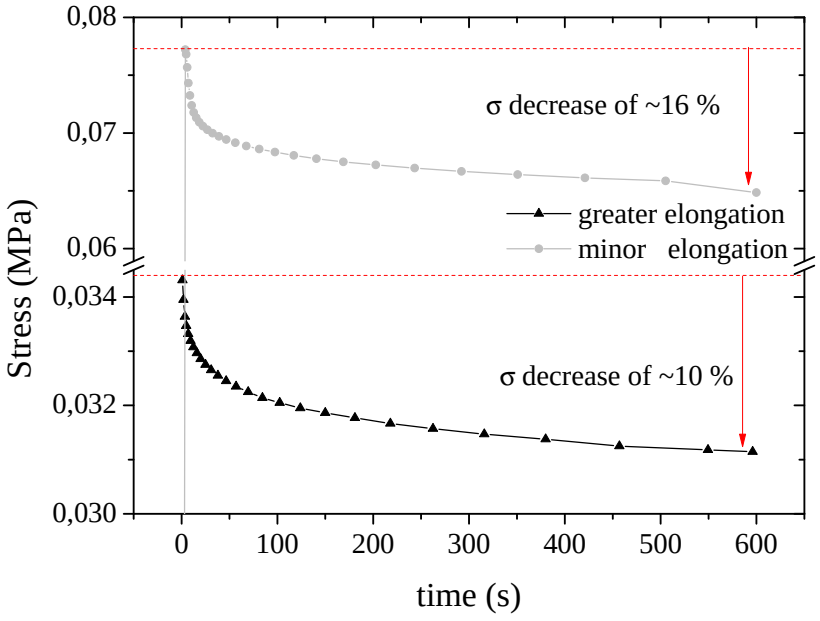

Figure 5.9: Relaxation experiment performed on elastic fabric with different behavior according to direction of applied tensile load. The stress needed to maintain constant strain of 30 % decrease in a different way depending on textile properties.

The final analysis on elastic fabric subjects with tensile load is the stress-strain testing. Samples are deformed under a constant linear strain rate of 20%/min until

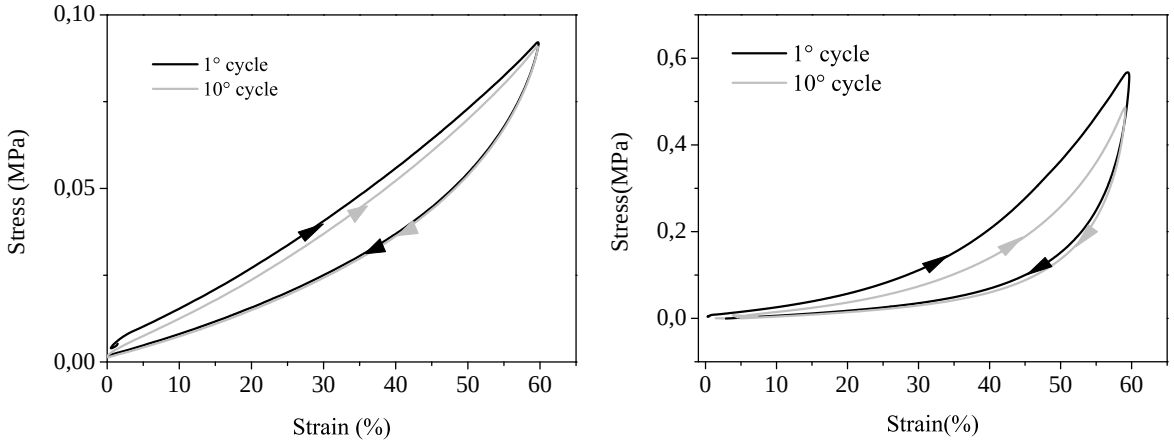

(a) *Greater elongation.* (b) *Minor elongation.*

Figure 5.10: Stress-strain curve of elastic fabric with the first and tenth cycle in loading and unloading tensile mode. The strain rate is of 20%/min.

a final deformation of 60%. Also the reverse process is performed to study the behavior of fabric when the tension decreases. The fulfillment of ten subsequent cycles allows to analyze the material response under repeated stresses and its potential deterioration.

In the figure 5.10 a) it can be observed that the stretch along the greater elongation direction exhibits a nearly Hookean trend in according to its elastic behavior. The same measure along a perpendicular direction points out the common J-shape curve for the knitted fabrics. In both cases there is an hysteresis effect due to viscoelastic behavior of material tested that absorbs some energy during deformation. Since the energy is absorbed from material, the stress-strain trend for the unload phase of the motion is different from the stress–strain trend for the loading phase. Energy is lost mainly into heat during the distortion of a viscoelastic material. In the figures below the loading of the material occurs along the black line and unloading of the material occurs along the gray line. The amount of energy absorbed by the material is equal to the area between the load (upper) and unload (lower) curves.

5.2.3 High performance sports technical fabric

Before starting the characterization of pressure sensors realized with this material, a description of mechanical properties is needed to understand its behaviors. Since in its real applications the textile is subjected to tensile as well as compression stress, the material response was studied under both stresses.

Compression mode

The fabric response to a compression stress has been studied again with the *DMA Q800* and the sample is cylindrical with dimensions: thickness of $(3,00 \pm 0,05)$ mm and diameter of $(12,30 \pm 0,05)$ mm. Two samples with same shape and dimension are investigated at different constant stress for the creep recovery experiment. The pre-load force, necessary to prevent the sample from moving, is $0,1$ N. The results, with the addition of creep compliance trend, are shown in figure 5.11. The samples are stressed for 2 min with 5 kPa and 50 kPa compression load, and the recovery time is 10 min. The high percentage of strain recovery means that this fabric has a more elastic behavior than cotton sample previously studied. In bulk compression,

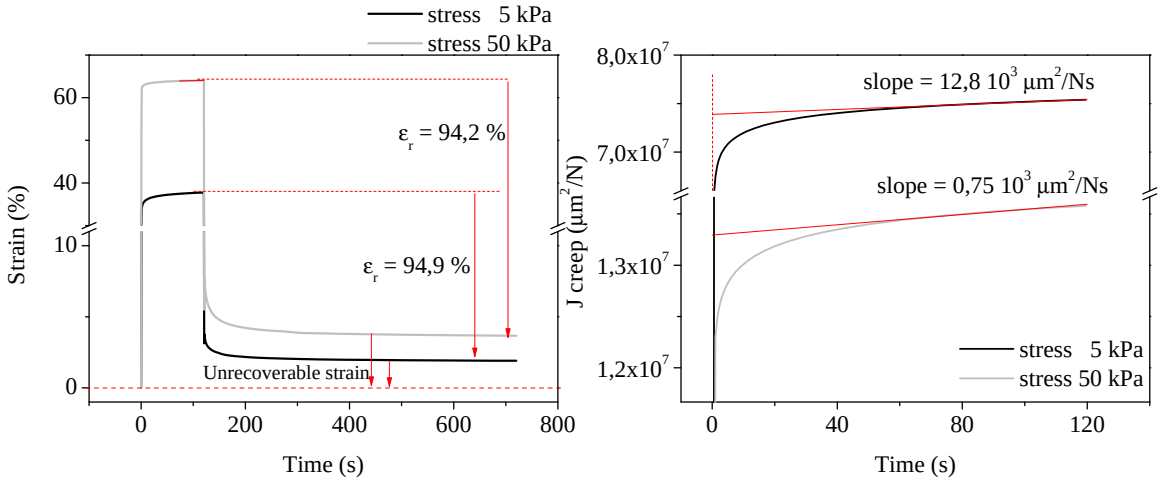

(a) *Creep recovery experiment.* (b) *Creep compliance against time.*

Figure 5.11: a) Creep recovery experiment for HP-STF is performed with two different values of constant stress to compare the response of materials at different real-life events. The compression stresses are 5 kPa and 50 kPa. Creep time is 2 min and recovery time is 10 min at a constant temperature of 30°C. b) Creep compliance plotted against time, with creep compliance rate.

an equilibrium compliance always exists and it is simply the thermodynamic compressibility. This value is reached when the deformation does not change anymore. The creep compliance rate is calculated for both cases. Neither of them seems to reach a constant value because the creep time is not enough to stabilize the deformation processes. However, as expected, when the sample is compressed with a greater pressure, the time required to reach a steady state is lower and the creep compliance rate is seventeen times smaller than the one calculated with the application of 5 kPa. The creep recovery experiment provides fundamental information on the response during compression and it will be useful for developing pressure sensors.

The classical stress-strain curve performed in compression mode, allows sample deformation until 60% and gives a J-shape graph typical of viscoelastic solid materials. In this operation mode, it is impossible to break samples and the maximum stress applicable depends on clamp limit switch. Figure 5.12 shows the stress needed to get the corresponding strain. When the strain overcomes 50%, the stress increases rapidly, meaning that the sample is about to reach the maximum deformation. The corresponding stress is about 30 kPa and it is comparable to the pressures reached during its real use.

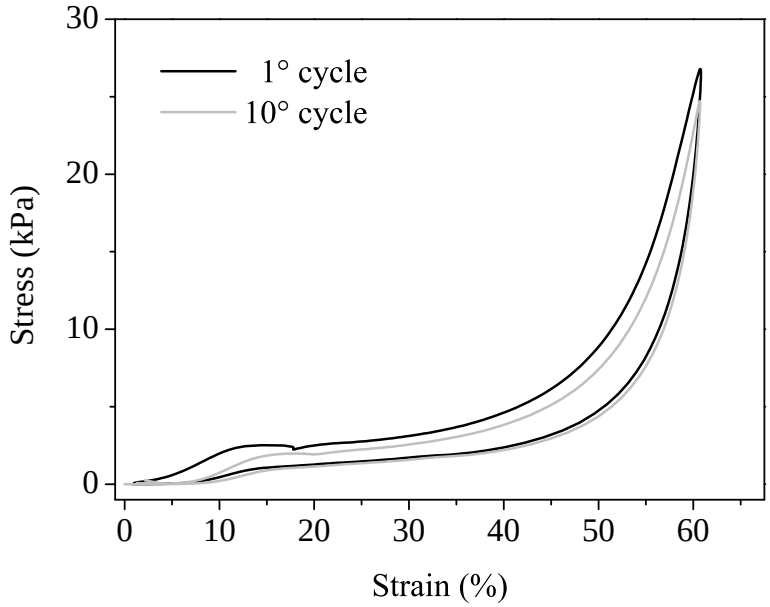

Figure 5.12: Stress-stain curve for HP-STF. The first and tenth cycles are plotted and an hysteresis occurs. The material are very soft and required small amount of stress to deform the sample until a 40%.

Tension mode

In this section, the results when a tensile load is applied to the HP-STF are reported. The geometry sample used for characterization with *DMA Q800* is rectangular with $2,50 \pm 0,05$mm length and $7,00 \pm 0,05$mm width. In figure 5.13 the main results are summarized, i.e. creep recovery experiment, relaxation test with its modulus and stress-strain plot.

The creep experiment is performed with a constant stress of 100 kPa and the high strain value reached means that the material has a low stiffness (which is the extent to which it resists deformation in response to an applied force). The stress

is applied for 10 min and during the 20 min of recovery the sample retrieves most of deformation. In figure 5.13 b) the trend of stress during a relaxation test is reported. The sample is subjected to a constant strain of 60% and after ten minutes the necessary stress to maintain the deformation is reduced by half.

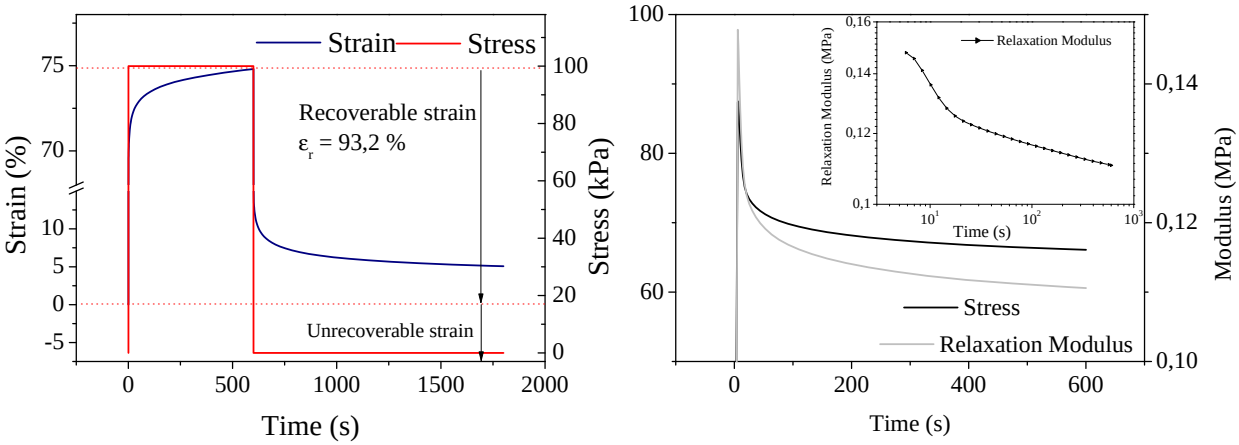

(a) *Creep recovery experiment.*

(b) *Stress relaxation experiment.*

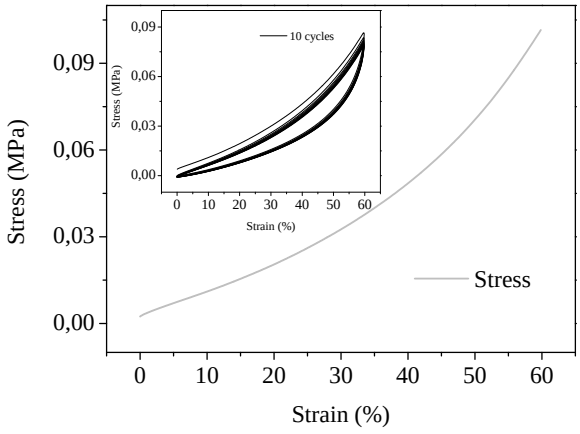

(c) *Stress-strain trend.*

Figure 5.13: a) Creep recovery experiment for HP-STF subject to a constant tensile stress of 100 kPa. The strain reaches a value of about 75%, stating the high flexibility of material; b) stress relaxation experiment with the stress and relaxation modulus trend against time. In the inset graph is plotted the modulus in logarithmic scale, c) stress-strain curve for a single loading cycle and, in the inset, ten successive forward and backward cycles until a 60% of deformation. The reproducibility is shown with the small hysteresis area.

The stress relaxation modulus, defined as the stress/strain ratio at constant deformation, is plotted against time with logarithmic scales in the inset graph of figure

5.13 b). Since the time scale is enormous, the only way to give a complete representation in a single graph is to make both coordinates logarithmic. The modulus shape has the typical trend of a lightly cross-linked amorphous polymer and, in a general way, in certain regions, modulus is approximately $1/J(t)$, so that the logarithmic plots have roughly the appearance of mirror images of creep compliance plot. At long time, the modulus for the cross-linked networks approaches values which are again nearly constant and it represents the equilibrium tensile modulus as treated by the theory of rubber-like elasticity. The region of time scale in which modulus falls sharply is often called the transition zone.

Lastly, the stress-strain curve for HP-STF loaded in tensile mode confirms the viscoelastic behavior of the material. When a stress is applied to a viscoelastic material like this fabric, parts of the long polymer chains that compose the material change positions and are rearranged in order to accompany the stress creating a back stress in the material. Unlike purely elastic substances that do not dissipate energy (heat) when a load is applied and then removed, a viscoelastic substance loses energy equal to the area of the loading-unloading loop.

Chapter 6

Textile pressure sensors: fabrication and characterization

In this chapter, fabrication methods, results of the electrical-mechanical characterization and a theoretical explanation for the working principle of wearable textile pressure sensors are reported. The devices developed in this work are a novelty in sensor field with low cost and fast-time manufacture. The proposed sensors are based on low amount of conductive polymer (<1ml) deposited on single layer of cotton fabric and connected with high stable commercial stainless steel yarns. Generally, as discussed in the Chapter 1, the textile sensors reported in literature usually have multilayer configuration that limit the flexibility and make intensive use of expensive materials [96, 97].

Pressure sensors fabricated on cotton fabric has been used to study the working principles, then the same configuration is carried on a high performance sport technical fabric (HP-STF). An example of application is the monitoring of rider pressure distribution on saddle. Figure 6.1 reports a representative average pressure distribution on a traditional road racing/sport saddle.

Similarly with a matrix of textile pressure sensor directly fabricated on cycling allow to monitor activity of athletes in order to improve performance, prevent injuries and help the fabrication to increase the saddle comfort.

The same image like that can be obtained manufacturing the pressure sensing elements directly on the cycling shorts, paving the way to sportswear with sensors to monitor activity of the athletes.

These pressure sensors are based on PEDOT:PSS conductive polymer that possess the piezoresistive property and it can be used as active material. It exhibits high flexibility, low cost fabrication process, light weight, and easy tailoring to obtained the required performance. The range of interest to detect pressure on a bicycle saddle

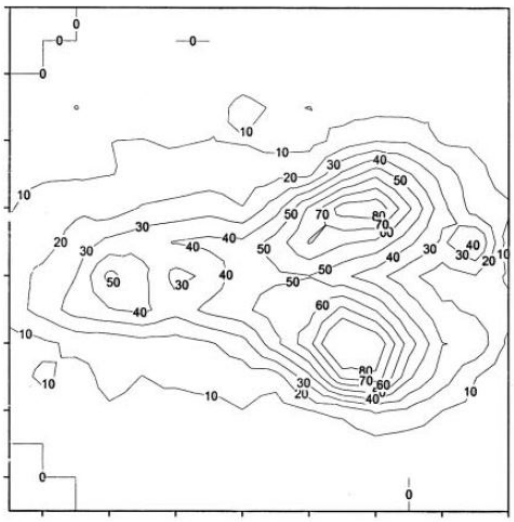

Figure 6.1: A representative average pressure distribution on a saddle. The pressure are reported in kPa [98].

is the medium-pressure regime ($<$ 100 kPa).

6.1 Geometry configuration

Conductive coating is an extrinsic alteration to the fabrics substrates and it can be achieved by solutions that act as conductive inks. In term of manufacturing process, drop casting and screen printing are used to achieve a high precision work and they allow printing of this conductive material on different substrates, such as natural (cotton) or synthetic fabric. PEDOT:PSS formulation are deposited both on standard 100% cotton fabric and then on *HP-STF*. Drop casting and screen printing techniques has been evaluated for the cotton fabric, while on the *HP-STF* only the drop casting method has been performed in order to obtained a proper sensor.

The configuration of these pressure sensors has been developed in our group and published by Josè et al in [99].

Figure 6.2 shows the operation mode of a single pressure-force element (**5**): it consist in a piece of base fabric (**1**) treated with a conductive polymer solution (as explained previously) at a crossing point (**4**) between top (**2**) and bottom (**3**) conductive threads that form a pressure-sensitive electrical connection with the treated fabric.

Conductive thread is made completely of 316L stainless steel. It is thin (measures 0,2 mm thick), strong and smooth. This thread is 2 ply and is sewn with the sewing machine *Elna eXplore 320*. It also has fairly low resistivity, 500 ohms per meter, and

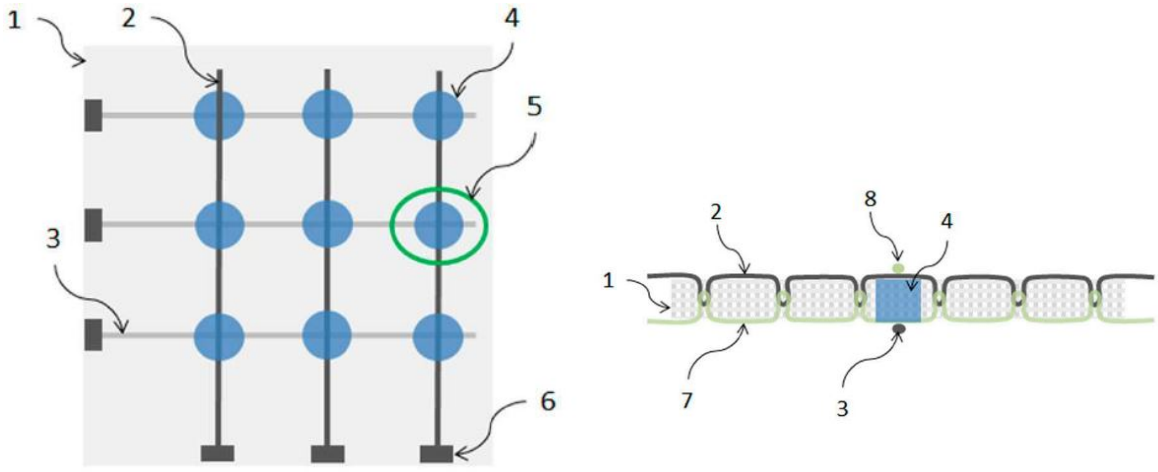

(a) (b)

Figure 6.2: Scheme of a textile pressure sensor. a) Top view of a 3 × 3 array where it is possible to identify: (*1*) base cotton fabric, (*2*) top conductive path, (**3**) bottom conductive path, (**4**) conductive polymer treated zone, (**5**) single sensing element and (**6**) connector or electrical contact for measuring; b) Transversal view of a sensel illustrating the relation between the base cotton fabric (**1**), the conductive threads (**2** and **3**), the non-conductive threads (**7** and **8**) and polymer-treated zone (**4**) that create the force-sensitive structure [99].

can connect electronic components that use under 50 mA (figure 6.3).

Figure 6.3: Sewing machine and 2-PLY stainless conductive thread.

After deposition, the stainless steel yarns have been sewed directly on the fabrics with lockstitch, the most common mechanical stitch formed by a needle thread passing through the material and interlocking with a bobbin thread, with the threads meeting in the center of the seam. Stitch looks the same on the top as well as the bottom and providing conductive paths on both sides of the fabric as illustrated on figure 6.2. Conductive paths on one side of the fabric are orthogonal to, and electrically isolated from, the conductive paths on the opposite side. Since each stitching line is made by two threads (needle and bobbin), bottom conductive paths (**3**) are obtained when using non-cunductive (100% polystirene) yarn as needle threads and the stainless steel yarn as bobbin thread. Conversely, top conductive paths (**2**) are obtained inverting and rotating the fabric, leaving the threads in the same arrangement. In order to avoid short circuits between top and bottom

conductive paths, single stitches are carefully distributed and arranged in such a way that top and bottom paths are not in contact with them. The thread crossing point is realized on the center of treated circular area.

6.2 Pressure sensing model

The resistance R_m measured at the ends of two orthogonal sewing paths (assuming all other paths driven to ground) can be expressed as:

$$R_m = R_{top} + R_s + R_{bottom} \tag{6.1}$$

where R_{top} and R_{bottom} are the linear resistance of the top and bottom conductive threads respectively (suitably insulated with a thermo-shrinkable), and R_s is the resistance of the sensel which in turn can be expressed as:

$$R_s = R_{c_{top}} + R_t + R_{c_{bottom}} \tag{6.2}$$

where R_t is the transverse resistance of the treated fabric and $R_{c_{top}}$ and $R_{c_{bottom}}$ are the contact resistances between the fabric and top and bottom threads, respectively. These resistances depend both on resistivity of threads and fabric fibers, and on the force that pressing produces contact between them. For practical reasons, however, the dominant physical phenomenon is assumed to be the contact of multiple conductive surfaces and that the overall behavior of the sensel resistance R_s can be modeled as [99]:

$$Rs = k \cdot F^{-n} \tag{6.3}$$

where k is a constant that depends on the geometric conditions and the resistivity of the materials and F is the equivalent force due to the pressure applied on the surfaces. The value of n depends on the nature of the contact and the elasticity of the materials, but it can be choose close to 1 for models where the load causes an increase of the size and number of contact points. Since F is proportional to the applied pressure P, and the resistances R_{top} and R_{bottom} can be assumed constants during a measure, equation 6.1 can be rewritten as:

$$R_m = \frac{a}{P} + b \tag{6.4}$$

with a and b constants. A good understanding of the resistance response at an applied external load is achieved if also the piezoelectric behavior of the active layer of PEDOT:PSS shall be take into account.

6.3 Electrical-mechanical characterization

To study the electrical response as a result of an external load, the *DMA Q800* and *Ketlhey 2400* are combined. The DMA works in compression mode to apply the external normal pressure and the resistance variation is measured with the source meter. Thermo-shrinkable polystyrene tube insulates the stainless steel threads which are connected with a copper wire to allow the connection with the source meter.

Figure 6.4 a) shows a cotton fabric sample in the DMA. The maximum force provided by DMA is 18 N and, using a top compression clamp with 15 mm diameter, a normal stress until $\sim$ 100 kPa can be applied. The top clamp, with an area of 1,77 cm^2 (larger than the active area), is used to provide an equal pressure distribution throughout the sensor area. The instrument is controlled with a specific software that allows the creation of custom measurement procedures.

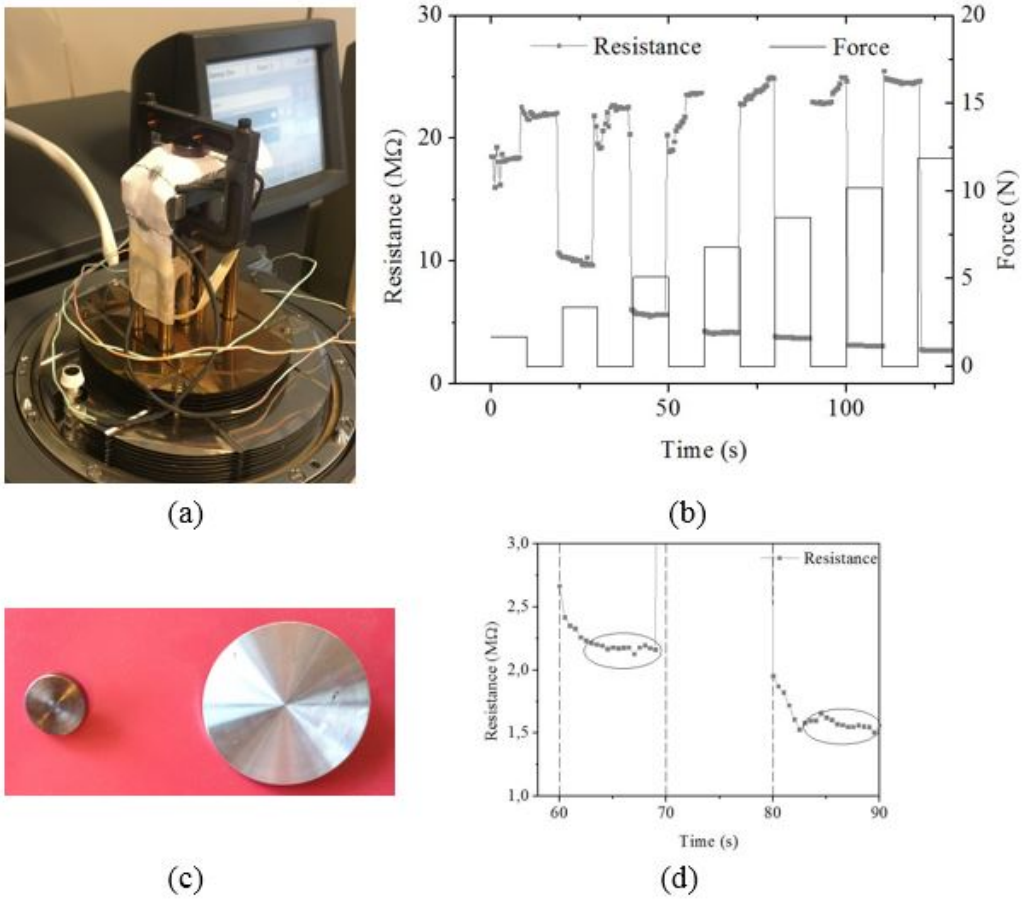

Figure 6.4: a) Application of normal pressure on a cotton fabric, b) load-unload force cycles and the corresponding resistance variation, c) right: top compression camp ($d = 15$mm), left: bottom compression clamp ($d = 40$mm), d) zoom in the resistance against time plot: the measurements need some second to stabilize.

The electrical data acquisition software is developed in LabView (figure 6.5) and the *Ketlhey 2400* supplies a constant current of 1 µA, measuring the voltage drop with a sampling time of 200 µs. These changes are due to the vertical resistance variations.

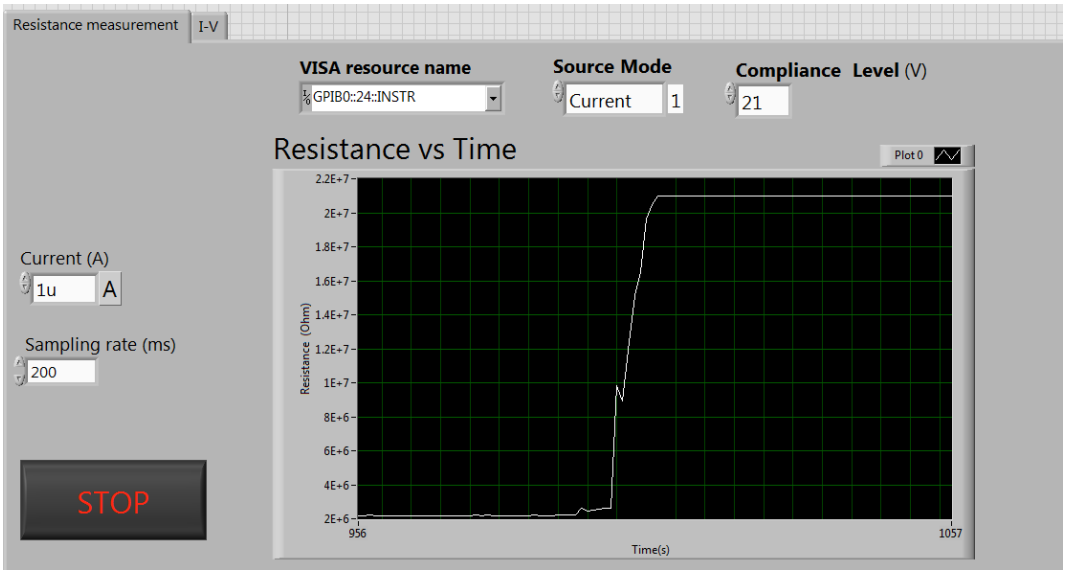

Figure 6.5: The front panel of the LabView program used to acquire the electrical signal.

The testing of the response properties of the pressure sensors is performed applying load-unload cycles (with a holding time of 10 s), increasing stress after each cycle (with step of ∼10 kPa). In the unload part, the applied force is 0,1 N; it is necessary to keep stable the sample and is called pre-load force. Figure 6.4 b) shows the typical mechanical procedure used to characterize the various samples and the corresponding resistance trend.

To analyze the behavior of these pressure sensors when external normal pressure is applied, it is important remember the fabric material responses. In chapter 5 the creep relaxation experiment on the cotton fabric has been reported, in which a stress of 5 kPa could deform the sample (in vertical direction) until 30%.

In this case, as well as the cotton fabric soaked with conductive ink, four different threads are present (geometry configuration illustrate in figure 6.2). Figure 6.6 a) shows a schematic cross section of the sensing element: the system is composed by a cotton fabric in the middle of two couples made up of one polyester yarn and one conductive thread; on the top side, the conductive thread is in contact with the fabric, whereas on the bottom side it is the yarn to be in contact with it. The DMA Q800 applies increasing pressure steps (∼ 0,9 N) and measures the instantaneous thickness

of the system (cotton plus thread). The loading and unloading times are 10 s. Figure 6.6 b) reports, as example, a typical thickness trend for Clevios P formulation while figure 6.6 c) shows the strain against pressure for the sample treated with Clevios P pristine, Clevios P + LC and Clevios P + HC. Here, the strain is defined as the ratio between thickness variation and initial thickness. As expected, the ethylene glycol presence does not change the mechanical response and all samples behave in the same way. With an external pressure of about 100 kPa the strain reaches a value greater than 60 %. The same architecture is chosen to overcame the different behaviors due to the geometry configuration.

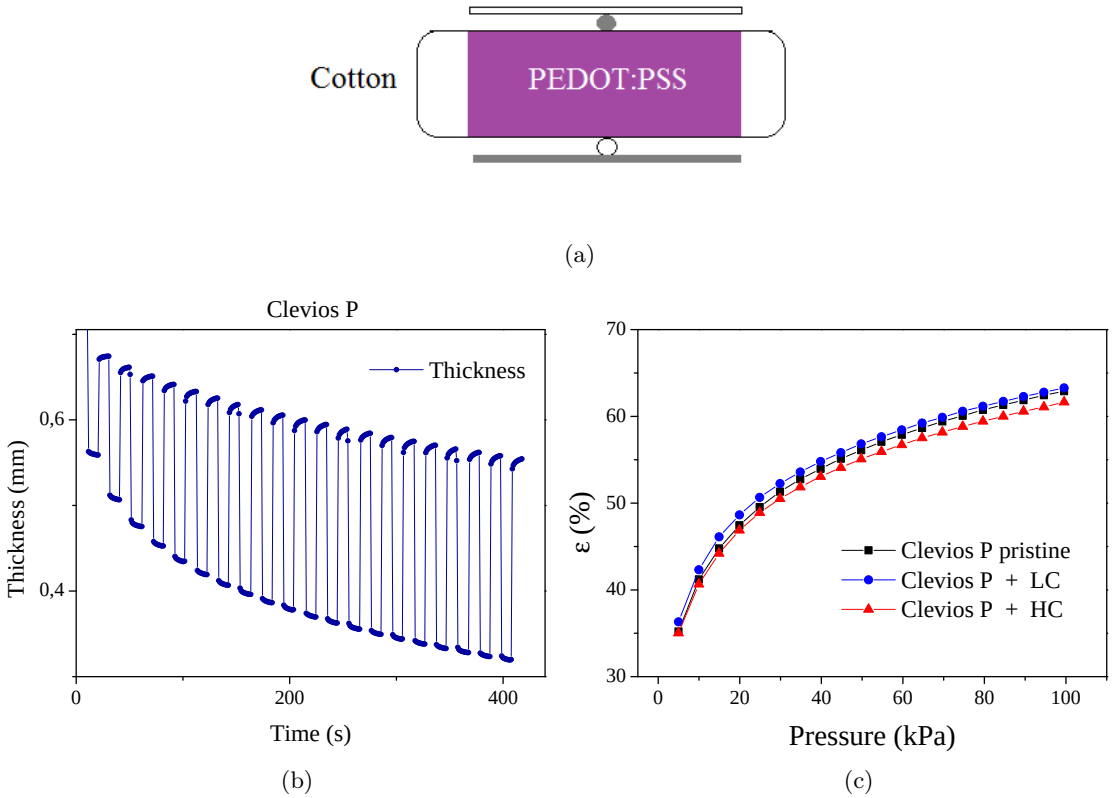

Figure 6.6: a) Schematic cross section of a circular pixel treated with PEDOT:PSS; b) typical trend of cotton fabric thickness when a normal pressure is applied. The load increase of about 0,9 N (untill 100 kPa) after each step and the loading and unloading times are 10 s; c) strain of cotton samples treated with different PEDOT:PSS formulation.

The resistance value corresponding to an applied stress is calculated averaging the resistances measured during load step. As reported in figure 6.4 d), the resistance values averaged are those acquired between 2 s and 10 s. A first important

consideration can be achieved by comparing, as an example, the electrical response at different pressures of sensors based on Clevios P pristine and Clevios P + HC formulations.

Figure 6.7 reports the electrical resistance trend when a pressure of 30 kPa and 90 kPa is applied (respectively, left and right columns).

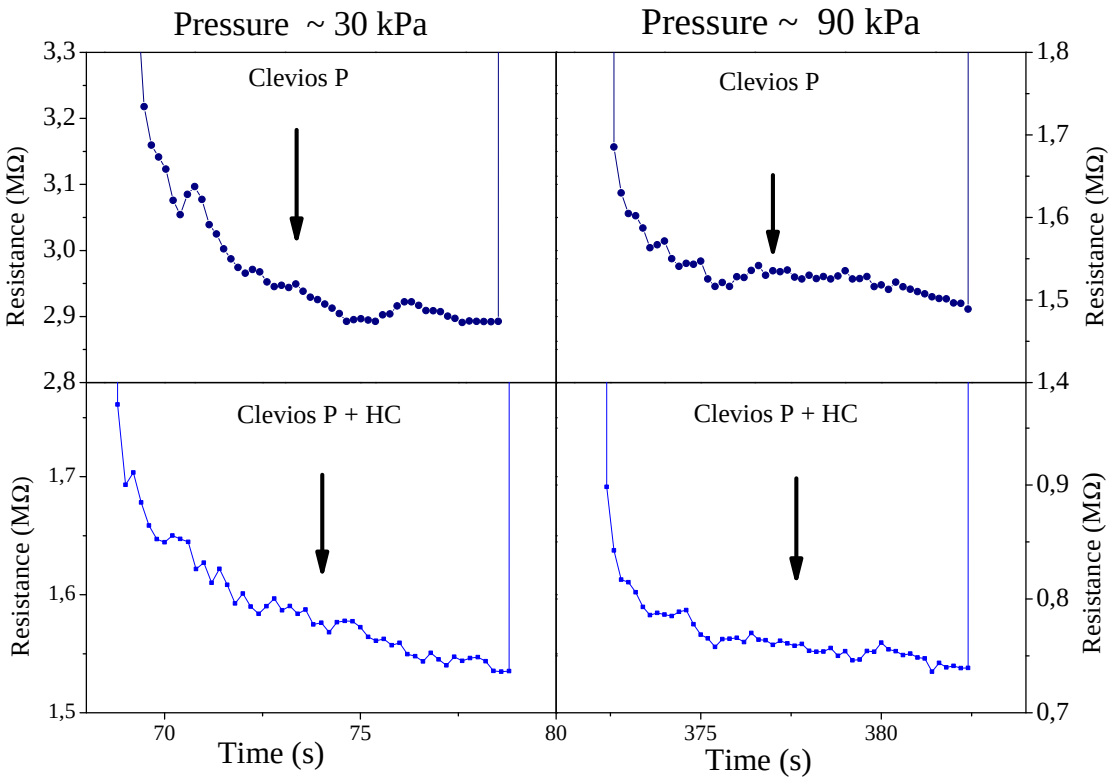

Figure 6.7: Resistances measure when a pressure of 30 kPa (left column) and 90 kPa (right column) are applied on a cotton pressure sensor. In the first row is shown the Clevios P behavior and in the second row is shown the Clevios P + HC behavior.

The first row shows the resistance trend for Clevios P and the second row shows the resistance trend for Clevios P + HC . It is possible to notice that, in both formulations, during the application of a low pressure, the time necessary to reach a steady state is larger with respect to the case of an applied high pressure. Table 6.1 shows the $\frac{\Delta R}{R_2}$ calculated as: $\Delta R = (R_2 - R_{10})/R_2$ where R_2 and R_0 are resistance after 2 s and 10 s from the application of pressure respectively. Increasing the pressure, the relative resistance variation is halved for both formulations. The presence of ethylene glycol does not change the overall behavior, and the relative resistance

variation is the same at both low and high pressures. This means that the additive does not change the stability of the measurement.

	30 (kPa)	**90** (kPa)
Clevios P pristine	6 %	3 %
Clevios P + HC	6 %	3 %

Table 6.1: Relative resistance variation $\Delta R = (R_2 - R_{10})/R_2$.

6.4 Cotton pressure sensors

In this section the responses of the sensing elements manufactured on cotton fabric with different methods are reported. A mechanical-electrical characterization is needed to understand the two most important parameters for these sensors: pressure working range and sensitivity ($\frac{\Omega}{\text{Pa}}$). These features depend on the desired final application.

The realization of conductive parts of these sensors are based on two different isopropanol or aqueous dispersion of PEDOT:PSS formulation (Clevios P and Clevios PH1000) mixed with a variable percentage (Low Conductive LC, Medium Conductive MC and High Conductive HC) of ethylene glycol which acts as the second dopant.

The Clevios P and Clevios PH1000 have been ultrasonicated before and after the addition of ethylen glycol for 15 min, and the cotton fabric can be treated via screen printing technique or drop casting methods.

6.4.1 Screen printing pressure sensors

The solutions used for these techniques have been heated in a oven at 70 °C to halve their weight. The dense conductive paste allows the screen printing method using an open mask with 2x2 matrix of circular holes. Subsequently, samples have been dry in a oven at 70 °C for 15 min.

To characterize the response of pressure sensors realized on cotton substrate, only one formulation of PEDOT:PSS is used. Four pixels of Clevios P + HC are deposited on cotton fabric and they are quickly tested with a home-made pressure setup. Since they respond to an external stress, a more precise electrical-mechanical characterization is performed using DMA Q800 and the *Kethley 2400* (as described in section 6.3). Figure 6.8 a) shows the resistance trend when the normal pressure

increases. The sensing pixels decrease their resistance and, since the unload resistance R_0 varies slightly for each sample, it is normalized dividing $R(P)$ by R_0. In this case, the unloading resistance is measured when the DMA Q800 provides a force of 0,4 N. Figure 6.8 b), instead, reports the resistance of Clevios P + HC formulation against a wide pressure operational range. This trend is the same to the pressure sensors on cotton fabric realized earlier in our research group by Jose et. al. [99]. The inset graph in figure 6.8 b) shows the previously results. The difference between the resistances values report in these graphs, is one order of magnitude and it may depend on the PEDOT:PSS used, and on the different deposition method.

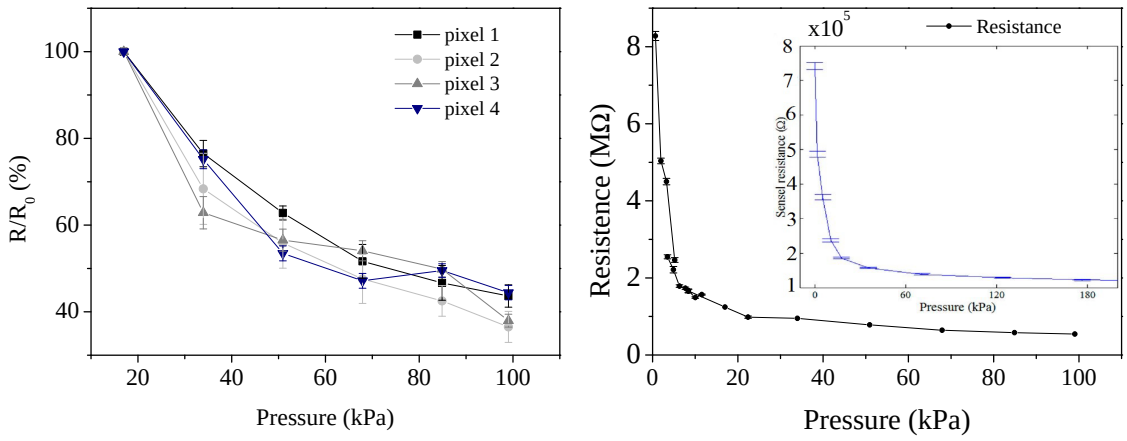

(a) (b)

Figure 6.8: **Clevios P + HC** a) Normalized resistance against pressure for four pixel fabricated with screen printing technique, b) resistance in a wide range on pressure compared with results presented in literature [99].

Drop casting pressure sensors on cotton fabric

In this section the results of electrical-mechanical characterization of different PEDOT:PSS formulations deposited by drop casting on cotton fabric are reported. One 5 µL drop of conductive solution formulations based on PEDOT:PSS is deposited on the cotton fabric. For each of the six solution formulations (the same formulations reported in chapter 4), a 2x2 matrix of 4 pixel equally spaced is realized. This geometry allows electrical-mechanical characterization of the cotton pressure sensors and it minimizes the seams to realize electric contact (figure 6.9).

Figure 6.10 reports the resistance (and conductance) responses of all different formulations during the application of a normal pressure.

These trends allow to understand the different features of each sample and the

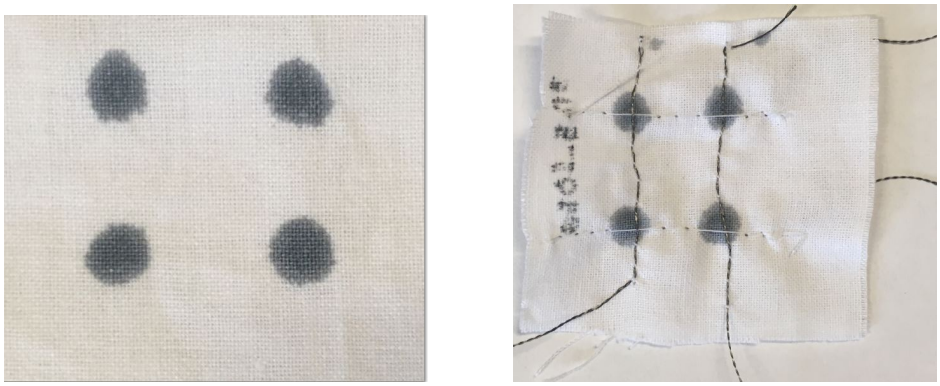

(a) (b)

Figure 6.9: a) 2x2 matrix with 4 PEDOT:PSS pixels deposited on cotton by drop cast with a standard pipette and b) electrical contacts realized with a sewing machine.

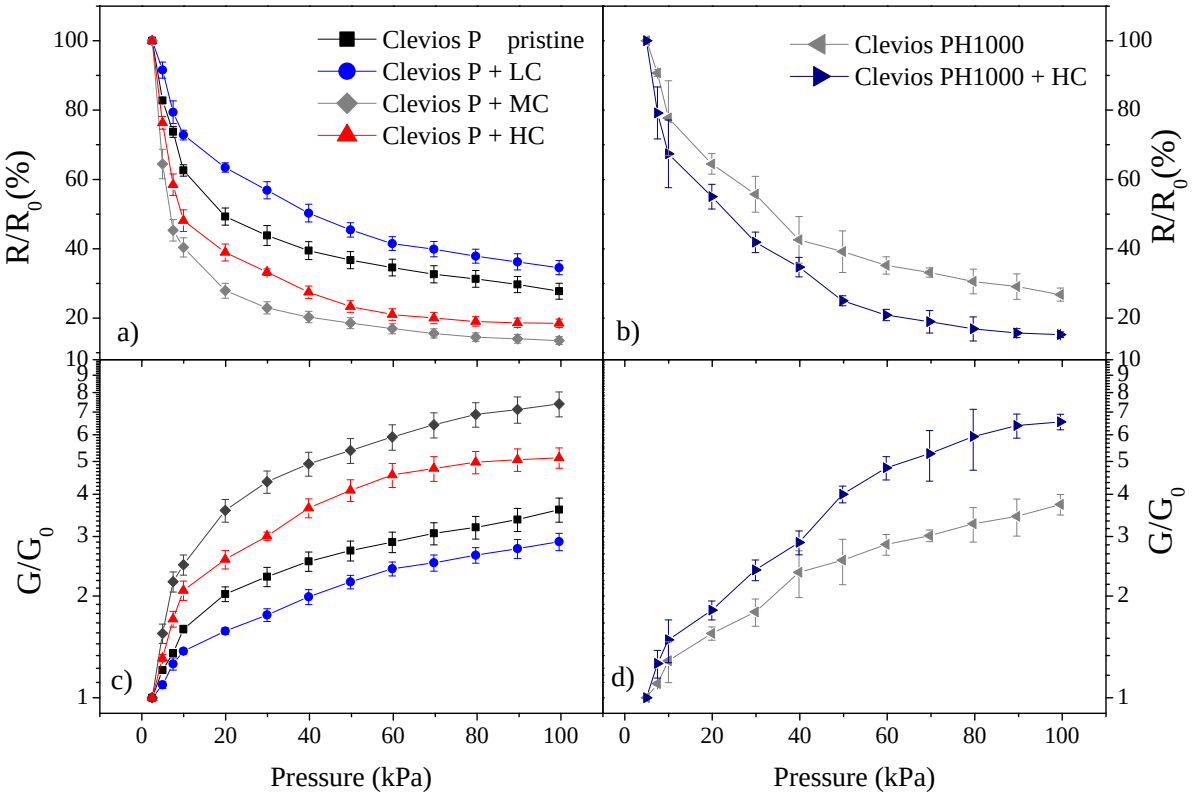

Figure 6.10: Relative resistance (conductance) variation against applied pressure for the six different formulations of cotton pressure sensors.

effect of ethylene glycol on the sensing properties. The resistances (conductances) are normalized with the value measured when the applied pressure is ~ 5 kPa ($R_0 = 1/G_0$). The results shown in the graphs are obtained averaging the R/R_0 value for each pixels.

6.4.2 Comparison

Comparing the response of sensors with the same formulation (Clevios P + HC) on cotton fabric but manufactured with two different methods, useful information about these techniques are obtained. Figure 6.11 reports the trend of normalized resistance in response to a normal pressure for pixels of Clevios P + HC realized with the screen printing (open mask) and with drop casting method. Even if the absolute resistance value of conductive pixel treated with drop casting method is greater than the one treated with screen printing (table 6.2), the normalized resistances have the same trend. This means that the deposition methods can affect the absolute resistance values, but does not the intrinsic behaviors.

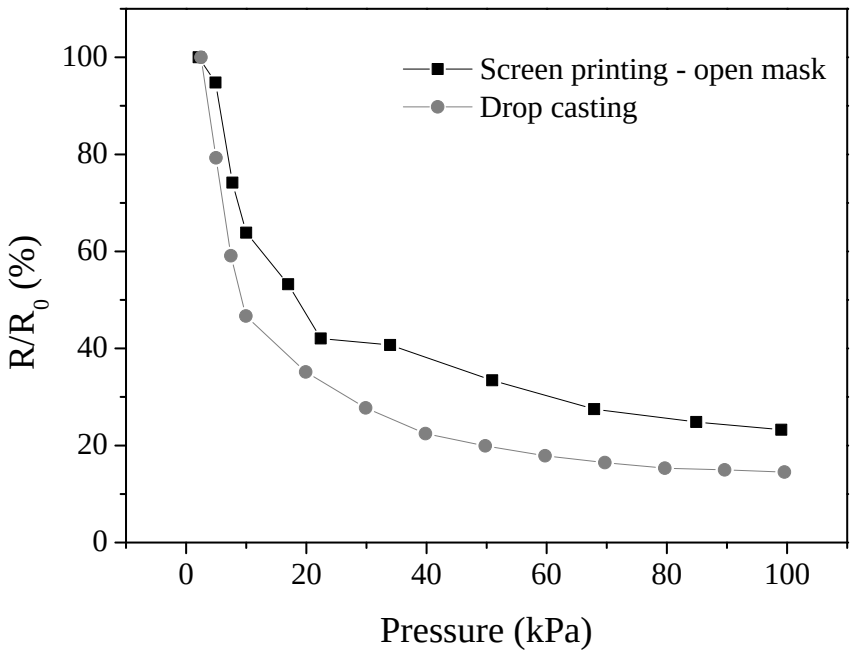

Figure 6.11: Comparison of normalized resistance trend between two cotton fabric pressure sensors realized screen printing and drop-casting. As example, only the Clevios P + HC formulation result is reported.

Pressure (kPa)	**Resistance** (MΩ)	
	Open Mask	Drop cast
~ 2	2,3 ± 0,4	7 ± 1
50	0,8 ± 0,1	1,4 ± 0,3
100	0,54 ± 0,08	1,0 ± 0,3

Table 6.2: Absolute resistance values for pressure sensors on cotton fabric treated with Clevios P + HC by screen printing and drop-casting methods.

6.5 Interpretation of piezoresistive behavior of PEDOT:PSS

As reported in [100], the PEDOT:PSS presents an intrinsic piezoresistive effect: when an external deformation is applied (in this case a compressive stress) the material change their resistivity. A change in this physical parameter leads to a change in the material resistance. In the development of a pressure sensor based on the resistance variation is very important understand the mechanism correlated with these variations.

The second Ohm's law describes the values that influence the electric resistance of a conductor: the resistance (R) of a homogeneous conductor of constant transversal section is directly proportional to its length and is inversely proportional to the area of its transversal section:

$$R = \rho \frac{l}{A} \tag{6.5}$$

with resistivity ρ, length l and area of transversal section A.

In the textile pressure sensors configuration developed in this work, the thickness of fabric material t correspond to the length that appears in the second Ohm's law, while ρ is the PEDOT:PSS resistivity that change due to the piezorestive behavior, and A is the sensor area which remains constant. When an external normal pressure is applied on sample, the fabric thickness, and the resistance, decrease. Since the conductive polymer used to fabricate the sensing layer has a piezoresistive behavior, it is important to separate the geometric contribution from the piezoresistive to the resistance decrease.

Figure 6.12 illustrates an example of resistance and thickness trend for Clevios P pristine formulation. The two plots have a different trend and this means that the pressure sensor resistance does not depend only by cotton thickness. As reported in section 6.3 in figure 6.6, the strain is the same for all formulations and the resistance variation with a pressure increase is affected also by the change of resistivity .

The schematic structures of cotton fabric treated with PEDOT:PSS before and after the application of a normal pressure are shown in figure 6.13.

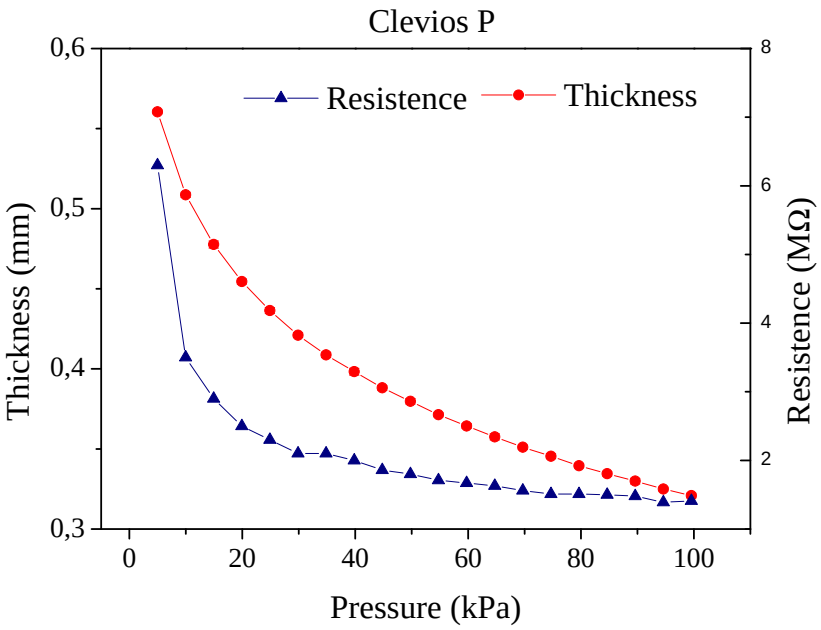

Figure 6.12: Thickness and resistance trend at different pressure for Clevios P.

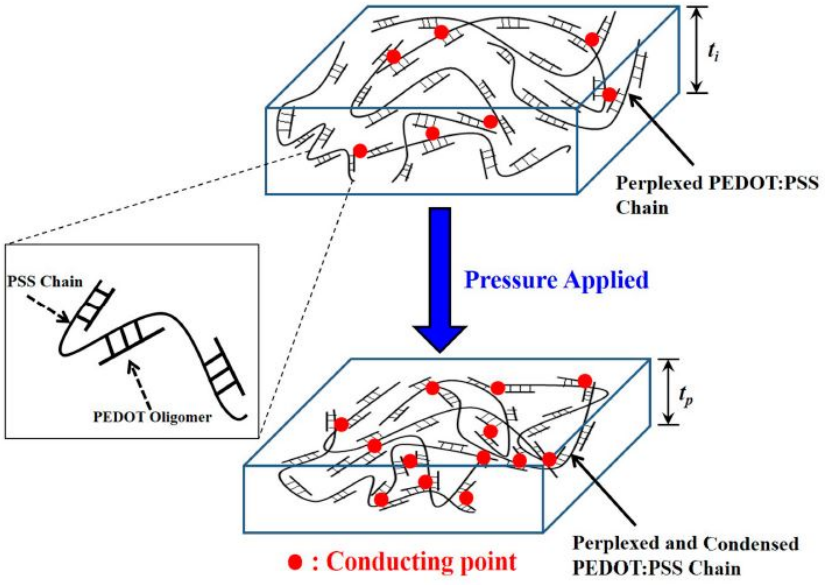

Figure 6.13: Conducting mechanism of the poly(3,4-ethylenedioxythiophene):polystyrene sulfonate (PEDOT:PSS) chains in the compressed mode. The red points illustrated the conducting points within the PEDOT:PSS. Perplexed PSS chain with connected PEDOT oligomers was shown in the enlarged figure [100].

It is possible to observe that the PEDOT oligomers (a molecular complex that consists of a few monomer units) are attached to the long perplexed PSS chain. As shown in chapter 2 the basic conducting mechanism of the PEDOT:PSS is nearest-neighbor hopping [101, 102]. When normal pressure is applied on the fabric soaked with PEDOT:PSS, the perplexed chain of PSS with the attached PEDOT is condensed from a thickness of t_i to t_p. Consequently, the possibility of carrier conduction is increased through the nearest-neighbor and non-nearest-neighbor PEDOT grains due to the reduced distance between PEDOT oligomers or the increased number of conducting points, as indicated by the red points in figure 6.13. This leads to the decrease of the resistivity of the PEDOT:PSS. Therefore, compressing the fabric treated with PEDOT:PSS the number contact points increases but there is a step beyond which its reaches a maximum value. From here on out, increasing the pressure, the resistance variation is related only to the thickness decreases.

6.6 Effect of different PEDOT:PSS formulation

The pressure sensors on cotton fabric are realized with the same structure and, eliminating the geometric factor that could affect the response, it is possible to evaluate the response by changing the PEDOT:PSS formulation. Figure 6.14 reports G/G_0 ratio for Clevios P and Cevios PH1000 formulations, and an example of linear fits performed at low and high pressure. These fits give the sensors sensitivity (the main results are reports in table 6.3). The theoretical model explained in the previous section is in agreement with these results.

The more conductive PEDOT:PSS formulations has many contact points and therefore responds immediately to the pressure, but they saturate soon. Conversely, the pristine PEDOT: PSS formulations have low conductivity and, when the applied pressure is low, there are few contact points. When the fabric is compressed, the contact points gradually increase and its response is linear in a wide pressure range.

In Clevios P pristine and with HC there are two different trend (figure 6.14 a) while in Clevios PH100 pristine and with HC there is not a different behavior between low and high pressure regime (figure 6.14 b). This effect is probably due to the presence of a great number of conductive points just in the pristine state.

The results reach in this section allow the realization of tunable textile pressure sensors based on PEDOT:PSS. Changing the conductivity of the PEDOT:PSS is possible to change the pressure response range. These behaviors allow to choose the best solution formulation according to the desired final applications.

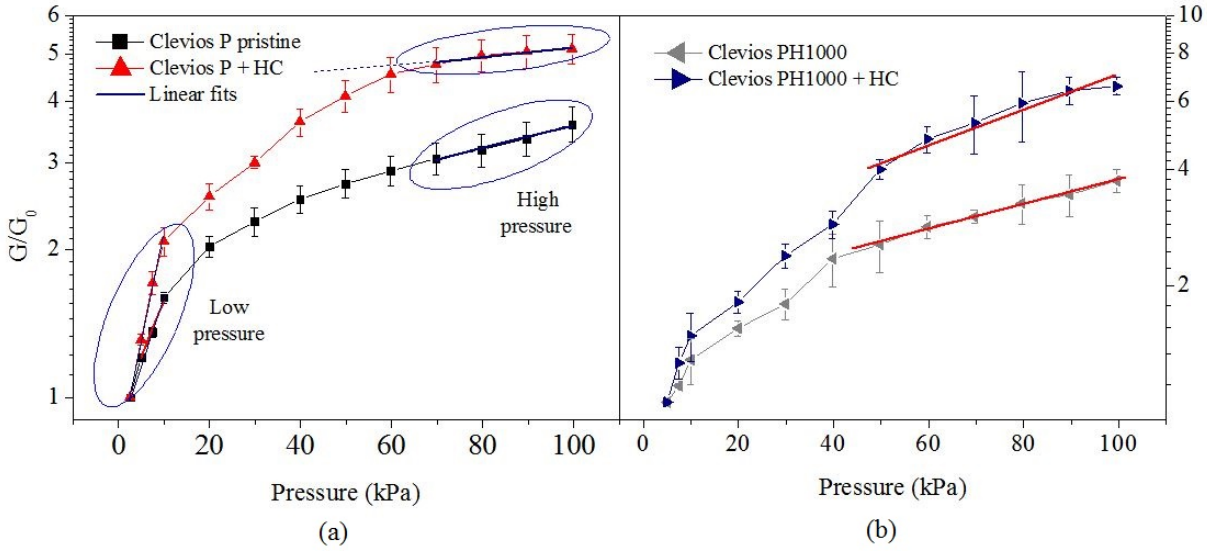

Figure 6.14: Trends of normalized conductance for Clevios P and Clevios PH1000 formulations and an example of the method used to obtained sensors sensitivity.

Formulation		$\frac{G/G_0}{P}$ $(\frac{1}{\text{kPa}})$	
		Low pressure	**High pressure**
Clevios P	pristine	0,054 ± 0,006	0,020 ± 0,002
	HC	0,09 ± 0,01	0,008 ± 0,001
Clevios PH1000	Pristine	0,04 ± 0,002	0,032 ± 0,001
	HC	0,05 ± 0,002	0,041 ± 0,004

Table 6.3: Slope values of linear fit in the low and high pressure regions for PEDOT:PSS formulations.

6.7 Application on HP-STF

In this section are reported the main results obtained from the electro-mechanical characterization of pressure sensors realized with the high performance sport technical fabric (a product of an Italian company). Starting from the model obtained from the cotton pressure sensors, it is possible to understand that, changing the conductivity of pristine formulation, different operation pressure ranges are obtained. Further, as showed in chapter 4, the deposition is closely related to the solvent present in the PEDOT:PSS dispersion. To combine these two effect, only four formulations are tested with the HP-STF : Clevios P (pristine and plus HC) and Clevios PH1000 + HC.

6.7.1 Fabrication

The HP-STF is a combination of a yellow elastic fabric thermoformed on top of a foam material, therefore the top and bottom faces are very different. The foam side is filled with holes in a density of 1,25 holes/cm^2 to allow transpiration of the fabric.. The foams can be made pressure sensitive by applying surface coatings and the application of pressure produces also a change in conductance due to an increase in volumetric contacts. According to its foam aspect, the drop-casting method is essential to allow solution diffusion into this system therefore, the conductive ink based on PEDOT:PSS is deposited with this technique. The screen printing method is not effective to soak the fabric due to its larger thickness (3 mm) and the dense conductive paste can not wet the textile from top to bottom.

For each formulations used, four pixels are deposited with drop casting methods. A 5 µL drop of conducting polymer solution has been dropped in- or off- holes like shown in figure 6.15. The geometry configuration used to realize the electrical contacts is the same described is section 6.1 and used in the cotton fabric pressure sensors.

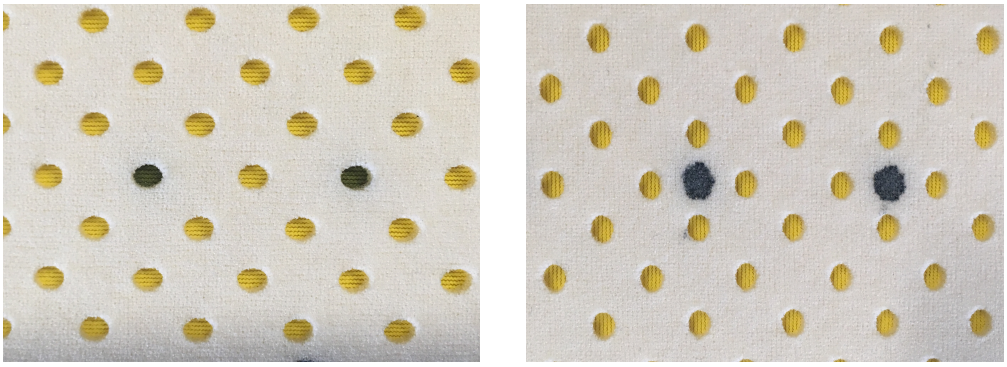

(a) (b)

Figure 6.15: *HP-STF* fabric treated with conductive solution based on PEDOT in (a) or out (b) of the holes.

6.7.2 Pressure sensors on HP-STF

According to its final application (detection of cyclist pressure distribution on a saddle), the pressure range of interest is between 10 kPa and 100 kPa (like reported in figure 6.1). The solution formulations developed until now are sensing in this range. The in- or off- hole deposition can change the response range and the sensitivity.

Figure 6.16 shows the normalized resistance (conductance) against applied pressure when the three formulations are deposited in- and off- hole.

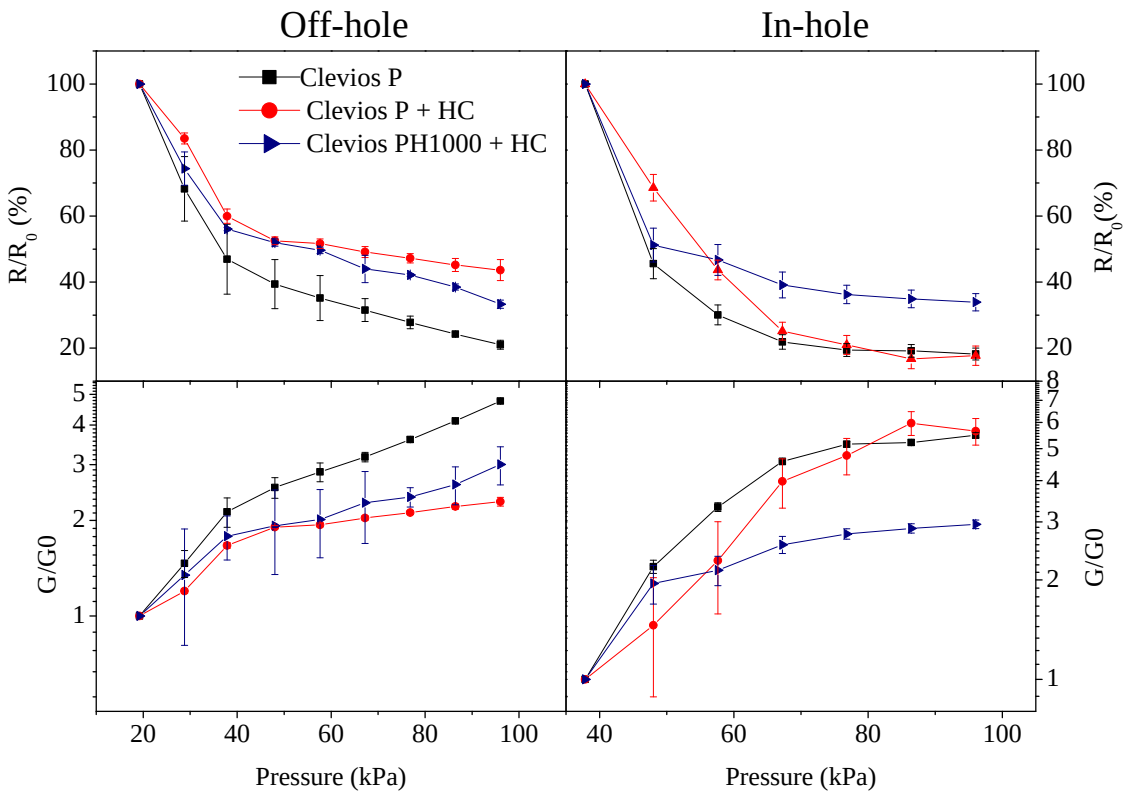

Figure 6.16: Normalized resistances (conductances) for the various formulation deposited on HP-STF. The graphs compare the response of the three different formulation in the off-hole and in the in-hole configuration.

In the off-hole case, the sample based on Clevios P has two distinct linear trends: the sensors sensitivity changes at 50 kPa but does not reach saturation. The samples with ethylene glycol (Clevios P + HC and Clevios PH1000 + HC) have a similar trend of those with pristine formulation, but a greater relative resistance variation R/R_0.

When the solution is deposited in-hole, only the sensing element based on Clevios P + HC has a linear trend between 40 kPa and 70 kPa; however, after that value, it saturates like the other samples. The in-hole configuration does not seem to be suitable to realize pressure sensors.

The main difference between the two configurations is that the in-hole configuration cannot detect low pressures. The presence of the hole requires enough pressure to make a contact between top and bottom conductive threads. Conversely, the off-hole configuration pressure sensors are sensitive also at pressure lower than 50 kPa.

Figure 6.17 reports a schematic cross section of the in-hole pressure sensors treated with conductive ink. This type of sensors measures the first resistance value when the normal pressure is $\sim$ 40 kPa.

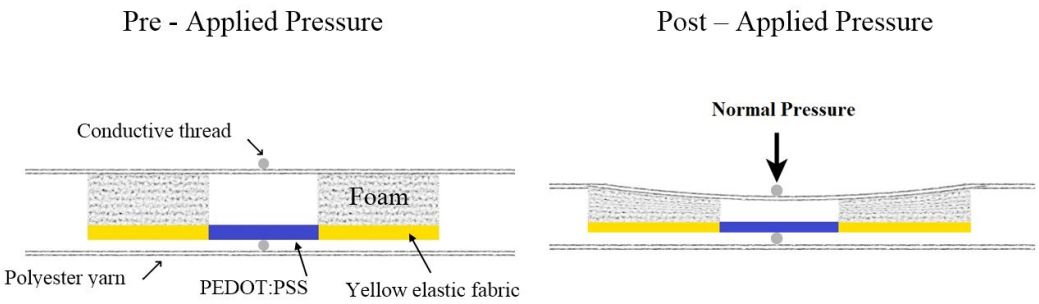

Figure 6.17: Schematic cross section of HP-STF sensing element with conductive solution deposited with drop casting method in the hole. When the pressure applied is low, the conductive threads (gray) do not contact each other.

As it is reported in figure 6.18, for Clevios P formulation, the in-hole configuration responses at high pressure and it reaches saturation at 80 kPa. In contrast, when the solution is deposited off-hole, the sensors do not saturate and it is possible to individuate two pressure ranges with a linear trend.

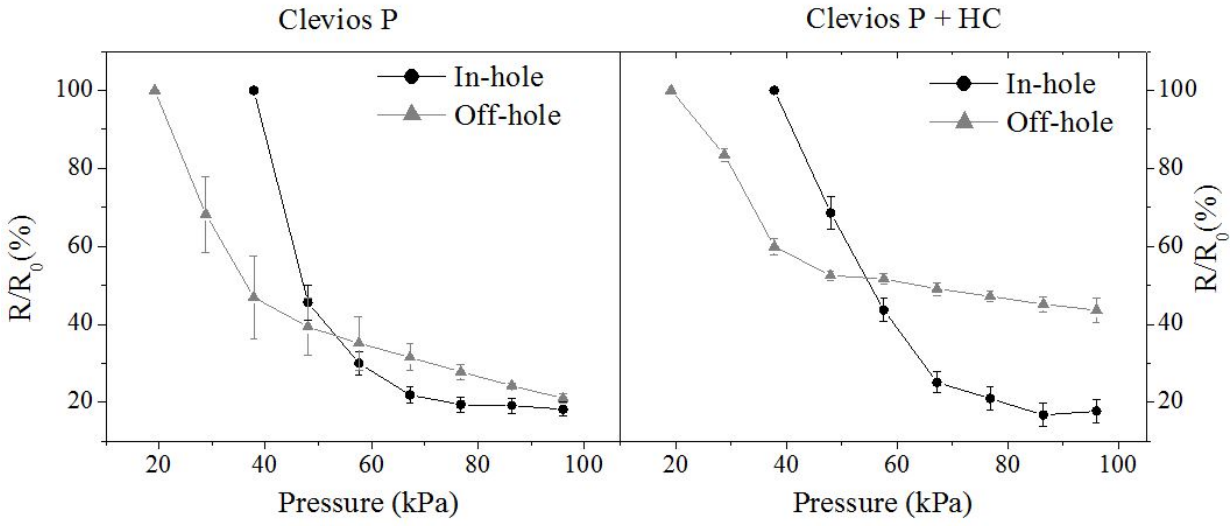

Figure 6.18: Comparison from the behavior of in- and off- hole configuration for Clevios P and Clevios P + HC formulations.

The sample treated with more conductive solution (Clevios P and high concentration of ethylene glycol) presents, at low pressure, a linear trend in both configurations but reaches saturation at 70 kPa. This behavior, when second dopant is present, is the same found for cotton pressure sensors.

The textile pressure sensors presented in this section, which are based on a commercial high performance sports elastic fabric, represent an example of a novel application of wearable technology in the sports world.

Chapter 7

Textile train sensors: fabrication and characterization

This chapter describes the fabrication, working principle and responses of a new kind of textile strain sensors. Strain sensors (or strain gauges) are devices that convert physical deformation into electrical signals. Traditional strain gauges are typically made of metals or rigid materials that offer limited stretchability and sensing range, making them unsuitable for practical applications if embedded within a textile structure.

Textile-based strain sensors are of particular importance: they exploit the functionality of traditional textiles such as flexibility and wearability, and at the same time are capable of sensing strains larger than 5%. Strain sensor textiles have important applications in body movement measurement [103], medical monitoring [104], sports rehabilitation and injury prevention [106], like just reported in section 1.4.2.

Several key factors must be considered in designing strain sensor textiles. The sensors should have high sensitivity (significant changes in the sensing response at different stretching conditions), high stability (repeatability of the sensing signals over many cycles) and large sensing range to cover the applied strain of the desired applications. To ensure a low time constant in the sensor response, the sensor structure should have high elastic properties and should be able to recover rapidly from the deformation. Finally, the sensor should be easily manufactured in large scale. A common mechanism of strain sensing is via resistive changes in the sensor device by strain to meet all the requirements: ease of fabrication, simplicity of the sensing, large sensing range, high stability, and high sensitivity.

In the textile resistive strain sensor, the textile sensitive element serves as a resistor when a voltage is applied and it changes its electrical properties with respect to the magnitude of the applied strain. Performance of the resulting strain sensor

is related to its fabrication, structure, and to the sensing behavior of its components. Textile strain sensors can be produced at the fiber or yarn levels and they can be knitting or weaving conducting to realize a co fibers or yarns [107]. Another method of fabricating strain sensor textiles is by coating a fabric with conducting materials such as polypyrrole, poly(3,4ethylenedioxythiophene):poly(styrenesulfonate) (PEDOT:PSS), and carbon nanotubes.

The strain sensors presented in this thesis are based on elastic fabric coated with PEDOT:PSS. They have a working range between low percentage deformation ($\sim$ 5%) and 60%. As the PEDOT:PSS-coated textiles conform to the shape of the human body, they work ideally as wearable biomechanical sensors that can be used in a range of applications to monitor human motion (intelligent knee sleeve [106] or wrist motion detector) or in personalized health-monitoring to realize breathing sensors.

7.1 Fabrication of fabric strain sensors

It is reported in chapter 6 that the presence of conductive elements gives piezoresistive properties to coated material and this enables the detection of local strain on the fabric. The textile used as substrate to develop the strain sensors is a knitted elastic fabric (EF). The EF is treated with the conductive polymer PEDOT:PSS, and four different formulations are used: CLevios P pristine, Clevios P + HC (high concentration of ethylene glycol), Clevios PH1000 pristine, Clevios PH1000 + HC. The solutions are placed in a sonic bath before and after the addition of EG. The PEDOT:PSS solutions are heated in an oven at 70 °C to halve their weight and increase its density. The fabrication of strain sensors over the elastic textile substrate has been done by screen printing technique, *serigraphy*, explained in 3.3.2. The pattern printed on textile has a rectangular form of 2,0 x 0,8 cm^2 and the fabric has been cut near the active area. After the deposition, the samples are heated in an oven at 70°C for 15 minutes. Figure 7.1 reports photographs of the samples: the zoomed images are realized with a CCD camera placed on an optical microscopy. To properly connect the sensor and record electrical response during strain, a 3-ply conductive thread (hand-sewn) realizes two terminal contacts in the opposite edges of the long side.

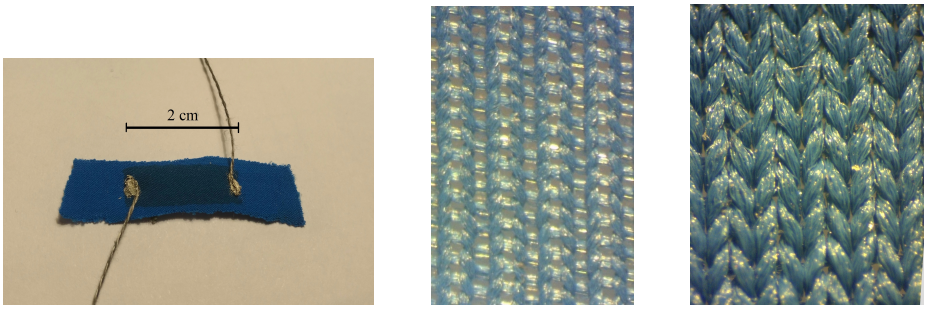

(a) (b) (c)

Figure 7.1: a) Strain sensor based on elastic fabric: optical microscope images of fabric (b) before stretching and (c) under ca. 40% stretching

7.2 Electrical-mechanical characterization

The electromechanical properties of the knitted textiles are evaluated by monitoring in situ the resistance using a digital multimeter (*Kethley 2400*) during cyclic deformations applied by a tensile testing instrument (DMA Q800 and an home-made experimental set up). A 3 cm-long knitted textile is used for electromechanical testing. This greater length is chosen to achieve the clamping in the non-covered textile area in the tensile testing instrument.

Before performing the electrical-mechanical analysis, it is useful recall the mechanical results reported in Chapter 5 about this elastic fabric. Since it is a knitted fabric, it has two elongation directions called "wale" and "course". The fabric strain sensors developed here are along the wale direction and the stress-strain curve presents a J-shape trend. Two different electro-mechanical experiments are performed on the strain sensors using the more suitable instrumentation: range and stability test.

The home-made set up allows the application of greater strains (up to 60%) to study the sensors response over a wide range. The textile is clamped on the home-made tensile instrument (figure 7.2 shows a brief view of its working principle), using tapes on the top and bottom clamps. A heat-shrinkable sleeve covers the conductive threads to avoid short circuit. These wires are then connected to the digital multimeter using alligator clips and the resistance signal is acquired on a personal computer using a GPIB interface.

This test (referred to as the range test) involved stretching of the textile to different applied strain magnitudes. The applied strain is increased from 0 % to about 60 % (the maximum value depends on the sample) in $\sim$ 4 % incremental steps. The textile is linearly stretched to the desired strain with a relaxation time of 10 s before increasing again the deformation. The resistance value is measured after

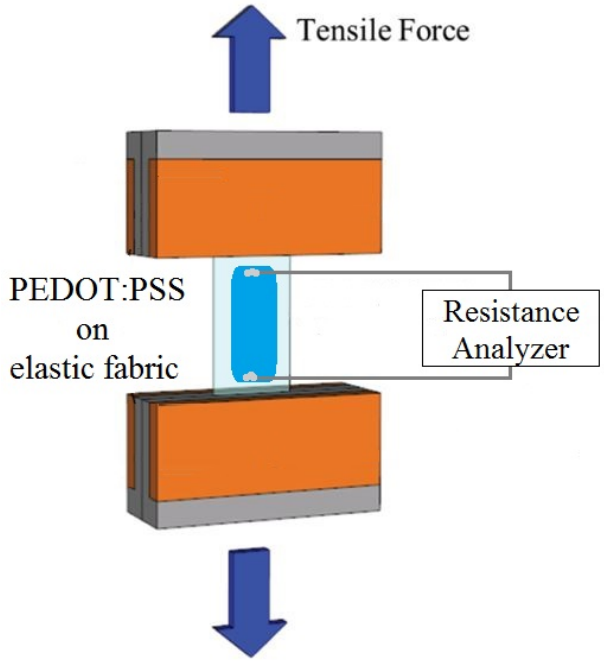

Figure 7.2: Experimental set-up for the in situ measurement of the electrical resistance of PEDOT:PSS coated elastic fabric during the tensile stretching.

5 s in order to allow the electrical stabilization.

To better understand the stability of the reported textile strain sensors, a second type of test has been carried out by means DMA Q800. This instrument allows the application of small deformations (up to 10%): two similar stability test are performed.

In the first test, the textile is stretched to 5% strain, then rest for 60 s before relaxing to zero strain. This relaxation time is introduced both after each loading and after each unloading step, and the test is carried out for 3 cycles (figure 7.3 a). In the second test, the textile is stretched to 10% strain and then allowed to relax (zero strain), without relaxation time from each loading and unloading step (figure 7.3 b). The strain speed, in both test, is 2%/min. During deformation, the sample resistance is measured through a source meter controlled by a custom-coded program in LabView. The DMA allows to do cyclical tests: the two tests described gives informations about how the sensors respond during a continuous stress application or when relaxation stage are present: these situations might have two different behaviors. In all experiments the samples are supplied with a current of 1 µA and the sampling time to acquire resistance values is 200 µs.

An important parameter to characterize the behavior of a strain sensors is called Gauge Factor (GF). The GF, defined as the fractional change in resistance per de-

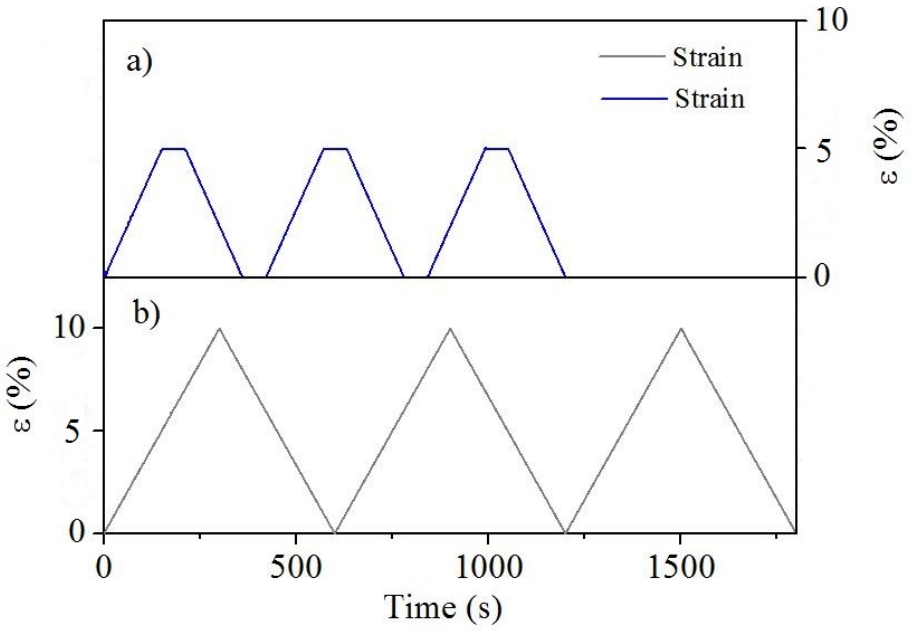

Figure 7.3: a) Strain ramp up to 5% with a relaxation time of 60 s from each loading and unloading step. The cycles have a duration of 1260 s; b) strain ramp up to 10% without relaxation time: the cycles have a duration of 1800 s.

formation unit, translates the resistance changes in the material as a function of the deformation caused by the applied mechanical stress [108], and is given by:

$$GF = \frac{\frac{R-R_0}{R_0}}{\epsilon} \tag{7.1}$$

where R_0 is the resistance of the sample before deformation. This parameter gives the sensitivity of the strain sensor and it is critical to assess the use of the sensor according to its applications. Typical commercial strain sensors, like metal foil or thin film metal (e.g. constantan) strain gauge have GF between 2 and 5.

7.3 Results

In order to develop an effective and textile strain sensor, it is necessary to study the sensing mechanisms of the conductive fabric. In this section, the strain sensing behavior of PEDOT:PSS-coated knitted fabric is studied, and the sensing mechanisms are investigated through the range and the stability test.

7.3.1 Range test on textile strain sensors

To characterize the strain sensors response in a wide range of deformation, four different samples, one for each PEDOT:PSS formulation, are studied with the home-made set up to reach high strain values. Formulations based on different solvents imply different coating on fabric. In order to properly investigate the performance of textile strain sensors fabricated on a new elastic fabric, both formulations of PEDOT:PSS Clevios P and PH1000, isopropanol and water dispersion, have been investigated. Moreover, to understand the effect of additive, the highest concentration has been evaluated.

Figure 7.4 reports the relative resistance variation against strain for the different formulations used. The resistance of the sample decreases when strain applied increases and this leads to a negative GF. Figure 7.4 a) shows the behaviors of Clevios P pristine and the other formulation with EG, while figure 7.4 b) reports the trend for Clevios PH1000 pristine and the other formulation with high concentration of EG. The sensors sensitivity is described by the GF and a linear relationship between $\Delta R/R_0$ and ϵ is obtained for both doped formulations with slope equal to GF (the GF values are reported near the trend line and in the table 7.1) but they present a lower GF compared to pristine formulation. The Clevios P + HC formulation has a GF two times larger than Clevios PH1000 + HC formulation.

Formulation		**GF**
Clevios P	pristine	l.s. (-1,3 ± 0,1) — h.s. (-0,45 ± 0,04)
	HC	-0,34 ± 0,02
Clevios PH1000	pristine	l.s. (-1,3 ± 0,2) — h.s. (-0,53 ± 0,03)
	HC	-0,53 ± 0,03

Table 7.1: Gauge factors for PEDOT:PSS coated elastic fabric strain sensors. (low strain=l.s.; high strain=h.s.)

It shows that this conductive fabrics have good sensing behavior and repeatability in the strain allowance. For the pristine formulations, the relationship between $\Delta R/R_0$ and the strain is nonlinear, reflecting a varying GF with the strain level. To determine the GF, the curves are divided in two regions. At low pressure, the two pristine states present the same GF value; at high pressure, the GF of Clevios PH1000 pristine is ∼18% greater than Clevios P pristine formulation.

There does not seem to be any difference in the deposition of the two materials although they have different solvents. From the strain response point of view, results like that, imply that it is not only the electrical conductivity that changes the performance, rather the effect of the additive seems to have the same effect on the

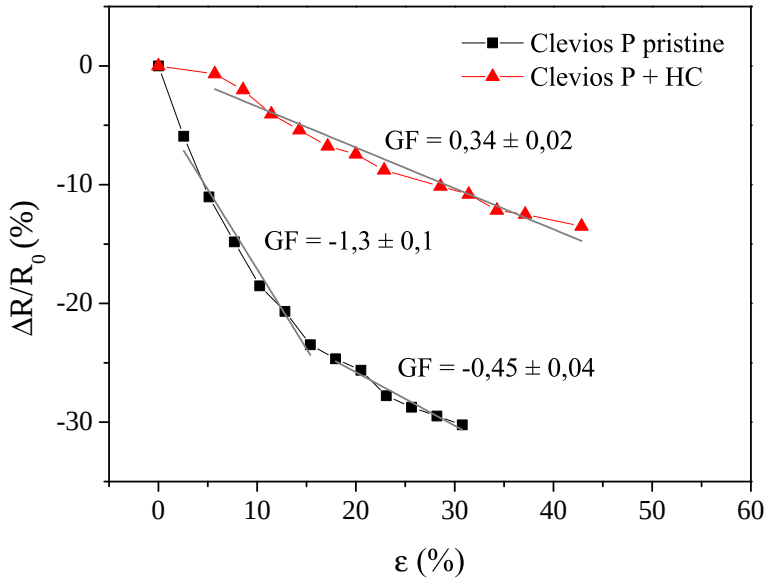

(a)

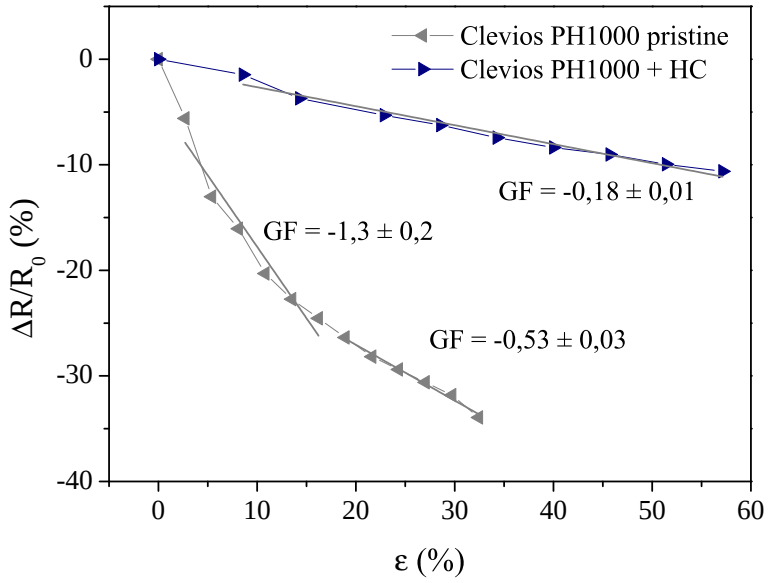

(b)

Figure 7.4: Relative resistance variation against strain for a) Clevios P based formulations and b) Clevios PH1000 based formulations. The GF are calculated with a linear fits. The pristine formulations have two different trends.

two formulations. To better understand what happens, further measurements (e.g. SEM images) are needed to understand the distribution of the coating in the fabric fibers.

7.3.2 Stability test on textile strain sensors

From the previous chapter, it appears clear that the concentration of additive in the pristine formulation of PEDOT:PSS allow to change their electrical properties and piezoelectric behavior. In order to evaluate the stability e reliability of the textile strain sensors, multi-cycles have been examined. As a results, the response is high stable during 3 cycles from 0% up to 10% of strain.

Since the stability tests show a behavior that depends mainly from the fabric elastic properties, similar results for the other formulations have been obtained. As an example to investigate these features, the experiments performed on elastic fabric coated with Clevios P pristine formulation are reported.

Figure 7.5 reports two different stability tests performed on the elastic strain sensor using DMA Q800 to apply the tensile stress, and gives the resistance variation in the wale directions with time under cyclic load.

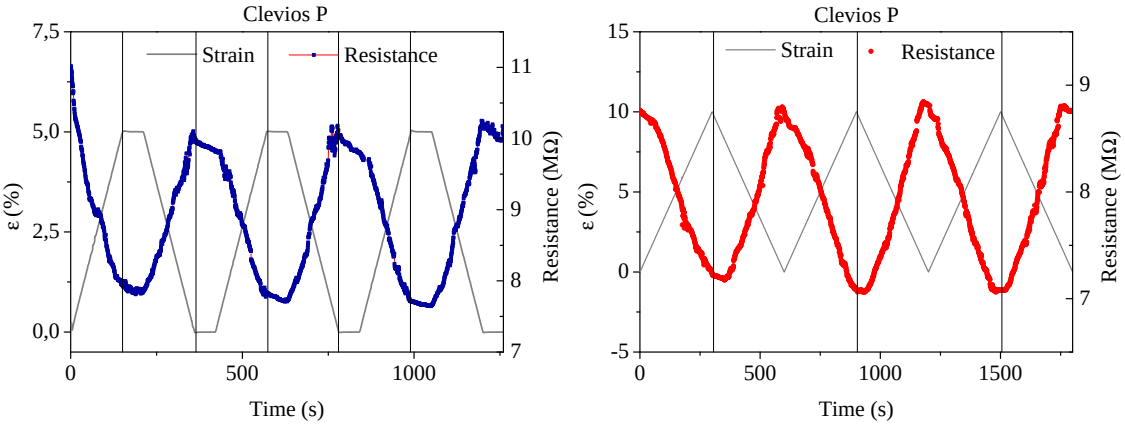

Figure 7.5: Stability test: a) cycle strain ramp until 5% and the resistance trend during deformation. The relaxation time between loading and unloading step is 60s; b) cycle strain ramp up to 10% without relaxation time between two consecutive cycle. The strain speed is 2%/min.

In both tests, the resistance variation caused by sample deformation is measured. When the deformation increases, the resistance of the sample decreases. Figure 7.5 a) shows that after one cycle, when the strain returns to zero, the resistance value does not remain constant but it undergoes a negative drift of $\sim 4\%$ (as highlighted in figure). Figure 7.5 b) reports a similar test with strain up to 10%. The load ramps of this three cycles are used to calculate the GF. At every unitary percentage deformation (for a total of 10 points) the resistance values are extracted from the graph in figure 7.5 b); these results are then combined in figure 7.6, which reports

the trend of relative resistance variation for the three loading cycle against strain. As it can be denoted, they have the same trend and this is confirmed by the value of GF (table 7.2).

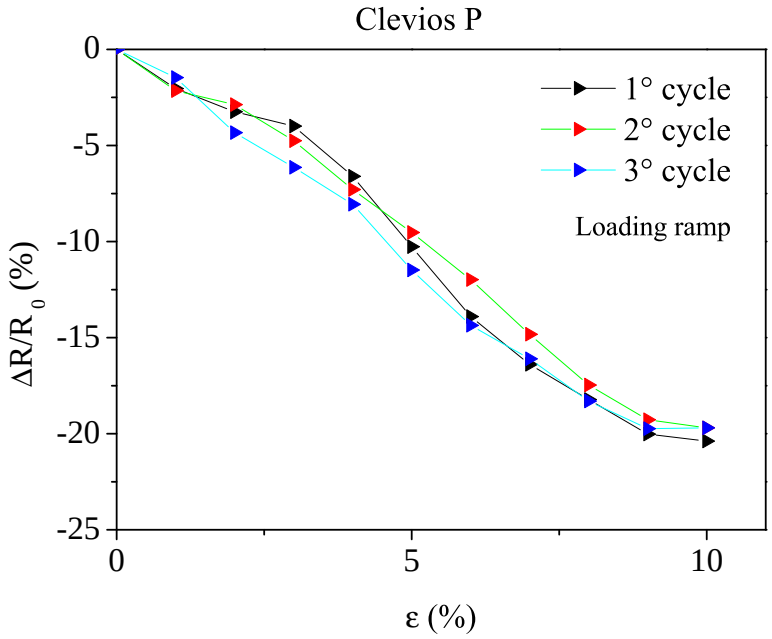

Figure 7.6: Relative resistance variation of Clevios P pristine deposited on elastic fabric during loading ramp. Three consecutive cycles are examined.

Cycle	**Gauge Factor**
1°	-2,3 ± 0,1
2°	-2,19 ± 0,08
3°	-2,2 ± 0,1

Table 7.2: Gauge factors of Clevios P pristine coated elastic fabric for three consecutive cycles.

These measurements show that PEDOT:PSS coated elastic fabric can be used to realize strain sensors with high stability.

7.3.3 Interpretation of textile strain sensors mechanism

The electro-mechanical behavior of the knitted textile is correlated to the possible deformations that occur within its structure. A knitted textile is made up of interlocks of rows (course) and columns (wale) of loops (figure 7.7 a). Each loop consists of a head, two legs, and two sinker loops that join the adjacent loops. The

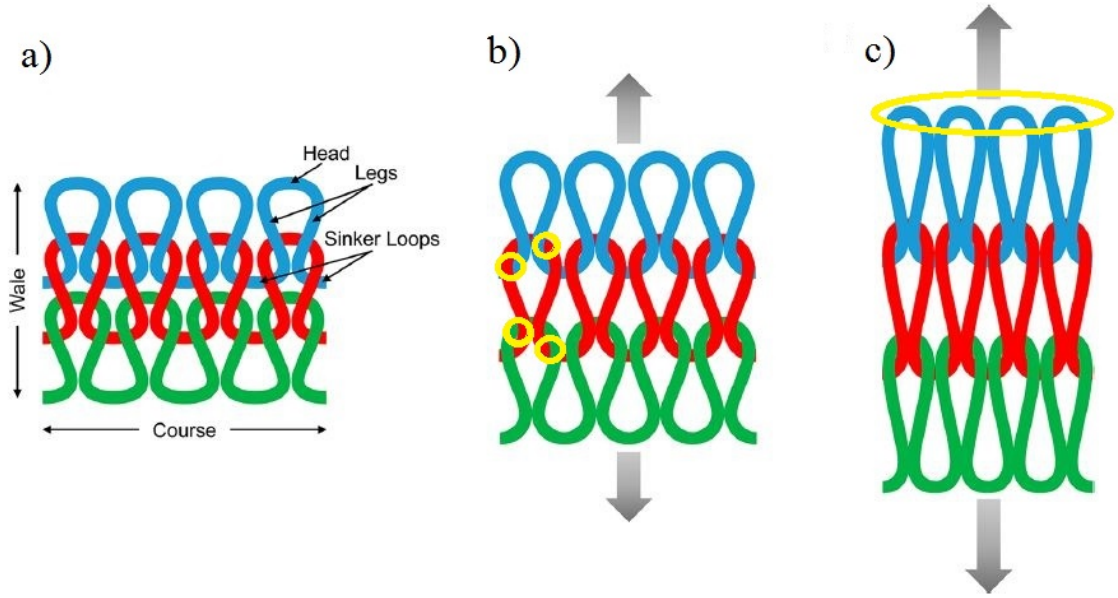

Figure 7.7: Schematic illustration of a weft-knitted textile with plain stitches at (a) unstretched and (b and c) different stretched states. Stretching is applied along the wale direction.

difference in deformation properties along the course and wale directions results in an anisotropic property in the textile. The height and width of the loop can be transferred under tension because of the large inter-space in knitted fabric.

The strain sensing properties of the knitted textiles coated with PEDOT:PSS are evaluated along the wale direction because the sensitivity and deformation range of a knitted sensor textile in this direction is much larger than the course direction. Considering two neighboring loops as example, four deformation steps can occur: slippage, increasing number of contacted fibers, bending, and stretching of the yarns. These deformation steps can be described as:

- length of the yarns can transfer between the arc segment and legs of a loop;
- at the contact point, the slipping caused reposition and redistribution of the fibers to be contacted (figure 7.7 b);
- yarns are bent during deformation and the curvatures of the fibers change (figure 7.7 c);
- at high strain, also the yarns are stretched.

It should be noticed that there are no clear demarcation points among the four stages. In order to explain the resistance variation during tension process, in this

section it will only discuss the contribution to the electrical resistance variation from the contact resistance.

The structural deformation development is shown in figure 7.7 when subjected to load along wale direction. In a *woven structure*, the resistance of the textile is independent of the fiber/yarn contact resistance while, in a knitted structure, the contact resistance plays an important role. In this textiles, the conducting fiber in a loop makes contact with the adjacent loops at the heads, legs and sinker loops. The contact resistance (R_c) between the two fibers can be described by the Holm's theory [109]:

$$R_c = \frac{\rho}{2}\sqrt{\frac{\pi H}{nP}} \tag{7.2}$$

where ρ is the resistivity of the fiber, n is the number of contact points (related to the number of PEDOT:PSS fibers in the knitted textile), P is the contact pressure, and H is the fiber contact hardness. Stretching the textile in the wale direction results in an increased contact pressure P between the interlocked fibers. Equation 7.2 shows that in a knitted textile, the contact resistance R_c of the fibers at the interlocks is indirect proportional to contact pressure P and the number of contact points n for a given fiber (assuming constant resistivity and hardness).

The decrease in resistance of the PEDOT:PSS coated textiles upon stretching can be attributed to the lowering of interfiber contact resistance due to the enhanced contact pressure in the stretched state. This results in the negative GF behavior of the knitted textiles.

Moreover, when a knitted textile is subjected to an uniaxial tensile strain in the wale direction, at a certain strain value the component yarns start to stretch. When this stage is reached, the sample resistance increase. Table 7.3 reports the initial resistance R_0, the maximum strain ϵ_m since begins the increase of resistance, and the unloading resistance R_f when the fabric returns in the un-stretched configuration. The difference in rest resistance for the different formulation is in agreement with results reported in chapter 4. It is possible to notice that, when the stretch is released, the un-stretched resistance increase because a large strain cause a permanent textile deformation.

Functional wearable textile sensing systems can monitor human motion, provide immediate, individual and objective biofeedback to the wearer without changing mechanical properties of fabric materials and without interfering with normal human body motion. When the coated fabric is stretched, the resistance will change with deformation. The different formulations of conductive inks leads to strain sensors with different behaviors. This theoretical model is a first approximation to explain

Formulation		R_0 (MΩ)	ϵ_m	R_f (MΩ)
Clevios P	pristine	1440	90%	1650
	HC	4,4	90%	5,4
Clevios PH1000	pristine	42,3	135%	58
	HC	0,681	62%	0,747

Table 7.3: Initial resistance R_0, maximum strain ϵ_m and unloading resistance R_f to the four tested elastic fabrics.

the behavior of this textile strain sensors, but further efforts are needed in order to understand the effect of EG on the sensors properties. The works in progress can achieve more details and an in-deep understanding of different cases.

In conclusion, the sensors presented in this work, with their high sensitivity, pave the way for developing new textile strain sensors for a great number of further potential applications which could be used for daily living, work and recreation.

Conclusions

The world of wearable electronics is an expanding field: in the recent years there has been considerable research effort devoted to the development of flexible and stretchable wearable sensors, in order to fulfill the requirements of future technology. The main scope is to measure and quantify signals generated by the human body for diagnosis, therapy, personal health-care, physiological and human-activity monitoring.

The fully textile wearable pressure and strain sensors developed in this work, are based on an organic conductive polymer (PEDOT:PSS) deposited into fabric by screen printing or drop-casting methods. Moreover, a model to describe the working mechanism of textile wearable pressure and strain sensors has been proposed in order to explain the behaviors in different pressure and deformation ranges.

The working principle of textile pressure sensors has been investigated using cotton fabric as substrate. By fixing the geometry configuration of textile sensing elements and changing the formulation of the active material, it is possible to investigate the pressure sensors response in order to realize tunable devices. The electrical electrical properties of fabric substrate treated with different conductive solution formulations are compare with PEDOT:PSS thin film deposited on glass. Similar trend in conductivity respect ethylene glycol concentration is obtained. Morphological characterization, performed via atomic force microscope and scanning electron microscope gives information about the structure of coated fibers that compose the woven fabric.

To properly describe the working mechanism of textile sensors, the intrinsic textile deformation during the application of an external stress has to be taken into account. Then, a purely mechanical characterization of the fabric used is needed to correlate it with the textile sensors performance.

Both deposition methods has been used to realize pressure sensors on cotton fabric and the final devices presents the same behavior. However, the drop casting technique represents the most efficient deposition method to functionalize every type of fabric substrate. The sensing element, combined with few stitching lines of

stainless steel threads, allows the realization of cotton pressure sensors.

The results of electro-mechanical characterization of textile pressure sensors based on different formulation can be explained with a theoretical model that describes the piezoresistive behavior of PEDOT:PSS. When the external normal pressure applied on the sensing elements increases, the electrical device resistance decreases due to its geometry configuration. The sensors realized with PEDOT:PSS mixed with ethylene glycol present a higher conductive feature with respect to the sensors based on the pristine solution. The ethylene glycol, which acts as second dopant, increase the number of contact points when the polymer chains are approaching under the action of an external pressure. The presence of a larger number of contact points leads to pressure sensors that saturate when the applied compression stress is sufficiently high ($>$ 70 kPa). Instead, the sensors based on pristine solution has low amount of conductive points, a lower conductance and consequently they response at high pressure (over 70 kPa).

The drop casting deposition methods, PEDOT:PSS formulations and geometry configuration studied for cotton sensors can be used to realize pressure sensing elements on a sport technical elastic fabric. The sensors based on this fabric allow the realization of cycling short that can monitor the cyclist pressure distribution on the saddle.

These devices have a behavior comparable to the pressure sensors based on cotton fabric and their features can be described with the same model. In fact, the electro-mechanical characterization shows that the sensing response is affected by solution formulation, and that the presence of ethylene glycol leads to more sensitive pressure sensors.

Nevertheless, the high performance sport textile is a more complex substrate and the pressure sensors can be fabricate in different configuration. For a complete description of sensor behavior the fabric features should be taken into account. To better explain the sensing behavior of these textile pressure sensors and achieve an in-deep knowledge of their working principles, further work is needed, e.g.: study of hydrophilic properties, dependence on solvent used and morphological analysis of the fibers coated with the conductive solution.

Moreover, the elastic fabrics are widely used to fabricate flexible strain sensors because of their high flexibility. In this thesis, to fabricate flexible strain sensing fabrics, the screen printing technique is used to coat the textile with the conductive polymers. Different solutions based on PEDOT:PSS and ethylene glycol endow elastic fabric with electrical conductivity. As been demonstrated, the mechanical properties of fabrics do not change after surface modification. The fabricated strain sensors exhibit good sensitivity (a gouge factor of $\sim$ 1,4 comparable with standard

strain gauge), a large workable strain range (0 - 60 %) and great stability. A theoretical model is developed to explain the resistance decrease when the strain linearly increases. It is based on fabric properties and on the wale-course structure deformations typical of knitted textiles. Future works should be focused to determine relationship between electrical properties of PEDOT:PSS formulations (with or without the ethylene glycol) and the strain behavior.

The results reached in this work allow the realization of tunable textile pressure sensors based on PEDOT:PSS. The simple configuration permits to fabricate pressure sensors directly embedded on textile resulting imperceptible from the outside. Moreover, by changing the conductivity of the PEDOT:PSS it is possible to change the pressure response range leaving the same geometry. These behaviors allow to choose the best solution formulation according to the desired final applications without loosing comfort. In addition, it has been demonstrated the production of strain sensors on elastic fabric with wide strain sensing capabilities that may be suitable for applications in wearable bionics and stretchable electronics.

In summary, although further work is required to optimize the sensors when fabricated on different fabrics, the results obtained in this thesis demonstrate that this textile sensors are promising to be applied on several applications. These results pave the way to develop new wearable sensors that may bring a technical revolution to daily life in the near future.

Bibliography

[1] W. Weng, P. Chen, S. He, X. Sun, H. Peng, *Smart Electronic Textiles*, Angew. Chem. Int. Ed. **2016**, 55, 6140 –6169.

[2] W. Zeng, L. Shu, Q. Li, S. Chen, F. Wang, X.M. Tao, *Fiber-based wearable electronics: a review of materials, fabrication, devices, and applications*, Adv. Mater. 26 (**2014**) 5310–5336.

[3] M. Amjadi, K.U. Kyung, I. Park, M. *Sitti, Skin-mountable, and wearable strain sensors and their potential applications: a review*, Adv. Funct. Mater. 26 (**2016**) 1678–1698.

[4] M. J. McGrath, C. N. Scanaill, D. Nafus, *Sensor Technologies: Healthcare, Wellness and Environmental Applications*, Apress, **2013**, 99.

[5] S. C. Mulkhopadhyway, *Wearable electronics sensors for safe and healthy living*, Springer, **2015**.

[6] M. Parrilla, R. Canovas, I. Jeerapan, F. J. Andrade, J.A. Wang, *Textile-Based Stretchable Multi-Ion Potentiometric Sensor*, Adv. Healthcare Mater. 2016, 5(9), 996-1001.

[7] A. Panneer Selvam, S. Muthukumar, V. Kamakoti, S. Prasad, *A wearable biochemical sensor for monitoring alcohol consumption lifestyle through Ethyl glucuronide (EtG) detection in human sweat*, Sci. Rep., **2016**, 6, 23111.

[8] J. Kim, W. R. de Araujo, I. A. Samek, A. J. Bandodkar, A. J, W. Jia, B. Brunetti, R. L. C. Paixao, J. Wang, *Wearable tattoo sensor for real- time trace-metal monitoring in human sweat* Electrochem. Commun., **2015**, 51, 41-46.

[9] T. Seesaard, P. Lorwongtragool, T. Kerdcharoen, *Development of fabric-based chemical gas sensors for use as wearable electronic noses*, Sensors **2015**, 15, 1885-1902.

[10] G.Liu, C. Ho, N. Slappey, Z. Zhou, S. E. Snelgrove, M. Brown, A. Grabinski, X. Guo, Y. Chen, K. Miller, J. Edwards, T. Kaya, *A wearable conductivity sensor for wireless real-time sweat monitoring*, Sens. Actuators, B **2016**, 227, 35-42.

[11] R. C. Reid, S. R. Jones, D. P. Hickey, S. D. Minteer, B. K. Gale, *Modeling carbon nanotube connectivity and surface activity in a contact lens biofuel cell*, Electrochim. Acta **2016**, 203, 30-40.

[12] J. Kim, S. Imani, W. R. de Araujo, J. Warchall, G. Valdes- Ramirez, T. R. L. C. Paixao, P. P. Mercier, J Wang, *Wearable salivary uric acid mouthguard biosensor with integrated wireless electronics*, Biosens. Bioelectron., **2015**, 74, 1061-1068.

[13] S. Gong, W. Schwalb, Y. Wang, Y. Chen, Y. Tang, J. Si, B. Shirinzadeh, W. Cheng, *A wearable and highly sensitive pressure sensor with ultrathin gold nanowires*, Nat. Commun., **2014**, 5, 3132.

[14] C. Pang, J. H. Koo, A. Nguyen, J. M. Caves, M.-G. Kim, A. Chortos, K. Kim, P. J. Wang, J. B. H. Tok, Z. Bao, *Highly skin-conformal microhairy sensor for pulse signal amplification*, Adv. Mater. **2015**, 27, 634.

[15] D. Kang, P. V. Pikhitsa, Y. W. Choi, C. Lee, S. S. Shin, L. Piao, B. Park, K.-Y. Suh, T.-i. Kim, M. Choi, *Ultrasensitive mechanical crack-based sensor inspired by the spider sensory system*, Nature **2014**, 516, 222.

[16] J.-W. Jeong, W.-H. Yeo, A. Akhtar, J. J. S. Norton, Y.-J. Kwack, S. Li, S.-Y. Jung, Y. Su, W. Lee, J. Xia, H. Cheng, Y. Huang, W.-S. Choi, T. Bretl, J. A. Rogers, *Materials and optimized designs for human-machine interfaces via epidermal electronics*, Adv. Mater., **2013**, 25, 6839.

[17] M. Amjadi, A. Pichitpajongkit, S. Lee, S. Ryu, I. Park, *Highly stretchable and sensitive strain sensor based on silver nanowire-elastomer nanocomposite*, ACS Nano, **2014**, 8, 5154 .

[18] R. C. Webb, A. P. Bonifas, A. Behnaz, Y. Zhang, K. J. Yu, H. Cheng, M. Shi, Z. Bian, Z. Liu, Y.-S. Kim, W.-H. Yeo, J. S. Park, J. Song, Y. Li, Y. Huang, A. M. Gorbach, J. A. Rogers, *Ultrathin conformal devices for precise and continuous thermal characterization of human skin*, Nat. Mater., 2013, 12, 938.

[19] T. Q. Trung, N. E. Lee, *Flexible and Stretchable Physical Sensor Integrated Platforms for Wearable Human-Activity Monitoring and Personal Healthcare*, Advanced Materials, 28, 4338-4372, **2016**.

[20] Y. Zang, F. Zhang, C. Di, D. Zhu*Advances of flexible pressure sensors toward artificial intelligence and health care applications*, Mater. Horizon, **2015**, 2, 140.

[21] S.C. Mannsfeld, B.C. Tee, R.M. Stoltenberg, C.V. Chen, S. Barman, B.V. Muir, A.N. Sokolov, C. Reese, Z. Bao, *Highly sensitive flexible pressure sensors with microstructured rubber dielectric layers*, Nat Mater, **2010**, 9(10), 859-64.

[22] C. Dagdeviren , Y. Su , P. Joe , R. Yona , Y. Liu , Y.-S. Kim , Y. Huang , A. R. Damadoran , J. Xia , L. W. Martin , Y. Huang , J. A. Rogers, *Conformable amplified lead zirconate titanate sensors with enhanced piezoelectric response for cutaneous pressure monitoring* Nat. Commun. **2014**, 5, 4496 .

[23] J. Park, Y. Lee, J. Hong, M. Ha, Y. D. Jung, H. Lim, S. Y. Kim, H. Ko, *Giant Tunneling Piezoresistance of Composite Elastomers with Interlocked Microdome Arrays for Ultrasensitive and Multimodal Electronic Skins*, ACS Nano **2014**, 8, 4689.

[24] X. Wang, Y. Gu, Z. Xiong, Z. Cui, T. Zhang, *Silk-Molded Flexible, Ultrasensitive, and Highly Stable Electronic Skin for Monitoring Human Physiological Signals*, Adv. Mater, **2014**, 26, 1336 .

[25] Q. Wang, M. Jian, C. Wang, Y. Zhang, *Carbonized Silk Nanofiber Membrane for Transparent and Sensitive Electronic Skin*, Adv. Func. Mat., 27 (9), **2017**.

[26] B. C. K. Tee, C. Wang, R. Allen, Z. Bao, *Flexible polymer transistors with high pressuresensitivity for application in electronic skin andhealth monitoring* Nat Nanotechnol, **2012**, 7, 825.

[27] C.-L. Choong, M.-B. Shim, B.-S. Lee, S. Jeon, D.-S. Ko, T.-H. Kang, J. Bae, S. H. Lee, K.-E. Byun, J. Im, Y. J. Jeong, C. E. Park, J.-J. Park, U. I. Chung, *Highly stretchable resistive pressure sensors using a conductive elastomeric composite on a micropyramid array*, Adv. Mater. **2014**, 26, 3451 .

[28] Y. Yang, H. Zhang, Z.-H. Lin, Y. S. Zhou, Q. Jing, Y. Su, J. Yang, J. Chen, C. Hu, Z. L. Wang, *Human skin based triboelectric nanogenerators for harvesting biomechanical energy and as self-powered active tactile sensor system*, ACS Nano **2013**, 7, 9213.

[29] X. Wang, T. Li, J. Adams, J. Yang, *Transparent, stretchable, carbon-nanotube-inlaid conductors enabled by standard replication technology for capacitive pressure, strain and touch sensors*, J. Mater. Chem. A **2013**, 1, 3580.

[30] S. Yao, Y. Zhu, *Wearable multifunctional sensors using printed stretchable conductors made of silver nanowires.*, Nanoscale **2014**, 6, 2345.

[31] J.-Y. Sun, C. Keplinger, G. M. Whitesides, Z. Suo, *Ionic skin*, Adv. Mater. **2014**, 26, 7608.

[32] G. Schwartz , B. C. K. Tee , J. Mei , A. L. Appleton , D. H. Kim , H. Wang , Z. Bao , *Flexible polymer transistors with high pressure sensitivity for application in electronic skin and health monitoring*, Nat. Commun., 4 , 1859, *2013*

[33] A. H. A. Razak, A. Zayegh, R. K. Begg, Y. Wahab, *Foot Plantar Pressure Measurement System: A Review*, Sensors **2012**, 12, 9884-9912.

[34] Novel Quality in Measurement. Available online: http://www.novel.de/ (accessed on 1 January 2012).

[35] Tekscan. Tactile Pressure Measurement, Pressure Mapping Systems, Force Sensors and Measurement Systems. Available online: http://www.tekscan.com/ (accessed on 1 January 2012).

[36] Q. Li, C. Liu, Y.-H. Lin, L. Liu, K. Jiang, S. Fan, *Large-strain, multiform movements from designable electrothermal actuators based on large highly anisotropic carbon nanotube sheets*, ACS Nano **2015**, 9, 409.

[37] S. Tadakaluru, W. Thongsuwan, P. Singjai, *Stretchable and Flexible High-Strain Sensors Made Using Carbon Nanotubes and Graphite Films on Natural Rubber*, Sensors, **2014**, 14, 868 .

[38] Y. Wang, L. Wang, T. Yang, X. Li, X. Zang, M. Zhu, K. Wang, D. Wu, H. Zhu, *Ultra-sensitive graphene strain sensor for sound signal acquisition and recognition*, Adv. Funct. Mater. **2014**, 24, 4666.

[39] S.-H. Bae, Y. Lee, B. K. Sharma, H.-J. Lee, J.-H. Kim, J.-H. Ahn, *A flexible graphene touch sensor in the general human touch range*, Carbon, **2013**, 51, 236 .

[40] J. J. Park, W. J. Hyu, S. C. Mun, Y. T. Park, O. O. Park, *Highly stretchable and wearable graphene strain sensors with controllable sensitivity for human motion monitoring*, ACS Appl. Mater Interfaces, **2015**, 7, 6317.

[41] C. S. Boland, U. Khan, C. Backes, A. O'Neill, J. McCauley, S. Duane, R. Shanker, Y. Liu, I. Jurewicz, A. B. Dalton, J. N. Coleman, *Sensitive, high-strain, high-rate bodily motion sensors based on graphene-rubber composites*, ACS Nano **2014**, 8, 8819.

[42] M. Yasin, T. Tauqeer, H. Rahman, K. S. Karimov, S. San, A. Tunc, *Polymer–Fullerene Bulk Heterojunction-Based Strain-Sensitive Flexible Organic Field-Effect Transistor*, Arab. J. Sci. Eng. **2015**, 40, 257.

[43] R. Matsuzaki, K. Tabayashi, *Wearables: Highly Stretchable, Global, and Distributed Local Strain Sensing Line Using GaInSn Electrodes for Wearable Electronics*, Adv. Funct. Mater. **2015**, 25, 3806.

[44] M. Z. Seyedin, J. M. Razal, P. C. Innis, G. G. Wallace, *Strain-responsive polyurethane/PEDOT:PSS elastomeric composite fibers with high electrical conductivity*, Adv. Funct. Mater. **2014**, 24, 2957.

[45] P. Slobodian, P. Riha, R. Benlikaya, P. Svoboda, D. Petras, *Can a wearable strain sensor based on a carbon nanotube network be an alternative to an isokinetic dynamometer for the measurement of knee-extensor muscle strength?*, Sens. J. IEEE **2013**, 13, 4045.

[46] Y. Li, X. Jiang, Z. Liu, Z. Liu, *Strain effects in graphene and graphene nanoribbons: The underlying mechanism*, Nano Res. **2010**, 3, 545.

[47] G. Latessa, F. Brunetti, A. Reale, G. Saggio, A. Di Carlo, *Piezoresistive behaviour of flexible PEDOT:PSS based sensors*, Sens. Actuators B Chem. **2009**, 139, 304.

[48] S. Savagatrup, E. Chan, S. M. Renteria-Garcia, A. D. Printz, A. V. Zaretski, T. F. O'Connor, D. Rodriquez, E. Valle, D. J. Lipomi, *Plasticization of PEDOT:PSS by Common Additives for Mechanically Robust Organic Solar Cells and Wearable Sensors*, Adv. Funct. Mater. **2015**, 25, 427.

[49] S. Hiremath, G, Yang, K. Mankodiya, *Wearable Internet of Things: Concept, architectural components and promises for person-centered healthcare*, 4th International Conference on Wireless Mobile Communication and Healthcare, **2014**.

[50] E. Sazonov, M. R. Neuman, *Wearable sensors: fundamentals, Implementation and Applications*, Accademic Press, **2014**, 1-13.

[51] Huang, C.-T.; Shen, C.-L.; Tang, C.-F.; Chang, S.-H. *A wearable yarn-based piezo-resistive sensor*, Sens. Actuators A Phys., **2008**, 141, 396–403.

[52] G. Mattana, P. Cosseddu, B, Fraboni, G. G. Malliaras, J. P. Hinestroza, A. Bonfiglio, *Organic electronics on natural cotton fibres*, Organic Electronics, 12, **2011**, 2033-2039.

[53] M. Stoppa, A. Chiolerio, *Wearable Electronics and Smart Textiles: A Critical Review*, Sensors **2014**, 14, 11957-11992.

[54] Y. Wang, T. Hua, B. Zhu, O. Li, W. Yi, X. Tao, *Novel fabric pressure sensors: design, fabrication and characterization*, Smart Mater. Struct. 20, 065015, **2011**.

[55] C. Lou, S. Wang, T. Liang, C. Pang, L. Huang, M. Run, X. Liu, *A Graphene-Based Flexible Pressure Sensor with Applications to Plantar Pressure Measurement and Gait Analysis*, Materials **2017**, 10, 1068.

[56] S. Takamatsu, T. Lonjaret, E. Ismailova, A. Masuda, T. Itoh, G. G. Malliaras, *Wearable Keyboard Using Conducting Polymer Electrodes on Textiles*, Adv. Mater.**2016**, 28, 4485–4488.

[57] S. Takamatsua, T. Kobayashib, N. Shibayamaa, K. Miyakeb, T. Itoh, *Fabric pressure sensor array fabricated with die-coating and weaving techniques*, Sensors and Actuators A 184 (**2012**), 57– 63.

[58] G. Cho , K. Jeong, M.J. Paik, Y. Kwun, M. Sung, *Performance evaluation of textilebased electrodes and motion sensors for smart clothing* IEEE Sensors J. 11, 3183–93, **2011**.

[59] L. M. Castano, A. B. Flatau, *Smart fabric sensors and e-textile technologies: a review*, Smart Mater. Struct. 23 053001, **2014**.

[60] G. Cai, M. Yang, Z. Xu, J. Liu, B. Tang, X. Wang, *Flexible and wearable strain sensing fabrics*, Materials **2017**, 10, 1068.

[61] D. I. Bower, *An introduction to polymer physics*, Cambridge university press, **2002**, 8-12.

[62] H. Shirakawa, E. Louis, A.G. MacDiarmid, C. K. Chiang, A. J. Heeger, *Synthesis of electrically conducting organic polymers: Halogen derivatives of polyacetylene, (CH) x*, Journal of the Chemical Society, Chemical Communications, **1977**, 16, 578.

[63] G. Inzelt, *Conducting Polymers A New Era in Electrochemistry*, Springer, **2012**, cap.1 - 2.

[64] MacDiarmid, *Synthetic Metals": A Novel Role for Organic Polymers*, A.G. Angew. Chem. Int. Ed., 40, 2581 **2001**.

[65] K. Tvingstedt, *Light Trapping and Alternative Electrodes for Organic Photovoltaic Devices*, Linkoping: Linkoping University Electronic Press, **2007**.

[66] A. Elschner, S. Kirchmeyer, W. Lovenich, U. Merker, K. Reuter, *PEDOT: Principles and Applications of an Intrinsically Conductive Polymer*, CRC Press, **2011**.

[67] A. J. Heeger, *Semiconducting and metallic polymers: The fourth generation of polymeric materials*, J Phys Chem B, 105(36), 8475–8491, **2001**.

[68] D. A. da Silva Filho, Y. Olivier, R. Silbey, V. Coropceanu, J. Cornil, J.L. Bredas, *Charge transport in organic semiconductors*, Chemical Reviews, 107(4): 926-952, **2013**.

[69] R. J. Kline, M. D. McGehee. *Morphology and charge transport in conjugated polymers*, Polym. Rev., 46(1):27-45, **2006**.

[70] O. Pyshkina, A. Kubarkiv, V. Sergeyev, *Poly(3,4-ethylenedioxythiophene):Synthesis and Properties*, Scientific Journal of Riga Technical University, vol 21, 51-54, **2010**.

[71] M. Zhang, Q. Zhou, J. Chen, X. Yu, L. Huang, Y. Li, C. Lia, Gaoquan Shi, *An ultrahigh-rate electrochemical capacitor based on solution-processed highly conductive PEDOT:PSS films for AC line-filtering*, Energy and Environmental Science, 6, **2016**.

[72] M. H. Yousefi, *Fabrication of flexible ITO-free OLED using vapor-treated PEDOT:PSS thin film as anode*, Journal of Display Technology, 12 (12), **2016**.

[73] G. F. Wang, X. M. Tao, R. X. Wang, *Fabrication and characterization of OLEDs using PEDOT:PSS and MWCNT nanocomposites*, Composites Science and Technology, 68 (14), **2008**, 2837-2841.

[74] Y. Wang, *Research progress on a novel conductive polymer–poly(3,4-ethylenedioxythiophene) (PEDOT)*, J. Phys. Conf. Ser., **2009**, 152, 12023.

[75] J. R. Reynolds, A. Kumar, J. L. Reddinger, B. Sankaran, S. A. Sapp, G. A. Sotzing, *Unique variable-gap polyheterocycles for high-contrast dual polymer electrochromic devices* Synth. Met. *1997*, 85, 1295.

[76] P. M. Borsenberger, D. S. Weiss, *Organic Photoreceptors for Imaging Systems*, New York: Marcel Dekker, **1993**.

[77] N. F. Mott, E. A. Davis., *Electronic Processes in Non-Crystalline Materials*, Oxford: Clarendon Press, **2012**, cap. 7.

[78] C. Qiu, J. Wang, S. Mao, W. Guo, S. Cheng, Y. Wang, *Preparation of poly(3, 4-ethylenedioxythiophene)/poly(styrene sulfonate) (PEDT/PSS) composite and its applications in anti-static coating*, Polymers for Advanced Technologies, 21, 9, **2010**, 651-655.

[79] D. Alemu, H. Y. Wei, K. C. Hod, C. W. Chu, *Highly conductive PEDOT:PSS electrode by simple film treatment with methanol for ITO-free polymer solar cells*, Energy and Environmental Science, 11, **2012**.

[80] A. G. MacDiarmid, A. J. Epstein, *The concept of secondary doping as applied to polyaniline*, Synth Met. 65(2–3), 103–106, **1994**.

[81] S. K. M. Jönsson, J. Birgerson, X. Crispin, G. Greczynski, W. Osikowicz, A. W. Denier van der Gon, W. R. Salaneck, M. Fahlman, *The effects of solvents on the morphology and sheet resistance in poly(3, 4-ethylenedioxythiophene)-polystyrenesulfonic acid (PEDOT-PSS) films* Synth. Met., 139(1), 1–10, **2003**.

[82] S.Timpanaroa, M.Kemerinkb, F. J.Touwslagerc, M. M. De Kokc, S.Schrader, *Morphology and conductivity of PEDOT/PSS films studied by scanning–tunneling microscopy Author links open overlay panel* S.Timpanaroa, M.Kemerinkb, F. J.Touwslagerc, M. M. De Kokc, S.Schrader, Chemical Physics Letters, 94, 4–6, **2004**, 339-343.

[83] J. Ouyang, C. W. Chu, F. C. Chen, Q. Xu, Y. Yang, *High-Conductivity Poly(3,4-Ethylenedioxythiophene):Poly(styrenesulfonate) Film and Its Application in Polymer Optoelectronic Devices*, Adv. Funct. Mater., 15, 290, **2005**.

[84] J.Y. Kim, J.H. Jung, D.E. Lee, J. Joo, *Enhancement of electrical conductivity of poly(3,4-ethylenedioxythiophene)/poly(4-styrenesulfonate) by a change of solvents*

[85] J. Ouyanga, Q. Xua, C. W. Chua, Y. Yanga, G. LiB, J. Shinarb, *On the mechanism of conductivity enhancement in poly(3,4-ethylenedioxythiophene):poly(styrene sulfonate) film through solvent treatment*, Polymer 45, **2004**, 8443–8450.

[86] Joseph Palathinkal Thomas , Liyan Zhao , Donald McGillivray and Kam Tong Leung , *High-efficiency hybrid solar cells by nanostructural modification in PEDOT:PSS with co-solvent addition*, J. Mater. Chem. A, 2014, 2, 2383-2389.

[87] X. Crispin, F. L. E. Jakobsson, A. Crispin, P. C. M. Grim, P. Andersson, A. Volodin, C. van Haesendonck, M. Van der Auweraer, W. R.

Salaneck, M. Berggren, *The origin of the high conductivity of poly(3,4-ethylenedioxythiophene)- poly(styrenesulfonate) (PEDOT-PSS) plastic electrodes*, Chem. Mater. 18(18): 4354–4360, **2006**.

[88] I. D. Cave, J. F. C. Walker, *Stiffness of Wood in Farown Plantation Softwood: The Influence of Microfibril angle*, Forest Product Journal, 4454348.

[89] S. Gordon, Y-L. Hsieh, *Cotton: Science and technology*, Woodhead Publishing Limited and CRC Press LLC, **2007**, cap. 1-2.

[90] S. Savagatrup, E. Chan, S.M. Renteria-Garcia, A.D. Printz, A. V. Zaretski, T. F. O'Connor, D.Rodriquez, E. Valle, D. J. Lipomi, *Plasticization of PEDOT:PSS by Common Additives for Mechanically Robust Organic Solar Cells and Wearable Sensors*, Advanced Functional Materials, 25 (3), **2014**.

[91] S. Zhang, P. Kumar, A. S. Nouas, L. Fontaine, H. Tang, F. Cicoira, *Solvent-induced changes in PEDOT:PSS films for organic electrochemical transistors*, APL Materials 3, 014911, **2015**.

[92] Pauw L J van der, Philips Res. Rep. 13, 1 (1958).

[93] A. Maksumov, R. Vidu, A. Palazoglu, P. Stroeve, *Enhanced feature analysis using wavelets for scanning probe microscopy images of surfaces*, Journal of Colloid and Interface Science, 272(2):365, **2004**.

[94] Keithley 2400 series Sourcemeter User's Manual.

[95] J.C. Wang, X.C. Ren, S.Q. Shi, C.W. Leung, P. K.L. Chan, *Charge accumulation induced S-shape J–V curves in bilayer heterojunction organic solar cells*, Organic Electronics 12, **2011**, 880–885.

[96] J. Meyer, B. Arnich, J. Schumm, G. Troster, *Design and modeling of a textile pressure sensor for sitting posture classification*, IEEE Sens. J. **2010**, 10, 1391-1398.

[97] W. Xu, M. C. Huang, N. Amini, L. He, M. Sarrafzadeh, *A textile pressure sensor array design and calibration for sitting posture analysis*, IEEE Sens. J. **2013**, 13, 3926-3934.

[98] B. D. Lowe, S. M. Schrader, M. J. Breitenstein, *Effect of Bicycle Saddle Designs on the Pressure to the Perineum of the Bicyclist*, Medicine and Science in sports and exercise, **2004**, 1055-1062.

[99] J. F. Saenz-Cogollo, M. Pau, B. Fraboni, A. Bonfiglio, *Pressure mapping mat for tele-home care applications* , Sensors (Basel), 16(3): 365, **2016** Mar.

[100] J. C. Wang, R. S. Karmakar, Y. J. Lu, C. Y. Huang, K. C. Wei, *Characterization of Piezoresistive PEDOT:PSS Pressure Sensors with Inter-Digitated and Cross-Point Electrode Structures*, Sensors (Basel), **2015**, 15(1): 818–831.

[101] A. M. Nardes, M. Kemerink, R. A. J. Janssen, J. A. M. Bastiaansen, N. M. M. Kiggen, B. M. W. Langeveld, A. J. J. M. van Breemen, M. N. de Kok, *Microscopic understanding of the anisotropic conductivity of PEDOT:PSS thin films*, Adv. Mater. **2007**, 19, 1196–1200.

[102] E. Vitoratos, S, Sakkopoulos, E. Dalas, N, Paliatsas, D. Karageorgopoulos, F. Petraki, S. Kennou, S. A. Choulis, *Thermal degradation mechanisms of PEDOT:PSS*, Org. Electron. **2009**, 10, 61–66.

[103] Yamada, T.; Hayamizu, Y.; Yamamoto, Y.; Yomogida, Y.; Izadi- Najafabadi, A.; Futaba, D. N.; Hata, K. A, *Stretchable Carbon Nanotube Strain Sensor for Human-Motion Detection*, Nat. Nanotechnol. **2011**, 6, 296 -301.

[104] F. Carpi, D. DeRossi, *Electroactive Polymer-Based Devices for e-Textiles in Biomedicine*, IEEE Trans. Inf. Technol. Biomed. **2005**, 9, 295 - 318.

[105] B.J. Munro, J.R. Steele, G.G. Wallace, *The Intelligent Knee Sleeve: A valid and reliable device to combat ACL injuries*, J. Sci. Medicine Sport 5 (4), **2002** Suppl: 10.

[106] B. J. Munro, T. E. Campbell, G. G. Wallace, J. R. Steele, *The Intelligent Knee Sleeve: A Wearable Biofeedback Device*, Sens. Actuators B, **2008**, 131, 541 - 547.

[107] Zhang, H.; Tao, X.; Yu, T.; Wang, S. *Conductive Knitted Fabric as Large-Strain Gauge under High Temperature*, Sens. Actuators A, **2006**, 126, 129-140.

[108] S. Beeby, G. Ensell, M. Kraft, N. White, *MEMS Mechanical Sensors*, Artech House, Boston, **2004**.

[109] Cherenack, K.; van Pieterson, L. *Smart Textiles: Challenges and Opportunities*, J. Appl. Phys. **2012**, 112, 091301.

Ringraziamenti

Al termine di questo lavoro di tesi desidero ringraziare il prof. E. G. Campari per la disponibilità e gentilezza con cui mi ha accompagnato in questo percorso. Sinceri ringraziamenti alla prof.ssa B. Fraboni che mi ha sempre supportato e accompagnato con i suoi preziosi consigli e alla dott.ssa M. Tessarolo che con il suo immancabile sostegno, pazienza e positività mi ha aiutato a superare ogni ostacolo.

Un profondo ringraziamento va alla mia famiglia: a mia madre Antonina e mio padre Enzo che mi hanno dato l'opportunità di intraprendere questo percorso e hanno sempre creduto in me; a mia sorella Francesca per la sua instancabile vicinanza e fiducia che mi ha continuamente dimostrato, a Giuseppe sul quale posso sempre contare e alle mie nipoti Caterina, Giorgia e Gemma che mi fanno sentire tanto amato.

Desidero ringraziare tutti i miei amici con cui, nel corso di questi anni, ho avuto la fortuna di condivide centinaia di esperienze, tra cui Giacomo, Luca, Michael, Gianluca, Michele, Dary, Francesco, Simone.

Un grazie speciale ai miei compagni di vita bolognese Gianmaria, Lorenzo e Filippo. Grazie in particolare a Riccardo, che mi ha sostenuto ed aiutato nelle serate di lavoro.

Ringrazio Alberto, il mio fedele compagno di studi con cui ho condiviso l'intero percorso di laurea magistrale.

Infine, voglio esprimere tutta la mia gratitudine a Noemi per la vicinanza e supporto che, *nonostante tutto*, mi ha sempre dimostrato. Grazie per aver condiviso con me, passo dopo passo, questo importante cammino dimostrandomi in ogni occasione il suo amore.